Ozone in the Tropical Troposphere

Wouter Peters

Ozone in the Tropical Troposphere

Ozon in de Tropische Troposfeer

(met een samenvatting in het Nederlands)

Proefschrift

ter verkrijging van de graad van doctor aan de Universiteit Utrecht op gezag van de Rector Magnificus, Prof. Dr. W. H. Gispen, ingevolge het besluit van het College voor Promoties in het openbaar te verdedigen op maandag 16 december 2002 des ochtends te 10.30 uur.

door

Wouter Peters

geboren op 15 mei 1975, te Hoorn.

Promotor:	**Prof. Dr. J. Lelieveld** Max Planck Institut für Chemie, Mainz, Duitsland oud-hoogleraar aan de Universiteit Utrecht
Co-promotor:	**Dr. M.C. Krol** faculteit Natuur- en Sterrenkunde, Universiteit Utrecht

This thesis is a contribution to the "Research on Atmospheric Dynamics and Chemistry in Suriname"(RADCHiS) program, sponsored by the Dutch National Association of Scientific Research (NWO).

ISBN 90-393-3206-1

Contents

Chapter 1

Introduction

Although ozone is only a minor constituent of the troposphere, it is involved in a wide range of atmospheric processes. I will start this thesis by discussing the many roles of ozone, to clarify the scientific interest in this molecule. Subsequently, I will explain the central role of the tropics in atmospheric chemistry research in general, and in ozone photo-chemistry specifically. This is followed by a description of ozone observation techniques and the global ozone distribution inferred from these observations. Our attempts to simulate this distribution with global chemistry-transport models will be discussed next. Finally, the scientific aims of this work are formulated, and an outline of this thesis is presented.

1.1 The role of ozone

Population growth and industrialization over the past century have changed the composition of the atmosphere. Atmospheric levels of trace gases that are by-products of human activities, such as carbon monoxide (CO), methane (CH_4), volatile organic compounds (VOC's), and nitrogen oxides (NO_x) have increased strongly, as emissions of these compounds more than doubled from their pre-industrial levels [*van Aardenne et al.*, 2001]. Although these trace gases constitute far less than 1% of the air surrounding us, their effect on the biosphere is considerable. The steady increase of the greenhouse gases carbon dioxide (CO_2) and CH_4 has caused a rise in global mean temperature [*IPCC, 3rd assessment report (TAR), 2001*], while traffic exhaust (mainly NO_x, CO, VOC's and aerosols) has led to urban 'smog' [*Haagen-Smit and Fox*, 1956], which is responsible for poor air quality and associated with respiratory problems and increases in allergies and juvenile astma [*Dockery et al.*, 1993]. Extreme surface ozone (O_3) concentrations impact human health and crop productivity and are estimated to cost several billion dollars per year in the United States alone [*US–EPA*, 1998].

Atmospheric change is common throughout the history of Earth even on timescales of several thousands of years. For instance, Antarctic ice-core records show that the atmospheric methane abundance was substantially (factor of five) smaller during the last glaciation (15K years before present) [*Petit et al.*, 1999]. What renders the changes over the past century so special is not only their absolute magnitude, but the

unprecedented rate at which they take place [*IPCC, TAR, 2001*]. Such rapid changes could potentially destabilize the atmosphere-climate system, and lead to severely altered environmental conditions. This includes for instance the possible collapse of the North Atlantic thermo-haline ocean circulation, the catastrophic removal of oxidants such as the hydroxyl-radical (OH) from the atmosphere, or a breakup of the West-Antarctic ice sheet [*IPCC, TAR, 2001*]. For example, only recently the catastrophic depletion of stratospheric ozone in the Antarctic vortex by minute quantities of chlorine, bromine and nitrogen was detected [*Farman et al.*, 1985] and explained by the breakdown of nitrous oxide and chlorofluorocarbons [*Crutzen*, 1970; *Molina and Rowland*, 1974]. After this realization, emissions of the responsible chemical were brought to a halt by the parties in the Montreal protocol. The timely recognition and effective response in this case illustrates the importance of monitoring trace gases, understanding atmospheric chemistry, and assessing system stability with respect to changes in composition.

In this thesis, studies of transport, photo-chemistry and system stability are focused on the troposphere. The troposphere covers the lower $\sim$10 km of the atmosphere, and differs from the stratosphere (10-50 km height) through relatively short transport time-scales (hours-months), and close proximity to surface sources and sinks of heat, moisture, and trace gases. This leads to a high degree of spatial coupling in the troposphere (processes occurring in one region can rapidly affect another), as well as strong photo-chemical interactions (many species are brought into contact with one another). In photo-chemistry of the troposphere, ozone plays a key role. Photo-chemical reactions that lead to the removal of many trace gases from our atmosphere are initiated either by sunlight, or by reaction with an oxidant. The most important oxidant in the troposphere is the hydroxyl (OH) radical, which is also called the 'cleaning agent' of the atmosphere [*Crutzen and Zimmermann*, 1991], as it is able to react with almost every organic and even many inorganic molecules. Other oxidants in the troposphere include for instance NO_3, H_2O_2, and also ozone. Of much greater interest is the role of ozone as a precursor for the production of OH, through the following reactions:

$$\begin{aligned} O_3 + h\nu(\lambda < 330nm) &\rightarrow O_2 + O(^1D) \\ H_2O + O(^1D) &\rightarrow 2OH \end{aligned} \tag{1.1}$$

Where $h\nu$ is the product of the Planck constant and the frequency of light at wavelength λ, and H_2O is water vapor. Thus, the tropospheric abundance of ozone (and water vapor + sunlight) determines the ability of the atmosphere to remove many trace gases. This property is called the 'oxidizing power' of the atmosphere[1].

Transport of ozone from the large stratospheric reservoir to the troposphere provides a baseline ozone concentration in the troposphere, which ensures a minimal oxidizing power everywhere. Additionally, net photo-chemical production of ozone maximizes in 'polluted' regions (where levels of NO_x, CO, and other pollutants are high), while it is negligible or even negative in unpolluted regions. As a consequence, the oxidizing power is increased in regions that are most polluted, providing a negative feedback on the growth of pollutant levels. This property of the atmosphere is governed by the following reaction cycles [*Crutzen*, 1973]:

[1] In this work, the oxidizing power is defined as the gross production of OH in the atmosphere in either [molecules/cm^3/s] or [Tmol/yr].

Production				Destruction			
$CO+OH$	$\rightarrow$	CO_2+H		$CO+OH$	$\rightarrow$	CO_2+H	
$H+O_2+M$	$\rightarrow$	HO_2+M		$H+O_2+M$	$\rightarrow$	HO_2+M	
$NO+HO_2$	$\rightarrow$	NO_2+OH		O_3+HO_2	$\rightarrow$	$2O_2+OH$	
$NO_2+h\nu(\lambda<420nm)$	$\rightarrow$	$NO+O(^3P)$					
$O(^3P)+O_2+M$	$\rightarrow$	O_3+M					
$CO+2O_2$	$\rightarrow$	CO_2+O_3	(1.2)	$CO+O_3$	$\rightarrow$	CO_2+O_2	(1.3)

M is a third body, usually N_2 or O_2, that removes excess energy from the intermediate reaction complex, preventing that this complex breaks up into the original reactants. Cycle 1.2 prevails under high NO_x abundances, and cycle 1.3 under low NO_x abundances. Note that CO in these cycles can be substituted by many different trace gases (such as methane, formaldehyde, or sulfate). Concentrations of ozone thus reflect the photo-chemical state (i.e. degree of pollution) of the atmosphere, and ozone is therefore often used as a diagnostic for atmospheric chemistry.

In contrast to OH which reacts in cycles 1.2 and 1.3 in mere seconds, ozone in the troposphere has a lifetime of several days to weeks depending on the abundance of water vapor and sunlight (see reaction 1.1). This allows ozone to be transported around the globe, and makes it a good tracer for atmospheric transport. The vertical distribution of ozone generally reveals a gradient from the surface, where the main sinks are located, to the stratospheric reservoir. The gradients are altered by turbulent transport and convection, allowing us to recognize these processes from a vertical ozone profile. Thus, the global distribution of ozone can reveal large-scale transport patterns, and is used for instance to detect frontal systems and stratosphere-troposphere exchange [*Holton et al.*, 1995].

Last but not least, ozone has important radiative properties. Ozone shields life on Earth from harmful ultraviolet radiation, but also acts as a greenhouse gas, trapping terrestrial long wave radiation in the lower atmosphere. Absorption of shortwave radiation by ozone mainly occurs in three wavelength intervals, called the Hartley, Huggins, and Chapuis absorption bands. The first two are in the ultraviolet range, while the latter is in the visible part of the spectrum (λ=620 nm). A fourth absorption peak in the infrared (9-10 μm) is largely responsible for an estimated climate forcing of 0.35 ± 0.15 W/m^2 since pre-industrial times (compared to 1.46 ± 0.2 W/m^2 for CO_2) [*IPCC, TAR, 2001*]. This makes tropospheric ozone the third most important greenhouse gas after CO_2 and CH_4. Estimates of ozone's radiative role are much more difficult and uncertain than that of the longer-lived greenhouse gases, since it is photo-chemically formed and displays considerable spatial and temporal variability. Projections of the future changes in ozone's greenhouse contributions therefore depend strongly on our knowledge of its photo-chemistry and variability.

In summary, our scientific interest in tropospheric ozone is based on its role as OH-precursor, as diagnostic for photo-chemistry, as transport tracer, and as absorber of long-wave and short-wave radiation.

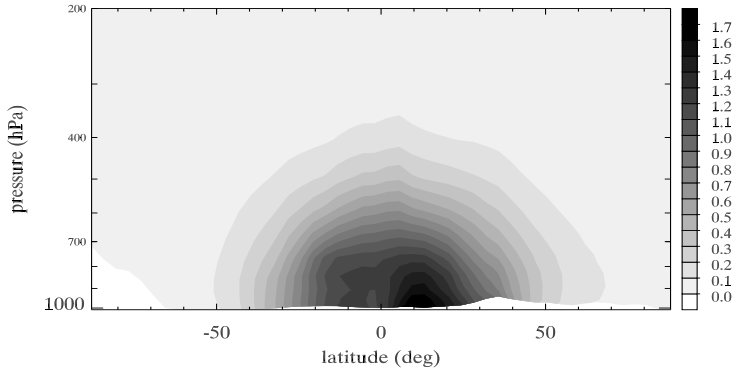

Figure 1.1: Yearly and zonally averaged OH-production from reaction 1.1 in units of 10^6molecules/cm^3/s. The figure illustrates the key role of the tropics in maintaining the 'oxidizing power' of the troposphere.

1.2 The role of the tropics

The extent of the tropics can be described in many ways, e.g. by climatic elements such as rainfall, by meteorological characteristics such as the location of the sub-tropical front, or by geographical extent (30°S to 30°N for example). Defined in this latter way, the tropical troposphere covers more than 60% of the Earth by volume. It receives up to twice as much solar radiation as the extra-tropics, while the thickness of the stratospheric ozone layer is only 60% of that at mid-latitudes. Thus, the amount of energy available to drive convection, evaporation, as well as photo-chemistry, far exceeds that in the extra-tropics. The maximum in temperature and evaporation leads to a maximum of moisture in the tropical troposphere, which, coupled to the large flux of UV-radiation, maximizes the production of OH in the tropical atmosphere (see reaction 1.1). Figure 1.1 shows the yearly and zonally average OH-production rate near the surface (10^6molecules/cm^3/s) from reaction 1.1, as calculated from a simulation of the present-day atmosphere. The figure illustrates that if OH is justly called the atmosphere's 'cleaning agent', the tropics can be deemed its 'laundry-room', as the bulk of the oxidizing power is contained in the tropics.

The tropical regions have generally developed less quickly than the Western world over the past century (economically), and population growth was not accompanied by strongly growing industrial emissions. Thus, anthropogenic pollution composes a relatively small fraction of the tropical atmosphere. Nevertheless, the tropical troposphere can not be characterized as a pristine environment. Considerable natural emissions of NO_x, CO, and VOC's from forests, savannas, and soils occur in the tropics as a result of plant physiological, but also microbial, and pyrogenic processes. For instance, *Guenther et al.* [1995] estimated that close to 1200 TgC is released in various forms annually from (tropical) vegetation alone, which is almost twice as much as the global total CO emissions. Likewise, tropical soils, savanna burning, and lightning likely release up to 10TgN in the form of NO_x per year, which is 25% of the yearly global total release of oxidized nitrogen compounds [*Pickering et al.*, 1993; *Yienger*

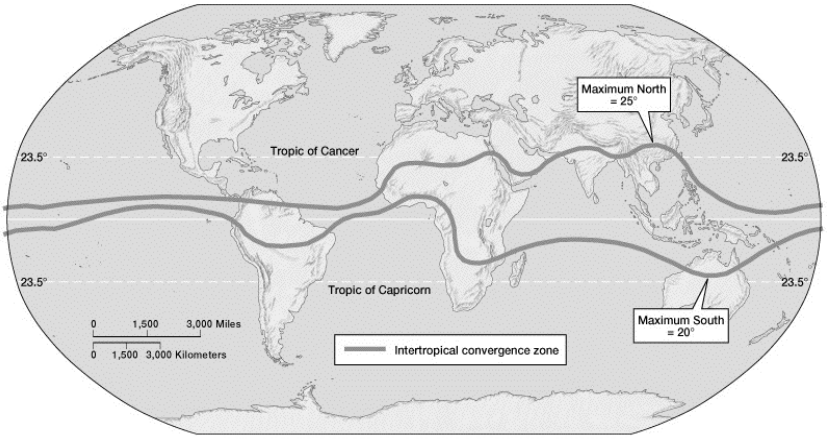

Figure 1.2: The ITCZ follows the position of maximum solar insolation between the two solstices, but displays considerable longitudinal variability due to the land-sea distribution and meteorological disturbances. Image: NASA Earth Observatory (*http://earthobservatory.nasa.gov*)

and Levy, 1995]. The largest contributor to the tropical emission budget however is the release of trace gases during burning of biomass.

Biomass burning can occur as a natural phenomena following droughts, but it is nowadays mostly a human practice for purposes of heating, cooking, deforestation, waste burning, or to revitalize agricultural land [e.g. *Andreae*, 1993]. Release of CO from biomass burning exceeds fossil fuel use as most important source of CO in the atmosphere [*Crutzen and Andreae*, 1990]. The location and timing of most biomass burning emissions follows a well-defined seasonality in the tropics, closely matching the precipitation patterns [*Hao et al.*, 1990]. However, these patterns display considerable interannual variability due to meteorological variability, and changes in land use [*Pinty et al.*, 2000] . In this thesis, as well as in previous work [e.g. *Roelofs et al.*, 1997; *Moxim and Levy*, 2000; *Galanter et al.*, 2000], our understanding of the photochemistry of the global troposphere was limited by our knowledge on the variability and chemical constitution of biomass burning emissions.

Meteorological variability in the tropics is strongly coupled to the migration of the Inter Tropical Convergence Zone (ITCZ). The ITCZ is an intermittent band of convective cloud systems oriented in east-west direction in the tropics. It follows the migration of the sun between winter and summer solstice (although never actually reaching these extremes), and is affected by the land-sea distribution and by atmospheric disturbances, giving it considerable variability on time-scales from days to years (see Figure 1.2). The convective systems in the ITCZ are caused by convergence of air near the surface, coupled to a strong heating of the surface which destabilizes the atmosphere (see Figure 1.3). The upward motions of moisture that are thus introduced result in release of latent heat through condensation of water vapor forming clouds and precipitation, but also result in vigorous exchange of air between the free troposphere and the boundary layer, on time-scales of hours. Once the convection ceases and the clouds disappear, layers that were vertically transported

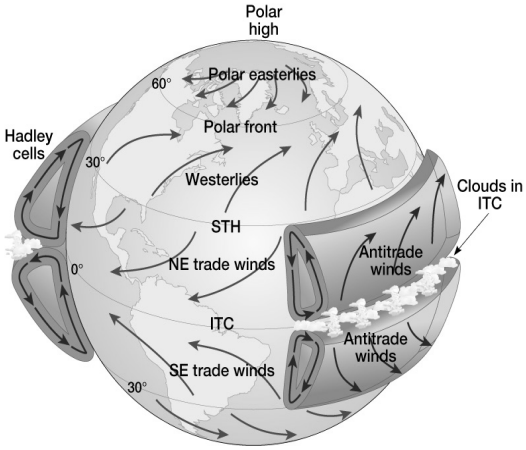

Figure 1.3: Convection in the ITCZ is induced by surface heating, and convergence of the surface trade-winds. Large-scale downward motions occur outside convective cells, closing the Hadley-cell circulation. Rapid horizontal transport at higher altitudes induces exchange between the tropics and extra-tropics. Image: NASA Earth Observatory (*http://earthobservatory.nasa.gov*)

while maintaining their chemical composition can be found at distinct altitudes in the troposphere. Convective transport has important implications for atmospheric chemistry, as the lifetime of many species increases considerably with altitude [*Lelieveld and Crutzen*, 1994]. Moreover, rapid horizontal transport occurs at higher altitudes, allowing exchange of chemical species between the tropics and extra-tropics. The coexistence of considerable emissions and an impressive vertical transport mechanism once again underline the importance of the tropics.

Finally, the rapid economic growth of economies in Asia, Africa, and South America will increase human influence on the tropics. Projected changes in industrial emissions, land-use, traffic, and population show that these will be most dramatic in these regions [*IPCC, TAR, 2001*]. Such changes will inevitably influence mid-latitudes as well, although our current knowledge of the tropical regions does not allow us to predict in what way. Scientific research specifically into this region is needed to increase our knowledge, allowing us to make more credible estimates of the consequences, and risks of climate change.

1.3 Observations of ozone in the tropics

Monitoring of tropospheric ozone is commonly carried out through the release of helium filled balloons equipped with a simple ozone measuring instrument. Most often, this instrument is an electrochemical cell (ECC), consisting of a Potassium Iodine (KI) solution that reacts with ozone in ambient air in a reduction-oxidation reaction. The ozone abundance determines the electric current in the redox-cell, and is continuously measured and relayed through a radio link to the ground for recalculation to a concentration. With concomitant measurements of pressure, this yields a vertical

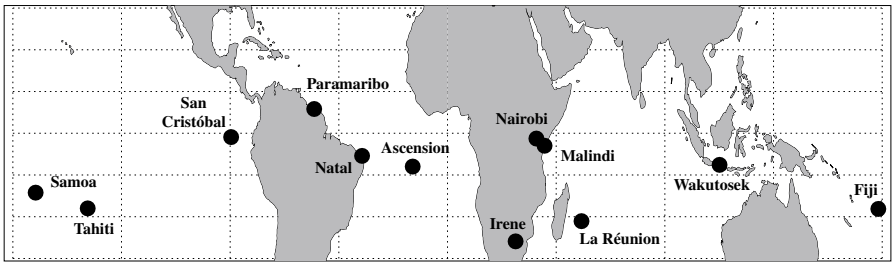

Figure 1.4: Location of stations in the Southern Hemisphere ADditional OZone sounding (SHADOZ) network.

profile of ozone with height. Such measurements are performed routinely, up to six times per day at over 100 stations in the world.

Although the number of such stations is quite large, their spatial coverage is quite poor. The Northern Hemisphere (NH) is much more densely covered by stations than the Southern Hemisphere (SH), and few stations are located in the tropics. The world's vast oceans are represented by a few island locations (Hawaii, Fiji, Tahiti, Samoa, La Reunion, Ascension). Some of the ozone stations have several decades of daily observations (e.g. Höhenpeißenberg, 11E, 47N operates since 1966), while others have weekly observations for only one year.

The oldest station in the tropics is Natal, Brazil (35W, 6S) [*Logan and Kirchhoff*, 1986], which provides a nearly continuous record dating back to 1979. Almost all other stations currently operating in the tropics were started in 1998, when NASA initiated the Southern Hemisphere ADditional Ozone Sounding (SHADOZ) program. This program was started specifically to increase the number of SH tropical monitoring stations, and support ongoing space-born ozone observation programs (e.g. TOMS, GOME, SCIAMACHY, OMI), which are expected to play an increasingly important role in atmospheric chemistry research.

Satellite observations of ozone started in 1978 with the launch of the NIMBUS-7 satellite, containing the Total Ozone Mapping Spectrometer (TOMS). This instrument uses the intensity of radiation in several UV-bands where ozone absorbs, to determine the total amount of ozone between the Earth's surface and the instrument. This quantity is often expressed in Dobson Units (DU), where one DU is 2.69×10^{16} molecules cm^{-2} of ozone, and 100 DU is the equivalent of a one mm layer of ozone at the surface (at standard pressure). TOMS instruments were flown on the NIMBUS, METEOR, ADEOS, and Earth Probe satellites to ensure a continuous dataset of ozone observations from 1978 until today. One of the most important accomplishments of the TOMS instruments is the imaging of the Antarctic ozone hole, providing a first glance on the huge geographical extent of the stratospheric ozone depletion in spring [*Farman et al.*, 1985].

The satellite observed distribution of total ozone columns (TOC) in the tropics also led to new scientific questions. Frequently, distinct maxima of TOC were seen over the Atlantic Ocean and the adjacent continents, while TOC over the Pacific was consistently lower [*Fishman et al.*, 1990]. This gave the impression of an equato-

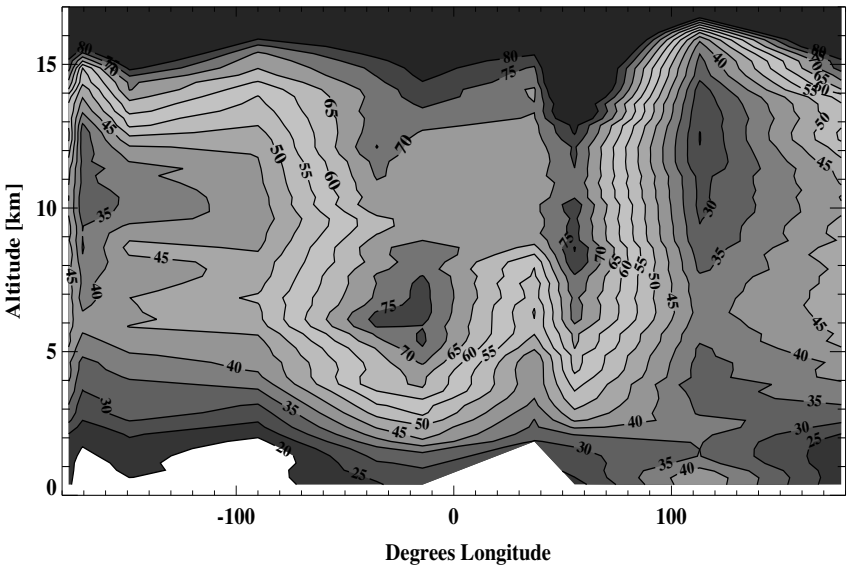

Figure 1.5: The zonal distribution of tropospheric ozone constructed from multi-year sonde observations from SHADOZ (units=ppbv). Reproduced from *Thompson et al.* [2002b].

rial wave pattern, with one maximum and one minimum. It was unclear whether this 'zonal wave one pattern' [*Shiotani*, 1992] found its origin in the stratosphere, or in the troposphere. This issue was resolved only recently [*Thompson et al.*, 2002b], using a large number of sondes from the SHADOZ project. Figure 1.5 shows that widespread ozone enhancements following a wave one pattern are found in the tropical troposphere, while the stratospheric ozone abundance is largely zonally invariant in the tropics (not shown). These tropospheric enhancements maximize during SH spring, concurrent with the local dry seasons, but are present throughout the year. Various studies on the composition of the Atlantic ozone maxima conclude that a complex mix of large-scale transport [*Krishnamurti et al.*, 1993], biomass burning related photo-chemistry [e.g. *Roelofs et al.*, 1997; *Galanter et al.*, 2000; *Moxim and Levy*, 2000], and lightning induced photo-chemistry [*Pickering et al.*, 1998; *Martin et al.*, 2000] underlie this feature.

This knowledge has been used to separate TOC observations into tropospheric ozone columns (TTOC) and stratospheric ozone columns [*Fishman et al.*, 1990; *Kim et al.*, 1996; *Hudson and Thompson*, 1998; *Ziemke et al.*, 1998]. Absolute values of satellite derived TTOC are quite uncertain (at least 10-25%), and different datasets are not always consistent with each other, or with independent measurements such as ozone sondes. Nevertheless, the distribution of TTOC as seen from space shows many interesting features, and is very well suited to study the large-scale ozone distribution in the tropics. Moreover, the spatial and temporal scales are very similar to those used in numerical modeling techniques, which renders satellite observations very useful to

test and improve our knowledge on tropospheric ozone with these tools.

1.4 Simulating the ozone distribution

Mathematically, the abundance and variability of trace gases in the troposphere is identified by a a set of coupled partial differential equations (PDE's), that describe the often non-linear interactions in chemistry and transport:

$$\begin{aligned} \frac{\partial \chi_i}{\partial t} &= S + D + T + C \\ C &= P - L[\chi_i] \\ P, L &= f(\chi_1, \chi_2, ..., \chi_n) \end{aligned} \tag{1.4}$$

This includes local non-chemistry sources (S), local non-chemistry sinks (D), transport (T), photo-chemistry (C), while χ_i denotes the trace gas concentration of species i at a fixed location. Net photo-chemistry is the sum of production (P) and loss (L) terms. The coupling between species is contained in photo-chemistry (C), while the coupling between locations is introduced by transport (T). Details on the individual processes (S, D, T, C), or the behavior of individual compounds (χ_i) can be studied in controlled laboratory environments, or by using measurements obtained in field campaigns, but numerical models are needed to study the fully coupled system.

As was seen in the previous sections, ozone is influenced by many processes, which should all be included in numerical models to determine its concentration from equation 1.4. The chemical lifetime of some species is sufficiently short to allow simplifications to Equation 1.4. For instance, OH has a chemical lifetime of a few seconds in the troposphere, which means that transport (T), deposition (D) and non-chemistry sources (S) can safely be neglected on the spatial scales that we are interested in. A short chemical lifetime also implies a large chemical production (or a negligible concentration). As a result, the rate of change ($\partial\chi/\partial$t) of such a 'fast' chemical species is small compared to its production and destruction rates. Thus, locally, the concentration of OH can be calculated from the concentrations of longer lived species as:

$$[OH] = \frac{P}{L} = \frac{P}{(k_1[\mathrm{CO}] + k_2[\mathrm{CH_4}] + ...k_n[\chi_n])} \tag{1.5}$$

Where k_n is the reaction constant for OH with species χ_n.

A trace gas with a longer lifetime such as CH_4 ($\tau \approx 8$ years) is relatively well-mixed in the troposphere (CH_4 local $\approx \overline{CH_4}$, where the bar represents a tropospheric average). We can thus consider the whole troposphere as one box. The tropospheric budget of the 'slow' chemical species CH_4 is then governed by surface emissions, and chemical loss, as transport to the stratosphere and surface deposition are negligible. The steady-state ($\partial\chi/\partial$t=0) tropospheric average CH_4 concentration can thus be determined from:

$$[\overline{CH_4}] = \frac{S}{(k[\overline{\mathrm{OH}}])} \tag{1.6}$$

Where the overbars again denote tropospheric averages. Measurements from ice-cores [*Petit et al.*, 1999] and a global monitoring network [*Dlugocencky et al.*, 1994]

indicate that $[\overline{CH_4}]$ has indeed increased by a factor of $\sim$2 (from 800 ppbv to 1700 ppbv) following a roughly two-fold increase in emissions since pre-industrial times [*Houweling*, 2000]. Paradoxically, Equation 1.6 thus implies that the tropospheric average hydroxyl concentration ($[\overline{OH}]$) has also remained roughly constant over this period, even though concentrations of the principal OH sinks CO and CH_4 (Equation 1.5) have almost doubled. This apparent paradox is one of the topics that will be addressed in this work (Chapter 5).

Numerical models can be applied in several ways to learn more about trace gases, including ozone in the tropical troposphere. First of all, by performing simulations to the best of our abilities and comparing them with observations, model deficiencies are recognized which can point out shortcomings in our knowledge of individual processes in the system, or make us consider other, previously unaccounted processes. For example, proposed catalytic ozone depleting cycles involving nitrogen-oxide [*Crutzen*, 1970] and chlorofluorocarbon (CFC) reactions [*Molina and Rowland*, 1974] on ice particles were not taken into account in numerical models of the stratosphere until after the discovery of the ozone hole [*Farman et al.*, 1985], which therefore came as a surprise. Secondly, numerical models can help us to quantify system dependencies and sensitivities, as well as feedbacks between processes. These feedbacks are not present in the uncoupled system, and can thereby help us prioritize directions for our research. Thirdly, models can provide information on processes or compounds that cannot be easily measured, by validating related compounds or processes which we understand and reproduce well. Finally and perhaps most importantly, models can be used to perform numerical experiments. In these, we can reproduce situations which are unavailable in reality, such as pre-industrial or future atmospheric conditions. Such simulations will be invaluable to study the effects of earlier mentioned changes in the tropics.

In this thesis, all these techniques will be used to learn more about ozone in the tropical troposphere, and provide guidelines for future research. This is done with the aid of a chemistry-transport model (CTM). This category of models combines the results of detailed atmospheric transport calculations with a numerical description of chemistry, sources, and sinks of several compounds. The atmospheric transport parameters are typically provided by another, dedicated, numerical model (such as a weather forecast model), so that more computer resources can be applied to chemistry and the complexity of the CTM is limited (this is called *off-line* chemistry transport modeling). This approach contrasts with that in general circulation models (GCM), which also perform all calculations of transport (*on-line* modeling), enlarging the complexity and demand of computer resources.

The CTM used is called the Transport Model version 3 (TM3), and has been developed over the past decade by a large number of persons in Mainz, Hamburg, Wageningen, and Utrecht. Typically, such model development starts with a 'core' model (the MOGUNTIA [*Crutzen and Zimmermann*, 1991] and TM2 [*Heimann et al.*, 1988] model in this case), to which more detailed and complex routines are added to improve its performance, as new insights develop and more observations become available. The consistent use and development by a large user community ensures that the model is properly tested and maintained, and documented in scientific journals [e.g. *Dentener and Crutzen*, 1993; *Kanakidou et al.*, 1995; *Houweling et al.*, 1998; *Jeuken*, 2000; *Lelieveld and Dentener*, 2000; *Bregman et al.*, 2001]. Due to the earlier mentioned excess of data available for the NH relative to the SH and tropics, the TM3

model (and virtually every other CTM and GCM) has been validated, tested, and developed with a bias towards NH mid-latitude conditions. This bias affects all aspects of the model, including the representation of the diurnal growth of the boundary layer, the treatment of convection, surface emissions, and even photo-chemistry. Now that more and more observations from the tropics are becoming available, most of these processes in the model need to be critically reexamined.

1.5 Research aims and thesis outline

The central theme of this thesis is the distribution of tropospheric ozone in the tropics, as deduced from measurements and model simulations. This theme was instigated by the inauguration in 1998 of an ozone monitoring station in Paramaribo, Suriname. It was started as part of recent efforts to better understand transport and photo-chemistry specifically in the tropics, which will eventually allow us to estimate the influence of (past, present, and future) population growth, industrialization, deforestation, desertification, and changing agriculture on the atmospheric composition. The ozone measurements from Paramaribo, combined with those at other locations, help to understand the ozone distribution on larger scales, but will also be used to validate satellite observations of tropospheric ozone. Finally, they will help to constrain and improve numerical modeling efforts that are required to study the coupled system of transport and photo-chemistry in the tropics.

The research questions that I set out to answer in this work can be summarized as follows:

1. Do we understand the horizontal and vertical distribution of ozone in the tropical troposphere, and specifically over the equatorial Atlantic?
2. Do we understand the variability of ozone in the tropical troposphere?
3. What is the nature of photo-chemical feedbacks involving ozone, and how do they contribute to the apparent constancy of oxidant levels?
4. Does the (human induced) changing atmospheric composition destabilize tropospheric hydroxyl photo-chemistry?

The first question is addressed in a very direct way in Chapter 2, where the 2.5 years of ozone measurements performed in Paramaribo are placed in a regional perspective through comparison of seasonal cycles of ozone observed at Paramaribo and other nearby monitoring stations San Cristóbal (90W, 1S), Ascension (14W, 8S) and Natal (35W, 6S). Contrasts between these stations are used to explain difficulties that were encountered with satellite retrievals of ozone over the NH equatorial Atlantic [*Thompson et al.*, 2000, 2002b]. The observations in Paramaribo also give a good frame of reference for the rest of this thesis, as it helps to sketch the ozone distribution in the equatorial Atlantic in more detail, and introduces transport patterns and photo-chemistry relevant to the region.

The interaction of large-scale transport and photo-chemistry justifies the use of a chemical-transport model. However, as stated previously, these have not been validated properly for the tropics. The next important step in this work is therefore to evaluate our current skills in modeling the tropical ozone distribution. In Chapter 3,

a 15-year simulation performed with the TM3 model is analyzed, that includes daily varying meteorology for this period, as well as monthly variations and trends in both stratospheric ozone content and surface emissions of ozone precursors over the whole period. Its results are compared to the few ozone monitoring stations operating in the tropics, focusing on seasonal and interannual time-scales. Related to the second research question, special attention will be given to ozone variability induced by the El Niño-Southern Oscillation (ENSO), as the model will be used to describe the pattern, vertical structure, and most important processes affecting ozone that change during alternate phases of ENSO.

Both interannual variability in transport, and observed discrepancies between model and measurements will be examined in more detail in Chapter 4, but now with the use of 14-years of satellite observed TTOC. An objective measure of error to quantify the differences between model and observations will be introduced, and applied to the monthly mean zonal wave one structure of TTOC. The results indicate several possible causes for the discrepancies, which are investigated through a large number of sensitivity experiments. These are used to suggest improvements to the model, and prioritize direction for future research and model development. The local budget of ozone will be analyzed to investigate strong feedbacks in ozone photo-chemistry, and the remarkable stability of ozone in the tropics (research question 3).

Chapter 5 continues research on the stability of photo-chemistry and the historic constancy of oxidant levels, but now focused on OH. This is coupled to the tropical ozone distribution through reaction cycles 1.1. The role of ozone in maintaining both the local and global oxidizing power of the atmosphere is examined. This is done using the novel concept of recycling probability, which describes the importance of ozone (through reaction 1.1) in the production of OH relative to other processes. This recycling probability is also used as a stability parameter to diagnose the sensitivity of OH-chemistry to perturbations such as induced by changes in CO, CH_4, or NO_x abundances. By comparing the model simulated pre-industrial atmosphere to the present, changes in OH-stability and OH-distribution over the past century are discussed, with a special focus on the role of (increased) ozone concentrations.

The main conclusions will be summarized in Chapter 6, in which also recommendations will be given for future research.

Finally, I also would like to note that the order in which the chapters were placed in this thesis does not represent the chronological order of the research. In reality, Chapter 3 was the first exploration of ozone in the tropics, at which time ozone sondes from the SHADOZ networks were available only sparsely, and station Paramaribo was in operation for only a few months. The comparison with sonde climatologies led to Chapter 4 in which a larger dataset was used to take a more quantitative approach, and to perform sensible sensitivity experiments. By then, the Paramaribo record had grown long enough to perform an interesting analysis, which was carried out at the University of Maryland under guidance of Dr. A.M. Thompson. Combined with our experience with the modified residual dataset, this gave rise to the analysis in Chapter 2. Chapter 5 was performed alongside the other research, as support to several papers published on methyl-chloroform measurements [*Krol et al.*, 2001, 2002; *Krol and Lelieveld*, 2002], CH_4-variability [*Dentener et al.*, 2002b, a], and OH-variability [*Lelieveld et al.*, 2002].

Chapter 2

Tropospheric ozone over a tropical Atlantic station in the northern hemisphere: Paramaribo, Surinam (6N, 55W)

[1]Submitted for publication in *Tellus B*, with P. J. F. Fortuin, H. Kelder, C. Becker, M. C. Krol, P. J. Crutzen, A. M. Thompson and J. Lelieveld as co-authors

Abstract

We present an analysis of 2.5 years of weekly ozone soundings conducted at a new monitoring station in Paramaribo, Surinam (6N,55W). This is currently one of only three ozone sounding stations in the northern hemisphere (NH) tropics, and the only one in the equatorial Atlantic region. Station Paramaribo is part of the Southern Hemisphere ADditional OZone Sounding program (SHADOZ). Due to its position close to the equator, the Inter Tropical Convergence Zone (ITCZ) passes over Paramaribo twice per year, which results in a semi-annual seasonality of many parameters including relative humidity and ozone. The dataset from Paramaribo is used to (1) evaluate ozone variability relative to precipitation, atmospheric circulation patterns and biomass burning; (2) contrast ozone at the NH equatorial Atlantic with that at nearby southern hemisphere (SH) stations Natal (6S,35W) and Ascension (8S,14W), (3) compare the seasonality of ozone with a satellite-derived ozone product: Tropical Tropospheric Ozone Columns from the Modified Residual method (MR-TTOC). We find that Paramaribo is a distinctly Atlantic station. Despite its position north of the equator, it resembles nearby SH stations during most of the year. Transport patterns in the lower and middle troposphere during February and March differ from SH stations, which leads to a seasonality of ozone with two maxima. MR-TTOC over Paramaribo does not match the observed seasonality of ozone due to the use of a SH ozone sonde climatology in the MR method. The Paramaribo ozone record is used to suggest an improvement for northern hemisphere MR-TTOC retrievals. We conclude that station Paramaribo shows unique features in the region, and clearly adds new information to the existing SHADOZ record.

2.1 Introduction

Tropospheric ozone is measured world-wide since it is important for the oxidation power of the atmosphere, as an air pollutant, and a greenhouse gas [*Thompson*, 1992; *Lelieveld and Dentener*, 2000]. Data from ozone sounding stations around the world is managed and stored by the World Meteorological Organization (WMO), and most is available through the internet (see *http://www.msc-smc.ec.gc.ca/woudc/index.html*). Although the number of ozone sounding stations is quite large (WMO archives data from more than 300 stations), their spatial coverage is poor. The northern hemisphere (NH) is much more densely covered than the southern hemisphere (SH), and fewer than 20 stations are operated in the tropics (10S-10N). Most of these stations are part of the SHADOZ program [*Thompson et al.*, 2002a], started by NASA in 1998 specifically to increase the number of tropical monitoring stations.

Although the SHADOZ project has provided more than 1500 soundings in the SH tropics since 1997, ozone measurements in the NH tropics are still limited. Ozone sounding stations are operated since 1992 in Kuala Lumpur, Malaysia (3N, 101E) [*Yonemura et al.*, 2002a] and on a bi-monthly base in Singapore (1N, 103E) [*Yonemura et al.*, 2002c] since 1996. A long-term record exists at Trivandrum, India (8N, 77E), and *Logan* [1999] reports some measurements from Panama (9N, 80W), dating back to the 1960's and 70's. This lack of data seriously complicates attempts to establish a global climatology of ozone. Therefore, trends for the NH tropics are associated with large uncertainties.

Measurements from stations Natal (6S,35W) and Ascension (8S,14W) have shown that two processes dominate the seasonal cycle of tropospheric ozone in the equatorial Atlantic region: (1) the annual migration of the ITCZ bringing alternate wet and dry seasons, and (2) photo-chemical production of ozone from biomass burning and lightning activity [*Thompson et al.*, 2002b]. The former influences the vertical redistribution of ozone through convection and subsidence, while the latter introduces vertical layers with strongly enhanced ozone volume mixing ratios (VMRs). Natal and Ascension are located several degrees south of the equator and convective overturning of the troposphere roughly dominates the first half of the year (Dec-June), while strong subsidence, biomass burning and lightning typically occur during the second half of the year (July-Nov). Extensive measurements during TRACE-A [*Jacob*, 1996; *Thompson et al.*, 1996; *Mauzerall et al.*, 1998] have established a similar picture for most of the SH Atlantic basin.

Does the NH Atlantic region show the same features? Based on the migration of the ITCZ, a different convective signal would be expected, as well as stronger transport of air from (polluted) NH source regions. Moreover, biomass burning may not have a similarly large influence, nor peak in the same months as in the SH. No systematic observations were available to test these hypotheses. The only prolonged ozone record in the NH equatorial region is that of Tropical Tropospheric Ozone Columns (TTOC) retrieved from the Total Ozone Mapping Spectrometer (TOMS) [*McPeters and Labow*, 1996] by the Modified-Residual (MR) technique [*Hudson and Thompson*, 1998; *Thompson et al.*, 2000]. These observations are consistent with sondes and *in situ* measurements on the SH [*Thompson et al.*, 2002b], but show remarkably high MR-TTOC in the NH eastern equatorial Atlantic. Moreover, the retrieval technique uses seasonal averages from SH ozone sondes to translate the observed zonal structure of MR-TTOC from one latitude to all other latitudes. Therefore, MR-TTOC for the

NH follows the same seasonality as that for the SH. The following important questions are thus associated with the ozone observations in the NH equatorial region: (1) Is there a strong contrast with stations south of the equator and if so, what causes these contrasts? (2) Do satellite observations of TTOC with the MR-method capture the seasonality of ozone over the NH tropics accurately? These questions can only be answered through independent measurements from a station in the area.

In September 1999, an ozone sounding station was established in Paramaribo, Surinam (6N, 55W). This station is currently the third measurement station in the northern hemisphere tropics with a regular (weekly) ozone sounding program, and the only one in the equatorial Atlantic region. In addition to the combined radio- and ozone sonde program, the station is equipped with a Brewer ozone spectrophotometer that continuously measures UV radiances, ozone column values, and twice daily stratospheric (Umkehr) ozone profiles. The sonde record also includes measurements of wind, humidity, and temperature.

In this work, we present and analyze the ozone measurements from Paramaribo, attempting to answer the questions stated above. Our analysis therefore focuses on the seasonality of ozone in the troposphere, as influenced by transport and photochemistry in the NH equatorial area. After describing measurement procedures at Paramaribo and the data processing in this work (Section 2.2), we will briefly describe the geographical location of Paramaribo in relation to the position of the other SHADOZ station, and to the ITCZ (Section 2.3). Using ozone and relative humidity data, Paramaribo will be contrasted with the SH stations Natal and Ascension during the unique short dry season, while it will be shown that conditions during NH summer are very comparable (Section 2.4) to those observed over the SH Atlantic. This includes the possibility of photo-chemical pollution from biomass burning. Integrated ozone columns will be used to show that satellite retrieval of MR-TTOC is not optimal for station Paramaribo (Section 2.5), and likely not for many locations in the NH tropics. The results are summarized and conclusions presented in Section 2.6.

2.2 Methods

Station Paramaribo uses Väisala RS80-15 radio sondes with an electrochemical concentration cell (ECC) sensor for ozone measurements, and a HumiCap humidity sensor [*Komhyr*, 1986] for moisture measurements. Location and wind speed are obtained from GPS navigation on the balloons. The ECC sensor is based on a reduction-oxidation reaction of ambient, ozone containing air with a 1.5% buffered potassium-iodide (KI) solution at a platinum anode. Simultaneous measurements with a Brewer spectrophotometer at the station show that the accuracy of sonde integrated total ozone is 2-5%. To date, no extensive validation or inter-comparison with nearby stations was performed. However, operating procedures and instrument preparation is the same as in other tropical stations in the SHADOZ project, for which estimated precision of total ozone is 5% [*Thompson et al.*, 2002a], and tropospheric accuracy 2-3% [*Johnson et al.*, 2002].

Data preparation

In this work, data from the period September 1999 to March 2002 is used. Ozone sonde quality is based on criteria set by WMO [*WMO*, 1995], and is calculated from a comparison of the integrated measured ozone profile to an independent measure for the total ozone column. At Paramaribo, this independent ozone column measurement is provided by direct sun observations from the station's Brewer spectrophotometer. An ozone profile obtained from a successful Brewer umkehr observation, or from the ozone climatology of *Fortuin and Kelder* [1998] is appended to the measured profile above the burst level to obtain a complete ozone profile, that is subsequently integrated and compared to the independent value. The resulting correction factor is typically close to 1.0 for ECC sondes [*Logan*, 1985, 1994]. Sondes with a correction factor between 0.8 and 1.2 are accepted for the WMO database.

Station Paramaribo has an excellent track record of correction factors, as 91% (122 out of 133) of the launches meet the WMO criterion. Most of the sondes that did not meet the criterion suffered from a burst at altitudes far below the ozone maximum. This causes an underestimate of the stratospheric ozone abundance above the burst height, which is used to determine the correction factor. Since the tropospheric data from these profiles was often not affected, 9 of these 11 sondes were included in our analysis after visual inspection, yielding a total of 131 sondes for the analysis. Launching of ozone sondes normally occurs at 13:00 GMT (08:00 LT), with a few early or late exceptions.

To facilitate the analysis, each profile was averaged to vertical bins of 0.25km. Standard deviations of ozone within these bins were within 10% of the mean for 92.5% of the points, indicating that the averages accurately represent their altitude bin. Near the tropopause, this criterion was not always met since the ozone gradients there can be large, even on a 0.25 km scale. Additionally, seasonal averages were constructed through averaging multiple gridded profiles within a calendar month. *Logan* [1999] derived that in the tropics, a minimum of 20 sondes is required to obtain a standard error (defined as $\sigma/\sqrt{N}$, with N the number of observations and σ the sample variance) within 7.5% of the mean, with a 95% confidence interval. In our analysis, the number of soundings per month ranged from 8-18, and the calculated standard errors are only within 15% of the mean in our analysis (with a 95% confidence interval). This shows that the seasonal cycles presented here are significantly influenced by interannual, and inter-monthly variations, and should not be interpreted as long-term averages.

The calculation of the tropopause is based on the temperature lapse rate, using a definition similar to *Craig* [1965]. We defined the tropopause as the level between 9 and 19 km altitude where the temperature lapse rate first exceeds 2K/km, and the ozone mixing ratio does not exceed 150 ppbv. Due to the sharp temperature change near the tropical tropopause, this criterion was easily checked visually, and no data was rejected though this procedure. We also calculated the chemical tropopause, defined as the level where the ozone mixing ratio equals 100 ppbv. On average, the thermal tropopause was 0.71 km higher than the chemical tropopause, and the difference maximized during the dry season (August-November), when enhanced ozone mixing ratios in the upper troposphere lower the 100 ppbv level. For a further analysis of tropopause heights, structure, and variability we refer to *Fortuin et al.* [2002].

Air mass origin

To discern the most probable origin of the air masses sampled over Paramaribo, trajectories were calculated for each time a balloon was launched. The trajectories were initialized at pressure levels 900, 800, 700, 600, 500, 400, 300, 200, 150, and 100 hPa, and calculated backwards for five days using a trajectory model based on ECMWF analyzed wind data. Brief quality assessments of ECMWF based trajectories can be found in *Pickering et al.* [1996]; *Fuelberg et al.* [1996] and *Stohl and Koffi* [1998].

We recognize the limited applicability of single trajectories in the tropics, due to the strong vertical motions and the role of diabatic processes, especially in the wet season. Moreover, five day backward trajectories from Paramaribo usually originate from the Atlantic Ocean, which complicates attribution of specific ozone features to its sources and sinks. Therefore, we applied some additional modeling techniques, focusing on the possible role of biomass burning emissions on the measured profiles.

In Section 2.4, we use plumes of a modeled tracer to illustrate transport patterns during the long dry season. These plumes were calculated using a global three-dimensional transport model, described in *Krol et al.* [2001]. This model calculates transport of an idealized tracer by advection and convection using the same meteorological information from the ECMWF data that was used to calculate the trajectories. The transport model employs a coarse geographical resolution of $9^\circ \times 6^\circ$ (lon$\times$lat) in the extra-tropics, a finer $3^\circ \times 2^\circ$ resolution in the tropics, and finest $1^\circ \times 1^\circ$ resolution over the northern part of South America. The idealized tracer is released throughout the boundary layer at the time and location where large fires were observed with the ATSR instrument [*Arino and Melinotte*, 1995]. This approach was chosen as a simple, qualitative alternative to trajectory calculations. Quantitative modeling of the Paramaribo profiles should be performed using a CTM with full chemistry, including a more detailed description of sources and sinks (see Chapter 4).

2.3 Regional perspective

The most prominent feature determining the seasons in Surinam is the ITCZ. Studies of the ITCZ migration in the vicinity of Surinam have been carried out on the basis of the GATE experiment *Frank* [1983], circulation and climate studies of South America [*Hastenrath*, 1966, 1977, 1997, 2000] and our current measurement program [*Fortuin et al.*, 2002].

A first distinction that can be made, based on the position of the ITCZ, is between the wet and dry season. The dry season (August-November) corresponds roughly to the period when the ITCZ is located over the northern equatorial Atlantic [*Hastenrath*, 1997], north of Paramaribo. The wet season (Dec-July) corresponds to the period when the ITCZ travels from this position southward and back, bringing it over Paramaribo twice. Convection and rain are abundant during the wet season, which can be viewed as a period with monsoon-like flow, by way of northeasterly inflow of air with the trade winds and southwesterly return flow at higher altitudes ($\sim$ 9-12km), which constitutes the northerly upper branch of the Hadley circulation.

During a short period in February and March, the ITCZ is at its southernmost position, and convection and precipitation over Paramaribo are suppressed by subsidence on the equatorward flank of the North Atlantic high [*Hastenrath*, 2000]. This period

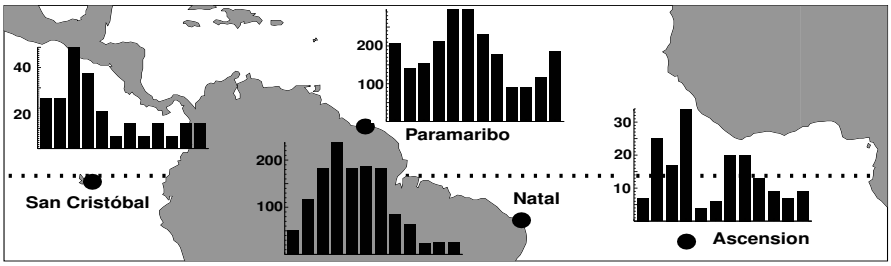

Figure 2.1: Location and seasonality (Jan-Dec) of rainfall (mm/month) in Paramaribo (6N, 55W), Natal (6S, 35W), Ascension (8S, 14W) and San Cristóbal (1S, 90W). Multiple year climate data provided by *http://www.weatheronline.co.uk* . Note that the y-axis has different values in each graph.

is called the short dry season, during which the station is part of the meteorological northern hemisphere. The short dry season divides the wet season in two parts, one in which the ITCZ approaches from the north (Dec-Jan) and one in which the ITCZ approaches from the south (April-July). This latter period lasts longer, and has more intense convection than the former because low level convergence and moisture advection are stronger toward NH spring, when the North Atlantic high intensifies [*Snow*, 1976] and the northeasterly trade winds are stronger to compensate the strong downward motions.

Figure 2.1 shows the location of stations Paramaribo, Natal, Ascension, and San Cristobal, as well as the seasonality of rainfall at each station. Clearly, the two continental stations Natal and Paramaribo receive much more rainfall than the two maritime stations Ascension and San Cristobal. As expected, the stations on the SH experience their maximum in rainfall earlier (March-April) than Paramaribo (May-June). Moreover, Paramaribo shows a clear double seasonality of rainfall, with maxima in Dec-Jan and May-June, whereas Natal shows a single, prolonged peak of rainfall from March-July. The other two stations receive little rainfall so that the seasonality is difficult to relate to the passage of the ITCZ.

The influence of the migrating ITCZ on the ozone concentration can clearly be distinguished for all stations (Figure 2.2). The most prominent feature is the low ozone concentrations during the local wet season, which appear to penetrate to over 12 km altitude. In Paramaribo, this starts in April with a relatively localized minimum between 9-12 km owing to outflow from the approaching ITCZ, while the ITCZ is positioned directly over the station in late May and June and mixes low ozone VMRs throughout the altitudes between 3-12 km. This relative ozone minimum agrees with the model calculations by *Lelieveld and Crutzen* [1994], who predicted that convective overturning reduces the ozone lifetime in the troposphere. A similar situation as in April occurs in late June, when outflow from deep convection that occurs elsewhere reaches Paramaribo at 9-12 km altitude.

Consistent with the rainfall patterns, ozone at Natal, Ascension and San Cristobal show signs of convective overturning throughout the first half of the year. The latter half of the year is characterized by enhanced ozone VMRs in the free troposphere as

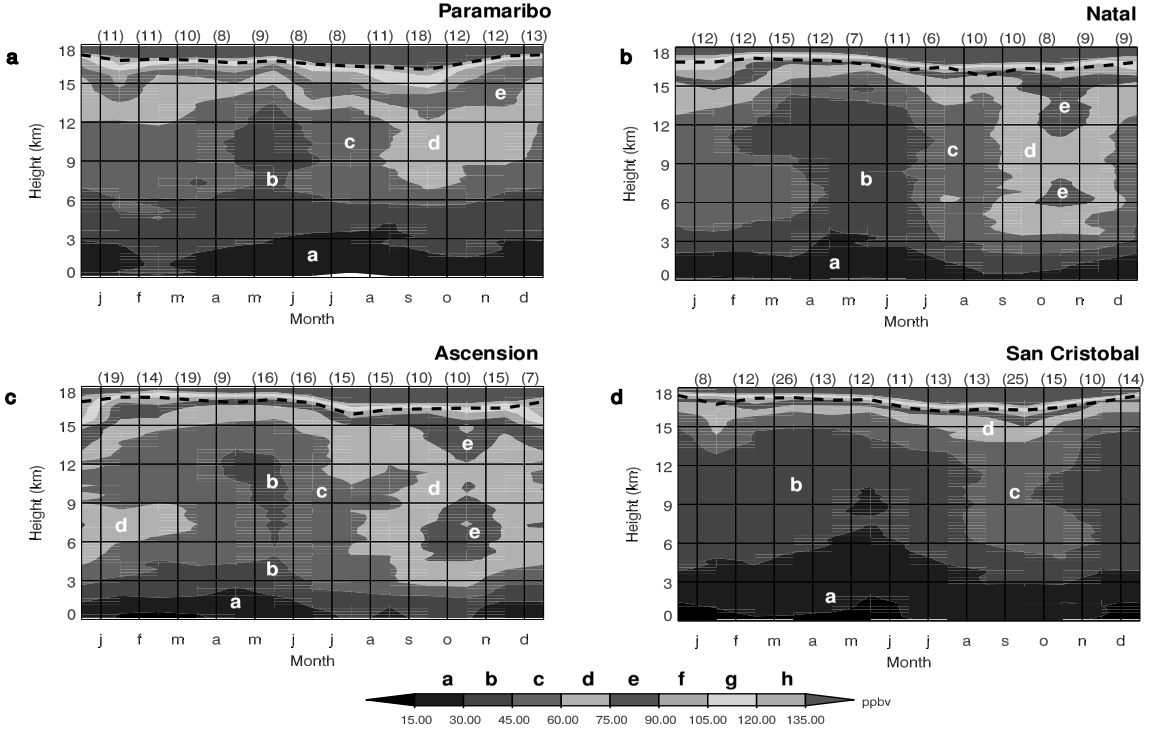

Figure 2.2: Seasonality of ozone (ppbv) as measured from the radiosondes at (a) Paramaribo (6N, 55W), (b) Natal (6S, 35W), (c) Ascension (8S, 14W), and (d) San Cristóbal (1S, 90W). Numbers in parenthesis denote the number of sondes used to construct a monthly average. The tropopause height is included as a dashed line.

described in Section 2.1. Paramaribo shows the same increase, suggesting that similar processes (subsidence, biomass burning, lightning NO_x) influence ozone here. As hypothesized, the influence is smaller than at the SH stations, as absolute values of ozone are generally highest at Ascension, lowest at San Cristobal, and higher at Natal than at Paramaribo. For instance, peak values of ozone at Paramaribo never exceed 100 ppbv (averaged over 0.25km bins) below 8 km, and rarely below 13 km altitude, whereas this occurs frequently at both Natal and Ascension [*Logan and Kirchhoff*, 1986; *Thompson et al.*, 2002a].

From a first glance at the seasonality of ozone at a NH Atlantic station, we can thus confirm that convective overturning in the ITCZ indeed introduces contrasts between NH and SH stations during the first half of the year, and that the processes that enhance ozone on the SH during the latter half of the year appear to affect Paramaribo as well. However, we cannot distinguish a 'strong contrast' (Section 2.1) with the SH stations, as the patterns in Figure 2.2 resemble each other quite closely. To see which processes cause the observed differences and similarities, we will analyze the sonde record in more detail for each season separately.

2.4 Wet and dry seasons

Figure 2.3a,b,c show the average vertical profiles of RH and ozone typical of wet season (N=22), short dry season (N=17), and long dry season (N=27) conditions. These profiles were constructed from selected sondes during these seasons, and illustrate the typical profile found over Paramaribo during the respective periods. Note that the typical profiles comprise $\sim$50% of the complete ozone dataset. The true seasonal average, based on all the profiles within a calendar month, is included in the figure as asterisks to show the result of our selection. By selecting specific profiles, we are better able to illustrate typical differences between the seasons, while excluding the effects of early and late onset of the seasons from year-to-year, as well as that of obviously anomalous profiles in the (short) record.

Looking at the RH profiles, convective moisture transport to the upper troposphere can be recognized during the wet season by values of RH exceeding 40% even at 10 km altitude. Subsidence during the short dry season dries the free troposphere rapidly above 3 km altitude, an effect that can also be seen during the long dry season although less strongly. While the latter was reported for much of the SH Atlantic region [*Krishnamurti et al.*, 1993], the former period of intense subsidence is unique to the NH Atlantic region and thus station Paramaribo at this time of year.

Although the ozone mixing ratios clearly minimize ($<$ 40 ppbv below 12 km) during the wet season, the mixing ratios are still high compared to measurements from Pacific stations during convective conditions. For instance, Pacific SHADOZ stations San Cristóbal (see Figure 2.2d) and Fiji often record tropospheric ozone mixing ratios below 20 ppbv during the wet seasons, and integrated ozone rarely exceeds 20 DU [*Thompson et al.*, 2002a]. The VMRs found over Paramaribo are comparable to those at Natal (Figure 2.2b and [*Thompson et al.*, 2002a]) during the wet season. This could be expected, because both are coastal stations and influenced by easterly surface winds bringing marine air from the Atlantic. Since this region shows higher ozone VMRs than found over the Pacific all year round [*Fishman et al.*, 1990; *Thompson et al.*, 2002a], background values of ozone are higher in Paramaribo and Natal

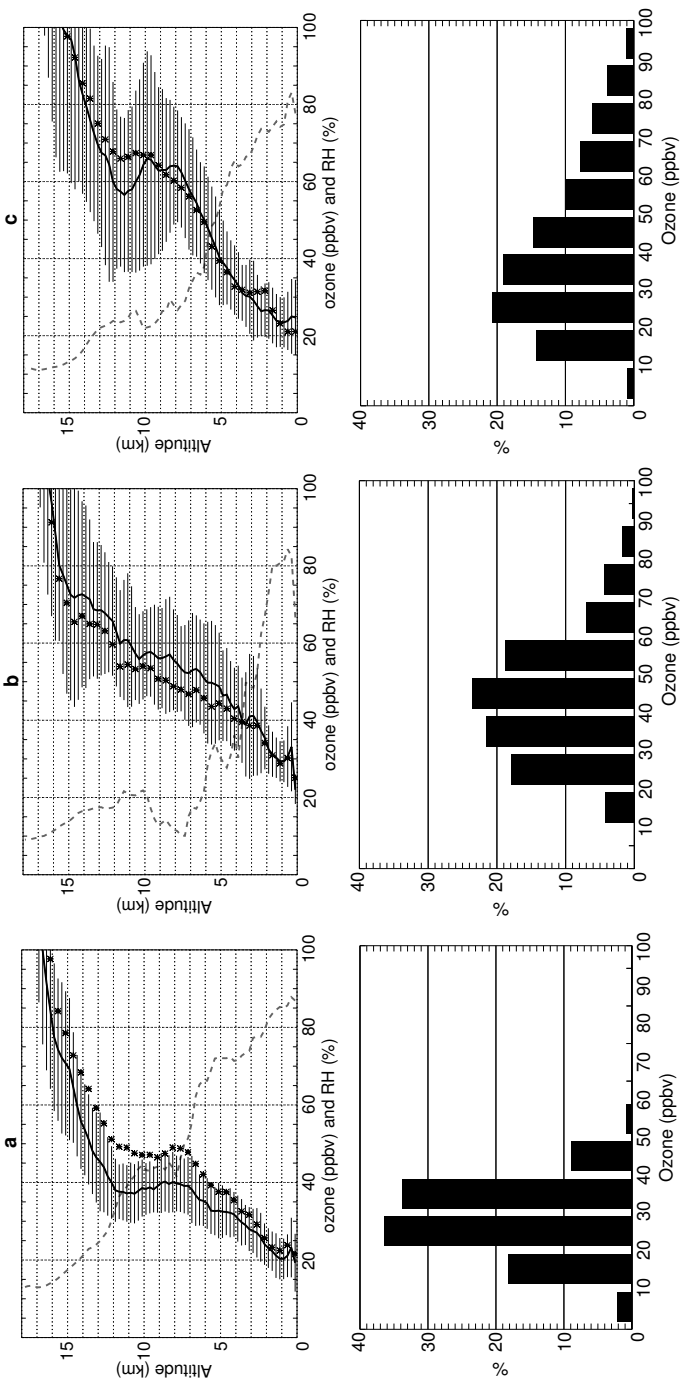

Figure 2.3: (top) Vertical profiles of ozone (solid) and relative humidity (dashed) for a selection of sondes from (a) the wet season (N=22), (b) the short dry season (N=17), and (c) the long dry season (N=27). One-sigma standard deviation of the averages per altitude are denoted by the horizontal bars, asterisks denote the true monthly averages without selection. (bottom) Histograms of the ozone VMR distribution in the typical profiles each season. Histograms are based on 0.25km averaged values for the lower 12km of the troposphere.

than over typical Pacific stations, even during wet season convective conditions.

VMRs during the short dry season are clearly much higher than during the wet season, but somewhat lower than during the long dry season, especially between 6-12 km altitude. There, the long dry season shows a broad ozone maximum with average values exceeding 65 $\pm$ 25 ppbv, which is introduced through the averaging of many more spatially confined peaks at different altitudes in different profiles. This also explains the large standard deviation of the average profile during the long dry season (Figure 2.3). Average values during the short dry season are just below 60 ppbv, and show a gradual increase up to the tropopause.

Based on the selected typical profiles used in Figure 2.3, histograms were constructed to show the distribution of VMRs in each season. In this analysis, 0.25km averages of the lower 12 km of the troposphere were used. The VMR distribution during the wet season shows >60% of the values between 20-40 ppbv, while mixing ratios >60 ppbv are not encountered below 12 km altitude during the wet season. Interestingly, the 20-40 ppbv range is also dominant in the profiles representing the long dry season, alongside many values exceeding 60 ppbv. This illustrates the fact that peak ozone values (80-100 ppbv) are found in vertically confined layers, which are superimposed on background values of 20-50 ppbv. In contrast, the background values during the short dry season are 40-60 ppbv, while peak mixing ratios are in the 60-80 ppbv range. Thus, the short dry season is characterized by elevated background ozone and increased VMRs throughout the column, while the long dry season is characterized by peak values of ozone superimposed on a less strongly enhanced background profile. This difference between the two dry seasons can be attributed to the underlying processes that cause the enhancements.

The short dry season

Two processes are responsible for the elevated background ozone values during the short dry season, both of which do not occur at stations south of the ITCZ, nor in the other seasons in Paramaribo. (1) air advected from the NH equatorial Atlantic has higher ozone VMRs during the short dry season than during the other seasons, and (2) strong subsidence of air originating from the upper troposphere brings ozone rich air to the middle troposphere over Surinam.

(1) The first feature is evident from trajectory origins and integrated ozone columns from the surface to 4 km. During the short dry season, trajectory origins at the levels 900-800-700-600 hPa levels (N=76) point to the northern Atlantic region around the Cape Verde islands (16N, 24W). This region was the focus of the 1983 GATE experiment [*Frank*, 1983], and has been traversed by ships, i.e. the R/V Polarstern in 1993 [*Weller et al.*, 1996] and the R/V Ronald H. Brown in March 1999 [*Thompson et al.*, 2000]. Based on ozone measurements from the ships, the area between 14N-30N was characterized as a region influenced by NH mid-latitude air of mixed stratosphere-troposphere origins, while the area between the equator and 14N was more tropical in nature and contained many peaks of ozone (> 60 ppbv) in the lower 5km (Figure 1, in *Thompson et al.* [2000]).

For trajectories to Paramaribo that originated from this region (68 out of 76), the integrated column ozone abundances in the lower 4 km over Paramaribo are 10.4 $\pm$ 2.1 DU. If we take all trajectories traversing that same region during other seasons (when this region is separated from the NH mid-latitudes by the ITCZ), the

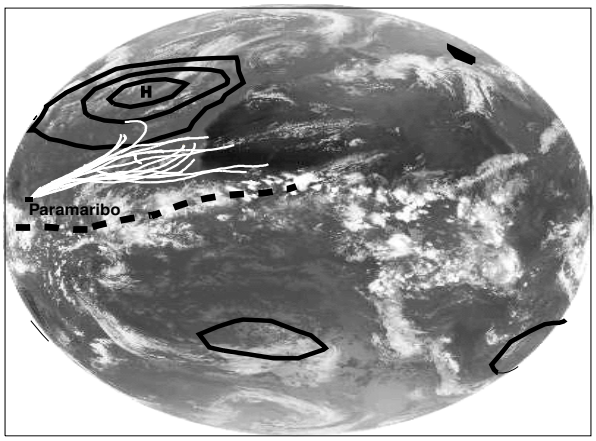

Figure 2.4: Composite illustrating the position of the ITCZ over the Atlantic Ocean and the starting point of 5-day backward trajectories. The satellite picture is a water vapor image from METEOSAT for March 31th 2001, while the trajectories (N=17) are from different days, and all end in the boundary layer over Paramaribo. The composite illustrates how the southern position of the ITCZ allows distinctly northern hemispheric air to reach the lower troposphere in Paramaribo during the short dry season.

integrated column ozone amounts to only 7.9 $\pm$ 1.7 DU. In total, 13 out of 17 sondes during the short dry season have ozone column abundances in the lower 4 km that exceed the average non-short dry season column abundance by more than one-sigma. This supports the view that elevated ozone VMRs from the NH are transported to Surinam in the trade winds from the north Atlantic region. The air mass origins in the meteorological NH are illustrated in Figure 2.4.

(2) In the middle troposphere, i.e. the region between 4-7 km, air mass origins differ strongly from those in the lower troposphere. This difference in origin is reflected in different ozone VMRs between the two different air masses, but also in a sharp decrease in relative humidity at 4 km altitude (see Figure 2.3b). Trajectories indicate that dry, ozone rich air originates from the upper troposphere over South America, and even from as far as the Pacific Ocean. It is transported to the middle troposphere over Surinam through subsidence in an area around Puerto Rico and the Lesser Antilles. This subsidence is a consequence of upper tropospheric convergence, induced by divergent outflow from convection near the equator, where sea surface temperatures are enhanced during this time of year [*Hastenrath and Lamb*, 1977].

Figure 2.5 shows an example of 13 of such trajectories associated with different launch dates, superimposed on a GOES-8 water vapor satellite image. The dark regions in the satellite picture denote areas where water vapor abundance is low due to downward motions. This large-scale feature is present throughout most of the short dry season. These trajectories undergo rapid downward motion north of Surinam. Similar motions and trajectories are found in other seasons, although they are less frequent, and the downward motions are weaker.

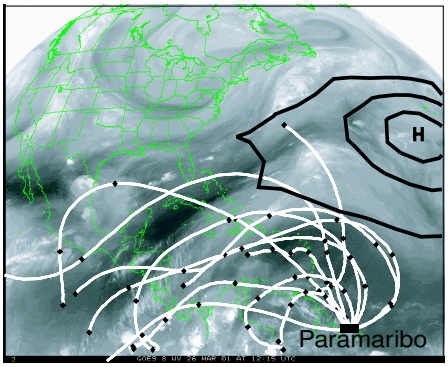

Figure 2.5: Composite illustrating the position of a strong area of subsidence over the Atlantic Ocean, as well as 5-day back trajectories that traverse this region. The satellite image is a water vapor image from GOES-west for March 25th, while the back trajectories are for several different days in March. All trajectories end in Paramaribo between 200-500 hPa, on a descending path. The composite illustrates how upper tropospheric air that is rich in ozone but low in water vapor reaches the middle troposphere over Paramaribo during the short dry season.

The long dry season

The most obvious reason for the similarity between Paramaribo, Natal and Ascension during the latter half of the year is the fact that all three stations are then part of the southern meteorological hemisphere, and not separated from each other by the ITCZ, which lies well north of Paramaribo. Thus, the same processes (biomass burning, lightning, subsidence) that cause ozone to increase over much of the SH Atlantic basin [*Fishman et al.*, 1990], as well as Ascension [*Thompson et al.*, 2002a] and Natal on the Brazilian coast [*Logan and Kirchhoff*, 1986], are likely to affect Paramaribo as well. The influence of subsidence during this period was already seen in Figure 2.3, the influences of biomass burning and lightning depend strongly on transport patterns in the area.

Figure 2.6 illustrates how African biomass burning products can reach the free troposphere over station Paramaribo. It shows the 10-day averaged wind field at 500 hPa, for the period July 31st-August 9th, 2000. Black dots over Africa indicate the location of intense fires during this period, as observed by both ATSR nighttime detection of fires [*Arino and Melinotte*, 1995], as well as by observations of burning scars [*Pinty et al.*, 2000] (see insert of Africa). From these locations, a tracer was released into a transport model as described in Section 2.2. The resulting modeled plume shows that biomass burning products are brought into the middle troposphere in a convective system off the coast of Nigeria, and subsequently transported (in 10 days) to Paramaribo by easterly winds over the Atlantic Ocean. Integrating the measured profile of tropospheric ozone at August 9th (not shown here) yields 42 DU of ozone, mostly due to VMRs of 70-100 ppbv between 5 and 10 km. Such enhancements require an average net ozone production ratio of $\sim$3-5 ppbv/day during the 10-day transport from the biomass burning source. This is within the range of estimates

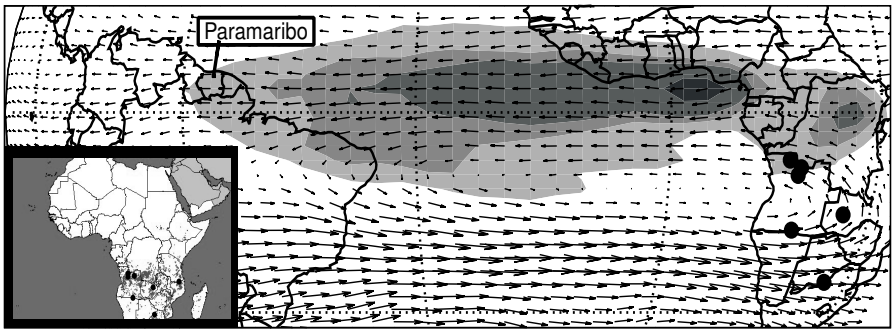

Figure 2.6: Composite illustrating transport of a plume of biomass burning products from Africa. Arrows denote the 10-day average wind fields at 500 hPa from July 31st to August 9th, 2000. Filled circles are locations of fires as observed by the ATSR instrument [*Arino and Melinotte*, 1995]. The insert of Africa shows burning scars from fires observed from METEOSAT [*Pinty et al.*, 2000]. Contours illustrate the dispersion of a modeled tracer released from the fires into the ECMWF wind fields, and transported to Paramaribo by convection and advection. Widespread ozone enhancements were observed in the Paramaribo ozone profile at August 9th.

(10-15 ppbv/day lower troposphere, 0 ppbv/day mid-troposphere) from TRACE-A [*Thompson et al.*, 1996; *Jacob*, 1996; *Mauzerall et al.*, 1998], as well as from modeling studies [*Moxim and Levy*, 2000]. In the days before August 9th, enhanced ozone was also seen over the equatorial Atlantic in the EP-TOMS TTOC observations and at station Ascension (51 DU at August 4th). These features support the possibility that aged biomass burning effluents from Africa enhanced ozone VMRs over Paramaribo on August 9th. No sondes were released from Natal in this period.

Biomass burning also occurs in South America during the dry season, possibly influencing our sonde record. Figure 2.7 shows an example of a case where this is likely to have occurred. In the days before August 30th, 2000, three day averaged wind fields at 400 hPa show transport of air around an upper tropospheric ridge (SH anti-cyclone), which advects air from the Pacific Ocean and Central Brazil to station Paramaribo. The location of fires (ATSR) over Brazil is again indicated by black dots. When we release a tracer from these fires, convection lofts it to the 400 hPa level, where ozone VMRs of $\sim$60 ppbv were sampled between 7-12 km at August 30th. The pattern of the tracer shows the advection to our site. As would be expected from the simulation, the measured profile at Natal is not affected (although sampled at August 31st), with only 17 DU of tropospheric ozone.

The situation in Figure 2.6 occurs most frequently during the long dry season, as the flow pattern shown closely resembles the monthly averaged winds. Therefore, the amount, frequency, and timing of ozone pollution events at Paramaribo depend mostly on the occurrence and intensity of fires over Africa, lofting of the plumes to the free troposphere by convection, and subsequent transport in the tropical easterlies. In contrast, the situation in Figure 2.7 is much less frequent, and is associated with anomalous southeasterly winds in the free troposphere. Note that the direction of

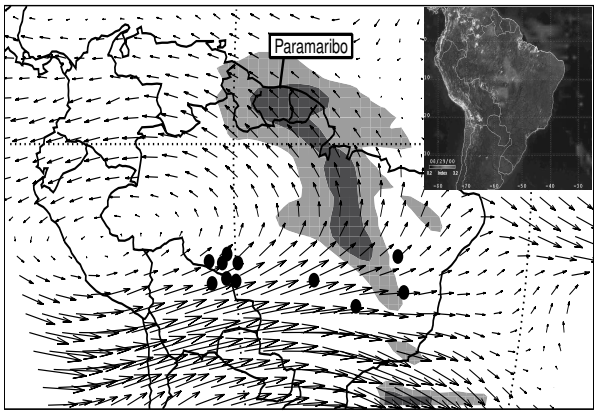

Figure 2.7: Composite illustrating transport of a plume of biomass burning products from South America. Arrows denote the 3-day average wind fields at 400 hPa from August 28th to August 30th. Filled circles are locations of fires as observed by the ATSR instrument [*Arino and Melinotte*, 1995]. The insert of South America shows enhanced aerosol index from biomass burning observed by the TOMS instrument (see *http://toms.gsfc.nasa.gov/aerosols*). Contours illustrate the dispersion of a modeled tracer released from the fire locations into the ECMWF wind fields, and transported to Paramaribo by advection and convection. Enhanced ozone VMRs were observed at 400 hPa in the Paramaribo ozone profile on August 30th.

transport (from Africa, westward to South America) is opposite to that of the 'global plume' [*Chatfield et al.*, 2002], which pollutes the Southern Hemisphere (sub)tropics through easterly transport of biomass burning emissions.

As a final check on the similarity between Paramaribo and the SHADOZ stations on the SH during the long dry season, we have placed the September-October-November (SON) data from station Paramaribo into the zonal wave structure deduced in *Thompson et al.* [2002b] (see Figure 1.5 on page 14 of this thesis). This zonal wave structure in tropospheric ozone shows a gradient in VMRs with highest values over the Central Atlantic (Ascension, 14W), decreasing westwards toward Natal (35W) and San Cristóbal (90W). A sharp decrease of VMRs can be seen between the latter two stations, separating the Atlantic region from the Pacific. Paramaribo (55W) is located exactly in this region with the strongest gradient between these stations. If we would include the SON average profiles from Paramaribo in the zonal wave one structure, the area of relatively high ozone VMRs would extend further westward. The separation between Atlantic and Pacific in the upper troposphere would be defined even more sharply, and placed longitudinally between 55W and 90W, i.e., over the western South American continent.

In conclusion, station Paramaribo generally falls within the relatively ozone-rich Atlantic region where the maxima in the zonal wave one pattern occur. Owing to its more remote location relative to the South Atlantic ozone maximum, and the fact that the lower troposphere is always influenced by maritime air masses, ozone VMRs are

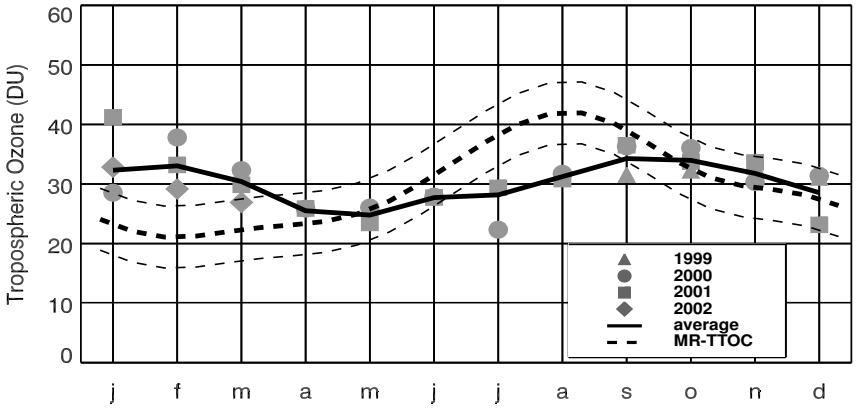

Figure 2.8: Seasonality of TTOC as observed in the 1979-1992 NIMBUS-7 TOMS data [*Hudson and Thompson*, 1998] (dashed line), and based on Paramaribo sondes (1999-2002) (solid line).

lower than at Natal, and fresh ($<$ 2 days old) biomass burning pollution is rarely encountered. The fact that the station's position relative to the ITCZ is different from the SHADOZ stations in the southern hemisphere introduces minor differences during the latter half of the year, but large differences during February-March when Paramaribo is north of the ITCZ.

2.5 Column integrated ozone

In Figure 2.8, the seasonality of TTOC as deduced from the 1999-2002 Paramaribo ozone record is shown. Although the monthly averages in different years show considerable interannual variability, a pattern with two maxima during each of the dry seasons is visible in the figure. Typical long wet season TTOC is 20-30 DU, again comparable to that at Natal. During the short wet season, convection penetrates only up to $\sim$7 km and TTOC can be as high as 30 DU. Especially in January 2001, ozone values were anomalously high when, for a short period, dry season conditions occurred very early in the year.

In the same figure, the seasonality of MR-TTOC as calculated from the 1979–1992 NIMBUS–7 TOMS record is shown (dashed line). MR-TTOC underestimates Paramaribo TTOC by 5-10 DU in February and March when the short dry season occurs, while it overestimates Paramaribo TTOC by up to 10 DU from June-September. Moreover, the seasonality of MR-TTOC displays one minimum during the first half of the year, and one maximum during the second half of the year, where the Paramaribo sonde record has two TTOC maxima. To understand the cause of this discrepancy, the procedures and assumptions in the MR-TTOC method need to be reviewed in some more detail.

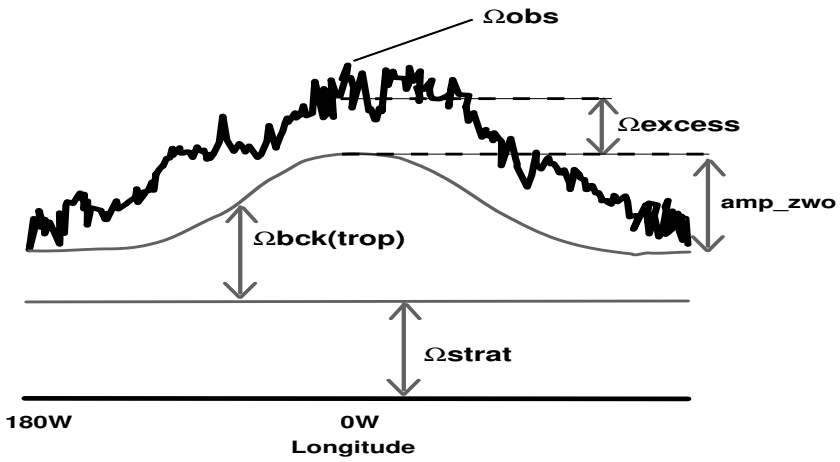

Figure 2.9: Illustration of the MR-method showing different components in the TOMS total ozone signal.

Modified Residual Method

The Modified Residual method, originally developed by *Hudson and Thompson* [1998] from methods already used in *Kim et al.* [1996], is based on the fact that TOMS total ozone columns [*McPeters and Labow*, 1996] can be separated into a stratospheric and a tropospheric ozone column. The separation between troposphere and stratosphere can only be made using added information in the form of assumptions, and/or external data. For instance, *Ziemke et al.* [1998] have used ozone observations from the Microwave Limb Sounder (MLS) and Halogen Occultation Experiment (HALOE) to obtain the stratospheric column amount at certain locations. In the MR-method, external data is added to the algorithm in the form of ozone sondes from Natal (6S, 35W), Ascension (8S, 14W), and Brazzaville (4S, 15E). Figure 2.9 illustrates some of the key points in the MR-retrieval. Here, we will explain the procedure as applied to one latitude, generalization to all tropical latitudes involves some additional steps described in the original work of *Hudson and Thompson* [1998].

The NIMBUS-7 TOMS (version 7, level 2) total ozone columns (Ω_{obs}) at one latitude are assumed to consist of three components: (1) a stratospheric column (Ω_{strat}), (2) a tropospheric background column (Ω_{bck}(trop)) which varies with longitude with a certain amplitude (amp_zwo), and (3) an amount of excess ozone (Ω_{excess}) ascribed to tropospheric pollution. The amount of ozone in the troposphere is given by:

$$\begin{aligned} \Omega_{trop} &= \Omega_{bck}^{trop} + \Omega_{excess} \\ \Omega_{trop} &= \Omega_{obs} - \Omega_{strat} \end{aligned} \tag{2.1}$$

The first important assumption in the MR-method is that the stratospheric ozone column is constant with longitude, e.g. any zonal variation in total ozone is in the troposphere. This is illustrated by the flat line in Figure 2.9. This assumption implies that if we know Ω_{trop} at a single location, we can determine Ω_{strat}, and subsequently calculate Ω_{trop} at each longitude (from equation 2.1). It would be ideal to have a measurement of Ω_{trop} somewhere along each tropical latitude and simply solve

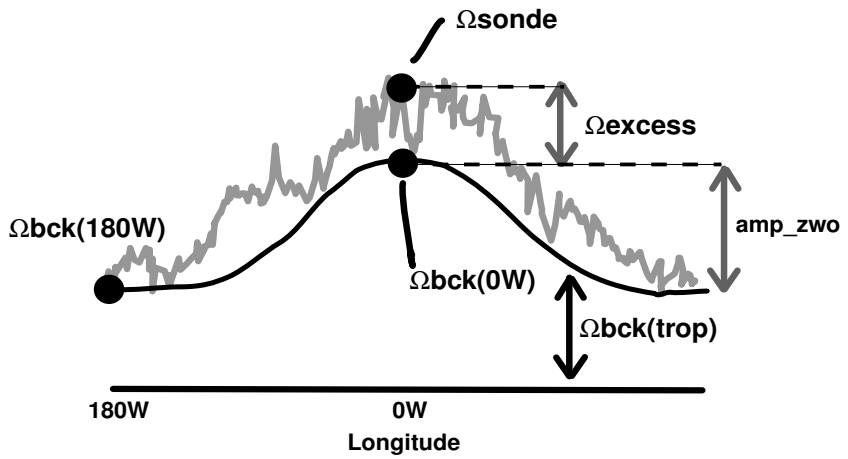

Figure 2.10: Same as Figure 2.9, now with Ω_{strat} subtracted. The figure illustrates how sondes at 0°W and the amplitude of the zonal wave one allow determination of Ω^{trop}_{bck}(180W).

equation 2.1. However, in practice the coverage of ozone sondes is too sparse to allow such a straightforward retrieval.

Therefore, a second assumption is introduced: at the dateline, the troposphere has a single *latitude independent* background (e.g. pollution free) value Ω^{trop}_{bck}(180W). With this assumption, Ω^{trop}_{bck}(180W) has become vital in the MR-method, since determining this value would allow us to calculate Ω_{strat} and Ω_{trop} everywhere. Whereas [*Kim et al.*, 1996] assumed this Ω_{bck}(180W) to be constant in time and taken from climatology (26 DU, [*Komhyr et al.*, 1989]), the Modified Residual technique uses ozone sondes to determine Ω^{trop}_{bck}(180W), and allows it to vary with season.

Unfortunately, there is no regular ozone sounding program at the dateline to determine Ω_{bck}(180W) directly. Instead, this value is derived from the TOMS observations combined with ozone sondes from Natal, Brazzaville, and Ascension. The sondes are averaged and assumed to represent the value of Ω_{trop} at longitude 0W, which corresponds to the wave maximum (see Figure 2.10). The amount of ozone measured by the sondes is then separated into two parts; a tropospheric background amount Ω^{trop}_{bck}(0W), and excess ozone (Ω_{excess}(0W)):

$$\Omega^{trop}_{sonde} = \Omega^{trop}_{bck}(0W) + \Omega_{excess}(0W) \tag{2.2}$$

To determine Ω_{excess}, a fast fourier transformation is applied, yielding the amplitude of the zonal wave one (as well as wave two, three,...) pattern (amp_zwo). The MR-method is only applied at latitudes where the wave-one component dominates over wave-two and higher contributions. Fitting the wave one contribution to Ω_{obs}(180W), and subtracting it from Ω_{obs} at all longitudes gives (Ω_{excess}), as illustrated in Figure 2.9.

With Ω_{sonde} and Ω_{excess}(0W) known, Equation 2.2 can be solved for Ω^{trop}_{bck}(0W). Combining this value with the amplitude of the zonal wave one pattern from fourier analysis (amp_zwo) then yields the wanted value of Ω_{bck}(180W). Note that the same

value can be found when calculating the Ω_{strat} from Ω_{sondes} and Ω_{obs}(0W), and subtracting this from Ω_{obs}(180W). However, if we know the climatological seasonality of Ω_{bck}^{trop}(0W), the method can be extended to other years by simply combining Ω_{bck}^{trop}(0W) with the observed wave amplitude (amp_zwo), without needing observations of Ω_{sonde} for each year.

With the values of Ω_{bck}^{trop} and Ω_{excess} determined, Ω_{trop} is calculated for each longitude. Since Ω_{bck}^{trop}(180W) is assumed latitudinally constant, this can subsequently be done for all other latitudes as well. The method has been used firstly to determine Ω_{trop} for 1991-1992 when ozone sondes were available from the three stations, and was later extended to the whole 1979-1993 TOMS record, using a fitted cosine function to the derived Ω_{bck}^{trop}(0W) in 1991-1992 [*Hudson and Thompson*, 1998; *Thompson and Hudson*, 1999].

Paramaribo retrieval

The questions that arises from the previous section and Figure 2.8 are: Which part of the Modified Residual method introduces the discrepancies at Paramaribo and can we do better? Using the ozone sondes from Paramaribo, we will show that the assumption of a latitudinal constant Ω_{bck}(180W) causes most of the observed differences, and can be improved.

The cosine function fitted to Ω_{bck}^{trop}(0W) and subsequently used for each month in the MR-method is given by the function [*Hudson and Thompson*, 1998]:

$$\Omega_{bck}^{trop}(0W) = 24.2 + 4.8\cos(\pi t/6 + 2.5) \tag{2.3}$$

Where t is given in months since January (0,1,...,11). This curve is plotted in Figure 2.11 (grey line). To illustrate realistically the different parameters in the MR-method, we have taken a short 'test' series of monthly mean total ozone data and applied the MR-method to them[1]. Function 2.3, together with the zonal wave one amplitude derived with an FFT-transform gives the monthly values of Ω_{bck}^{trop}(180W) (black diamonds) that would be used in the MR-method based on these data. Obviously, the Ω_{bck}^{trop}(180W) inherits the SH seasonality present in the original function in Equation 2.3. Since this same Ω_{bck}^{trop}(180W) is used to derive MR-TTOC at the latitude of Paramaribo (6N) as well, Ω_{trop} at the latitude of Paramaribo is biased toward this value. This bias is linear, in so far that under(over)estimates in the Ω_{bck}^{trop}(180W) will lead to equal over(under)estimates in Ω_{trop}. If we apply this to the differences observed in Figure 2.8, this means that the observed 5-10 DU underestimate of MR-TTOC in January-March would be caused by a 5-10 DU underestimate of Ω_{bck}^{trop}(180W) at 6N, and 5-10 DU overestimates of MR-TTOC in July-December would be caused by a similar overestimate of Ω_{bck}^{trop}(180W) at 6N during the respective months. Differences between MR-TTOC and Paramaribo sondes are illustrated by the black line in Figure 2.12.

What should Ω_{bck}^{trop}(180W) look like to ensure an optimal retrieval for Paramaribo? Using the same method as illustrated in Figure 2.10, we have derived the $\Omega_{bck}^{trop}{}'$(180W), which is based on the seasonal cycle of Paramaribo ozone sondes and the zonal wave

[1]Here, monthly mean total column ozone data for 1998-2000 from EP-TOMS were used. Efficiency correction factors were not applied in these examples. This should not affect the retrieved seasonal cycles, but will affect the yearly average values. These will not be interpreted here however.

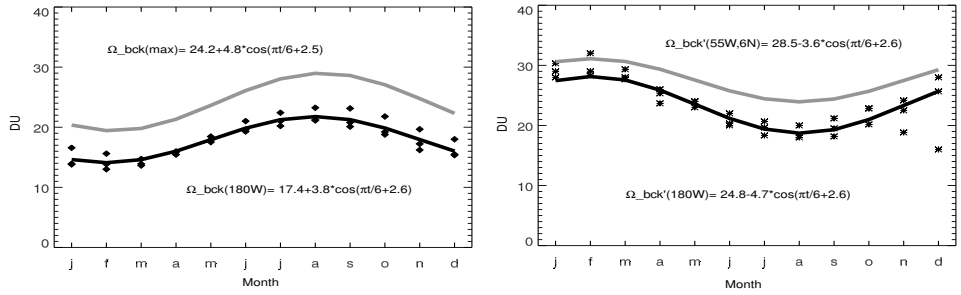

Figure 2.11: (left) Seasonal cycle of Ω_{bck}^{trop}(0W) as given in *Hudson and Thompson* [1998] (grey line) and the derived Ω_{bck}^{trop}(180W) (diamonds and black line). (right) As left, but now with the retrieval based on ozone sondes from Paramaribo to provide $\Omega_{bck}^{trop}{}'$(55W,6N) (grey line), from which $\Omega_{bck}^{trop}{}'$(180W,6N) (asterisks and black line) is calculated. The yearly averages depend critically on the total ozone values, the shape of the zonal wave one, and the instrument efficiency and should therefore not be interpreted from the analysis presented here (also see footnote on page 37).

one amplitude at latitude 6N. Figure 2.11 (right) shows the results. The grey line is a cosine fit to the $\Omega_{bck}^{trop}{}'$(55W,6N) calculated from excess ozone at Paramaribo and the sonde seasonality (see equation 2.2). The solid line is a fitted cosine curve to the derived $\Omega_{bck}^{trop}{}'$(180W) values (in asterisks). The cosine functions have the form:

$$\begin{aligned} \Omega_{bck}^{trop}(180W) &= 17.4+3.8\cos(\pi t/6+2.6) \\ \Omega_{bck}^{trop}{}'(55W,6N) &= 28.5-3.6\cos(\pi t/6+2.6) \\ \Omega_{bck}^{trop}{}'(180W) &= 24.8-4.7\cos(\pi t/6+2.6) \end{aligned} \tag{2.4}$$

Note that the yearly average difference between Paramaribo (55W) and the dateline (180W) is only 3.7 DU (28.5-24.8) in our analysis, while it is 6.3 DU in Figure 2.11. This is due to the fact that Paramaribo is located quite far westerly (e.g. closer to the wave minimum) on the curved flank of the zonal wave one in Figure 2.10, while our analysis in Section 2.3 showed that the sharp transition to more Pacific values occurs west of the station. This average difference is therefore most likely underestimated. Since the yearly averages (first terms on right hand side of equation 2.4) also depend on the total ozone column and the retrieval efficiency factor that varies with latitude, we will not interpret these in our simple analysis and focus on the seasonal variations instead.

The seasonal cycles of $\Omega_{bck}^{trop}{}'$(180W,6N) and $\Omega_{bck}^{trop}{}'$(55W,6N) are almost 6 months out of phase with that derived from the Natal, Ascension, and Brazzaville sondes. In other words: *the seasonality of Ω_{bck}^{trop}(180W) needed to optimally retrieve observed ozone values at Paramaribo is opposite to that derived from SH sondes*. The assumption of one single, latitudinal invariant Ω_{bck}^{trop}(180W) does thus not appear to be valid. Maximum differences in Ω_{bck}^{trop}(180W) solely due to the seasonality (and not due to the yearly average) are as large as 8 DU, enough to explain most of the observed discrepancy at Paramaribo as can be seen in the grey curve in Figure 2.12.

As a final check on this important conclusion, we have illustrated in Figure 2.12

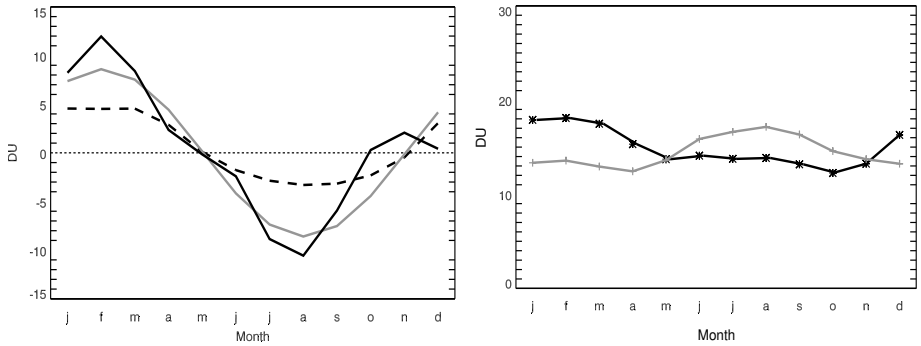

Figure 2.12: (left) The difference (sondes-satellite) between integrated ozone sondes at Paramaribo and MR-TTOC (black solid) can be minimized by using Ω_{bck}^{trop}/(180W) (Equation 2.4), reducing the discrepancy by an amount shown in the grey line. The dashed line shows the reduction in discrepancy when using the model calculated seasonalities of Ω_{bck}^{trop}(180W) from the figure to the right. (right) Seasonal cycle of tropospheric column ozone from a chemistry-transport model simulation for [180W, 6S] (grey line) and [180W,6N] (black line). The model confirms the opposite seasonality of TTOC at either side of the equator.

the seasonal cycle of tropospheric ozone columns near the dateline from a 15-year chemistry-transport model simulation [*Lelieveld and Dentener*, 2000]. The model used was shown to capture the seasonal cycle of TTOC over Samoa and Hilo well (Chapter 3), and is expected to perform well for most remote locations (Chapter 4). Once again, the contrasting seasonal cycles at 6S (grey line) and 6N (black line) appear, with maximum differences here in the order of $\sim$5DU.

The contrasting seasonalities of integrated ozone at either side of the equator around the dateline are introduced by the migration of the ITCZ. In the first months of the year, the ITCZ is in a southerly position, reducing convection at the NH side of the equator, and also allowing relative ozone rich air from more northerly latitudes to influence the region, and increase TTOC. Likewise, the ITCZ takes a more northerly position from July-October, with similar effects on the SH side of the equator. Correcting Ω_{bck}^{trop}(180W) for this effect should be relatively straightforward, and we have shown that this can be done using ozone sondes or possibly chemistry-transport models. In this respect, we should also mention that new algorithms currently under development no longer use the ozone sondes, and are not expected to show the bias explained here.

However, based on our results, it is highly likely that every location on the NH in the existing 1979-1992 MR-TTOC dataset has a bias toward SH ozone values. This bias is expected to increase with distance from the equator, where seasonal cycles become stronger. It would be interesting to better quantify this bias with more observations, but there are no other distinctly NH stations available for this. Nevertheless, our results suggest that station Paramaribo can be used to improve the seasonality of MR-TTOC over the NH, which highlights again the importance of this new station.

2.6 Conclusions and summary

The ozone measurements over Paramaribo are largely controlled by meteorological variability, which is strongly linked to the annual migration of the ITCZ. As expected, ozone and relative humidity vary on a semi-annual time scale due to the passage of the ITCZ in May and December. Although the seasonality of ozone at Paramaribo resembles that at SH stations Natal and Ascension, the existence of the short dry season (Feb-March) distinguishes it from all SH stations in the SHADOZ network.

In February and March, the station is part of the northern meteorological hemisphere, and relatively polluted air from the NH Atlantic region and even from NH mid-latitudes is transported into the lower 4 km of the atmosphere. Moreover, downward transport of ozone rich-air occurs on the equatorward side of the North Atlantic high, which contributes to high ozone VMRs in the middle troposphere during the short dry season.

In the latter half of the year, Paramaribo is typically a SH Atlantic station, and fits well in the zonal wave one structure of tropospheric ozone that displays its strongest maxima in September-October-November. Besides downward transport of dry, ozone-rich air, we have shown that transport of biomass burning products from Africa is a plausible source of ozone in the free troposphere in this latter period. In contrast, transport of biomass burning products from South American sources is less likely to occur given the prevailing winds. Some meteorological situations can nevertheless occasionally favor this transport, as we have shown in Section 2.4. Based on the Paramaribo sonde record, the division between the Atlantic and Pacific regime in tropospheric ozone (and relative humidity) can be placed west of Paramaribo (55W), and east of San Cristobal (90W), making the natural barrier of the Andes mountains the region where the strongest zonal gradients in tropospheric ozone occur.

We have shown that satellite observed tropospheric ozone columns (MR-TTOC) do not reproduce the observed seasonality at Paramaribo correctly. Underestimates occur during the first months of the year, and overestimates during the second half. Analysis suggests that this is due to an assumption on background ozone over the Pacific (180W) in the MR-method. By lack of suitable data, this background value was derived using SH ozone sondes. The Paramaribo data and chemistry-transport model results suggest that the seasonality of this background value reverses for the NH, and that data from station Paramaribo can be used to improve the MR-retrieval algorithm.

Acknowledgments.

We would like to thank the ozone station operators in Paramaribo, who have done a superb job in collecting the data presented here, maintaining the instruments, and assuring high data quality. Also, we acknowledge the support and enthusiasm received from the government of Suriname in establishing this site. Part of this analysis was performed during a visit to NASA Goddard Space Flight Center, who I thank for their hospitality. This research was conducted as part of the RADCHiS program financed by the Dutch Research Council (NWO).

Chapter 3

Identification of an El Niño-Southern Oscillation signal in a multiyear global simulation of tropospheric ozone

[1]Published in *Journal of Geophysical Research*,**106**,10,673-10,696, with F. J. Dentener, M. C. Krol and J. Lelieveld as co-authors.

Abstract

We present the first study of the El Niño-Southern Oscillation (ENSO) interannual variability in tropical tropospheric ozone in a multiyear simulation with a global three-dimensional chemistry-transport model. A 15-year period (1979-1993) was simulated using European Centre for Medium-Range Weather Forecasts meteorological reanalysis data and a time-varying emission data set. A comparison of model calculations with observations shows good agreement for surface ozone, seasonal cycles, and ozone concentrations at remote stations, but reveals an underestimate of ozone in the free troposphere, which is most pronounced during biomass burning seasons. The ENSO signal is the most important component of interannual variability in tropical tropospheric ozone columns (TTOC), being responsible for nearly 25% of the total interannual variability of ozone in the tropics. The amplitude of the modeled ENSO signal in TTOC is 3 Dobson units, in close agreement with satellite observations. This signal is evenly distributed with height, indicating that rapid vertical transport plays an important role. The ENSO signal is also detectable at the surface, for example at the Pacific island Samoa, for which model-calculated and measured ozone agree well.

3.1 Introduction

The interest in tropical tropospheric ozone has intensified in the past decade, since it provides important insights into transport processes, photochemistry, and the oxidation power of the atmosphere. Photochemistry is particularly active in the tropics due to the high insolation. Measurements of ozone are conducted at only a few stations in the tropics (*Logan 1999*, and references therein]), while most of the in situ observations have been performed during intensive campaigns [e.g., *Browell et al.*, 1990; *Diab et al.*, 1996; *Kley et al.*, 1996; *Thompson et al.*, 1996; *Fenn et al.*, 1999; *de Laat et al.*, 1999]. These data sets, however, are insufficiently comprehensive to infer trends and large-scale distributions, as they lack spatial and temporal coverage.

Total tropospheric ozone columns (TTOC) were retrieved from satellite measurements in several studies [e.g., *Fishman et al.*, 1990; *Kim et al.*, 1996; *Hudson et al.*, 1995; *Hudson and Thompson*, 1998]. These studies are based on so-called residual methods, where TTOC is calculated as the difference between total column ozone and stratospheric column ozone. The Total Ozone Mapping Spectrometer (TOMS) [*McPeters and Labow*, 1996] provides a 15-year record (1978-1993) of total ozone columns, while calculation of the stratospheric ozone contribution differs from one method to the other. *Hudson and Thompson* [1998] described the modified residual (MR) method, where stratospheric ozone is obtained from a combination of TOMS observations and ozonesondes launched near the Atlantic Ocean ozone maximum. *Ziemke et al.* [1998] used cloud observations from the TOMS instrument to estimate the stratospheric ozone content (cloud convective differential or CCD method). These two methods have been shown to be successful in reproducing TTOC values from ozonesondes [*Ziemke et al.*, 1998; *Hudson and Thompson*, 1998; *Thompson and Hudson*, 1999].

Satellite observations of TTOC have been used to describe the 'zonal wave one' distribution of ozone in the tropics [*Fishman and Larsen*, 1987; *Kim et al.*, 1996]. This zonal wave one pattern is characterized by an ozone minimum associated with strong convective upward motions over the Pacific warm pool, and an ozone maximum associated with oceanic anticyclones over the tropical Atlantic. These motions are part of large-scale zonal transport which is induced by convection, and their effect on TTOC has been described previously [*Lelieveld and Crutzen*, 1994; *Krishnamurti et al.*, 1996; *Chandra et al.*, 1998; *Wang et al.*, 2000]. *Fishman et al.* [1990] recognized that the TTOC maximum over the Atlantic Ocean is strongest in Southern Hemisphere spring (September-November), when the biomass burning intensity reaches a maximum over Africa and Brazil. Later studies from the 'TRansport and Atmospheric Chemistry near the Equator-Atlantic' (TRACE-A) campaign [*Fishman et al.*, 1996; *Thompson et al.*, 1996] indicated that production of ozone from precursors in biomass burning plumes can lead to a 10-15 Dobson unit (DU) increase of ozone over the Atlantic Ocean during austral spring.

In addition, the observed mean distribution of tropospheric ozone is influenced by interannual variability in the tropics. Phenomena such as the El Niño-Southern Oscillation (ENSO) introduce variability in tropospheric transport patterns, the amount and location of biomass burning emissions, the UV flux entering the troposphere, and other parameters. Signatures of ENSO were recognized previously in measurements of various chlorofluorocarbons (CFCs) at Samoa [*Prinn et al.*, 1992]. They noted that transport of methylchloroform (CH_3CCl_3) from the Northern Hemisphere

to Samoa was inhibited by migration of the Intertropical Convergence Zone (ITCZ) during ENSO events. *Ziemke et al.* [1999] showed that owing to shifting convection patterns during ENSO, TTOC over the eastern part of the Pacific decreases (3-4 DU), while the western Pacific shows an increase in ozone (2-3 DU).

Most previous studies of tropical tropospheric ozone with models were largely limited to validation of off-line and on-line chemistry-transport models [e.g., *Wang et al.*, 1998; *Brasseur et al.*, 1998; *Hauglustaine et al.*, 1998; *Lawrence et al.*, 1999]. Although most models seem to generally reproduce ozone observations well, all studies report difficulties with representing tropical ozonesondes. This is usually attributed to a poor representation of biomass burning and lightning NO_x emissions, insufficient model resolution, or limitations of the chemistry scheme used. Several studies that focused on the impact of biomass burning on ozone [e.g., *Chatfield et al.*, 1996; *Roelofs et al.*, 1997; *Galanter et al.*, 2000; *Wang et al.*, 2000; *Marufu et al.*, 2000] have yielded important insights on the interaction of (convective) transport and photochemistry during the biomass burning season. However, these model studies focussed on reproducing observed ozone distributions during specific years and for specific regions, while none was aimed at reproducing a long-term tropical ozone record, including interannual variability.

In this study we present for the first time an analysis of a 15-year tropical ozone record simulated with an off-line chemistry-transport model. European Centre for Medium-Range Weather Forecasts (ECMWF) reanalysis meteorological data have been combined with a time-varying emission data set to perform such a long-term integration. Some results from this integration were previously published by *Lelieveld and Dentener* [2000], focusing on the relative roles of chemistry and transport in global tropospheric ozone. In the work presented here, we focus on tropical ozone and address two questions: (1) How well can the model reproduce the ozone distribution in the tropics? and (2) how well can the model reproduce ENSO variability?

In Section 3.2 the chemistry-transport model (CTM) is described, as well as the details of the long-term integration. The analysis method (principal component analysis or PCA) is discussed in Section 3.3. After analyzing the modeled tropopause heights (Section 3.4), we compare annual cycles of ozone at several stations with climatological values of *Logan* [1999] (Section 3.5). In Section 3.6 we focus on ENSO variability in modeled TTOC, and show that this agrees well with satellite-derived observations of *Ziemke et al.* [1999]. We show the effects of ENSO on surface ozone at the tropical Pacific station Samoa, where a significant increase in ozone is observed during ENSO. Finally, we discuss our results in Section 3.7 and present our conclusions in Section 3.8.

3.2 Model Description

In this model study, the off-line chemical tracer transport model version 3 (TM3) is used to calculate atmospheric concentrations of 47 trace species over the period 1979-1993. Transport of chemical tracers is prescribed using ECMWF reanalysis data [*Gibson et al.*, 1997], which encompass the period January 1979 to April 1994, as meteorological input. Six-hourly global fields of geopotential height, temperature, specific humidity, clouds, precipitation and horizontal mass fluxes are retrieved from the ECMWF archive and extrapolated to a horizontal resolution of 5°x3.75°, corre-

Table 3.1: Processes included in the model and references to the original work

Process	Based on	Discussed in[a]
Advection	*Russel and Lerner* [1981]	*Dentener et al.* [1999]
Convection (subgrid)	*Tiedtke* [1989]	*Dentener et al.* [1999]
Turbulent mixing (subgrid)	*Louis* [1979]	*Dentener et al.* [1999]
Stratospheric boundary[b]		LD2000[c]
Photolysis[b]	*Landgraf and Crutzen* [1998] *Krol and van Weele* [1997]	
Dry deposition	*Wesely* [1989]	*Ganzeveld et al.* [1998]
Wet deposition	*Guelle et al.* [1998]	*Jeuken* [2000]
Biomass burning emissions[b]	*Hao et al.* [1990]	*Marufu et al.* [2000]
Lightning NO_x[c] emissions	*Price and Rind* [1992] *Levy et al.* [1996]	
Other emissions[b]	*van Aardenne et al.* [2001]	LD2000[c]
Chemistry, CBM-IV[c]	*Gery et al.* [1989] *Houweling et al.* [1998]	*Houweling et al.* [1998]

[a]This column refers to previous work with the TM3 model.
[b]This process is discussed in Section 3.2.
[c]This process is discussed in Section 4.2.
[d]LD2000 is *Lelieveld and Dentener* [2000].

sponding to about 600x400 km in the tropics. Between the surface and 10 hPa, 19 hybrid sigma-pressure layers are applied with approximately five in the boundary layer, nine in the free troposphere, and five in the stratosphere. Although the long-term integration spans the 1979-1997 period, only the period corresponding to the reanalysis was used for consistency. A short list of processes included in the model and further references to previous applications of the model is given in Table 3.1. We will limit ourselves to a description of processes that are relevant for this study. These include treatment of stratospheric ozone, calculation of photolysis rates, and the emission scenario used in this study.

In the model, stratospheric chemistry is not explicitly accounted for, because it would strongly increase the computational burden. Since ozone is produced in the stratosphere, an upper boundary condition has to be applied for this compound. For this purpose the TOMS data set from the Nimbus 7 satellite (1979-1992) has been used in combination with the ozone climatology from *Fortuin and Kelder* [1998]. The ozone concentrations between the top of the atmosphere and 10 hPa in the model are fixed at climatological values. Between 10 hPa and 60 hPa, zonally averaged ozone

Table 3.2: Estimated 15-year average global emission magnitudes of CO, NO_x and nonmethane hydrocarbons (NMHC) for categories relevant to the tropics[a]

	CO, TgC yr^{-1}		NMHC, TgC yr^{-1}		NO_x, TgN yr^{-1}	
Source Category	Range	Avg	Range	Avg	Range	Avg
Biomass burning						
Savannah	68-77	73	13-15	14	2.6-2.9	2.8
Agricultural waste	87-94	89	13-15	14	2.2-2.4	2.2
Trop. deforestation	43-49	46	7-8	7.5	1.0-1.1	1.0
Temp. wildfires		46		4	1.6-0.8	1.2
Lightning					4.4-4.9	4.63
Agricultural soil					2.7-3.5	3.2
Natural soil/ Vegetation		115		403	3	3

Here Tg=10^{12} g. Data are from J.A. van Aardenne (see footnote to Table 3.1) and *Benkert* [1997].
[a]Numbers in the table signify the range and average for 1979-1993.

values are forced toward zonally and monthly averaged TOMS data with a relaxation time of 2.5 days. For this purpose the TOMS total ozone is distributed in the vertical direction by means of the climatology [*Fortuin and Kelder*, 1998]. The ozone between the Earth's surface and 60 hPa, as well as the zonal distribution and variability, is fully determined by transport and chemistry of the model [*Lelieveld and Dentener*, 2000]. The TOMS data of 1992 were used to constrain the model in 1993, when Nimbus 7 TOMS was no longer available. Therefore relatively little attention is given to 1993.

Photodissociation frequencies for 20 trace gases are calculated on-line in the model with a scheme based on *Landgraf and Crutzen* [1998] and *Krol and van Weele* [1997]. In this scheme, photodissociation frequencies depend on the thickness of the stratospheric ozone column. As noted above, part of the stratospheric ozone column in the model is prescribed by the 14-year TOMS record. Thus interannual variability in the stratospheric ozone column that is present in TOMS observations is also introduced in photodissociation frequencies of ozone, and in species with absorption bands overlapping with ozone. The effect of (multiple) scattering of clouds is also incorporated in the photodissociation scheme, which allows for possible feedbacks associated with convection in the troposphere.

Trace gas emission estimates for the 1978-1993 period are based on the Emission Database for Global Atmospheric Research (EDGAR) [*Olivier et al.*, 1996]. Anthropogenic emission calculations have been performed for 10-year intervals since 1860 [*van Aardenne et al.*, 2001]. The emission trends for anthropogenic ozone precursors between 1979 and 1993 that were not explicitly calculated were scaled with regional trends of fossil-fuel-related CO_2 emissions [*Benkert*, 1997]. Biomass burning emissions are based on *Hao et al.* [1990], and African emissions were recently evaluated by *Marufu et al.* [2000]. Emission magnitudes of sources that are specifically important to the tropics are given in Table 3.2. It is important to note that in the current

study natural biomass burning emission distributions do not vary from year to year and that the same emission distribution is used in each year of our simulation. Therefore the effect of ENSO on ozone precursors is reflected only in different transport patterns, and not in enhanced burning in unusually dry areas or prolonged duration of the burning seasons [*Chandra et al.*, 1998; *Fujiwara et al.*, 2000].

3.3 Principal Component Analysis

A principal component analysis (PC analysis) is used to analyze variability of TTOC in the model data set. Since a detailed description of this technique can be found in most statistical analysis textbooks, we will limit ourselves to a short description. A comprehensive comparison between different variability analysis methods was published by *Bretherton et al.* [1992] and *Kim and Wu* [1999].

PC analysis (sometimes called empirical orthogonal function decomposition) is a tool to investigate spatial and temporal variability in a data set. It is based on the concept that the bulk of the variability in a data set is controlled by only a few physical processes, which modify the field on certain timescales with specific spatial patterns. PC analysis uncovers these patterns and their associated timeseries. The patterns are called empirical orthogonal functions (EOFs), while the time series are called principal components (PCs). The data set is decomposed into (latitude $\times$ longitude) EOFs, and individual EOFs and corresponding PCs from this technique might relate to a physical mechanism that caused the variability. Whether this is the case for any EOF has to be decided afterward. This can be done by relating the EOF pattern to a known physical process, but also by investigating the corresponding PC. The dominant frequency in the signal, and whether or not it correlates with a known time series (such as the ENSO index) can help to isolate the physical mechanisms. A similar technique was applied by *Martin et al.* [2000] to find patterns of variability in the annual cycles of TTOC.

A second analysis technique applied in this work is that of linear regression. We use the same linear regression model as described by *Stolarski et al.* [1991], *Randel and Cobb* [1994] and *Ziemke et al.* [1999], which is the following:

$$\begin{aligned} X(t) = \alpha(t) + \beta(t)t + \gamma(t)QBO(t) + \\ \delta(t)solar(t) + \varepsilon(t)ENSO(t) + R(t) \end{aligned} \tag{3.1}$$

In (3.1), t is the index for the month (t=1, 2, ..., 180, corresponding to January 1979 to December 1993). The equation simply states that a given signal *X(t)* can be decomposed into contributions from five different proxies: a seasonal cycle (α), a linear trend (β), a contribution on the timescale of the quasi-biennial oscillation (γ), a contribution on the timescale of the solar cycle (δ), and a contribution on the timescale of ENSO (ε), plus a residual term *R(t)*. Each of these time-varying coefficients consists of a combination of 4-month, 6-month, and 12-month sine and cosine functions. For the proxies we have used the 10.7-cm solar flux series (*solar(t)*), the Singapore zonal winds at 30 mb (*QBO(t)*), and the Tahiti-Darwin pressure difference (*ENSO(t)*).

There are two important differences between PC analysis and more traditional linear regression techniques. First of all, in linear regression the most important physical mechanisms are defined in advance, and their temporal behavior is prescribed in the

analysis using indicator functions (or proxies, see also *Ziemke et al.* [1997]). Second, linear regression analysis is performed by fitting curves to all the individual time series in the domain. In contrast, PC analysis is performed on the entire temporal and spatial domain at once, and both patterns and time series are selected for their ability to explain the variance of the complete domain. These two features make PC analysis more general than a linear regression. It must be noted that to gain confidence in our results, we also applied the linear regression model (3.1) to the modeled TTOC time series. These results do not differ much from those presented in Section 3.6 and are not further discussed.

Before performing the PC analysis, we removed the seasonal cycle from the signal to isolate interannual components. This was done by subtracting the 15-year average annual cycle from the actual signal for each of the 15 years. By filtering the solar cycle, the results further improved, since the number of solar cycles ($\pm$ 11 years) is too small in our 15-year data set to be isolated as an independent component of variability.

3.4 Tropopause Heights

The first step in calculating the model TTOC is the definition of the tropopause. In contrast to satellite retrieval methods that provide only limited information on the spatial distribution of the tropopause height, the model tropopause can be defined for every grid point using the temperature profile. The main problem is the poor vertical resolution at the tropopause. At the tropopause, model levels are typically spaced approximately 2 km apart, which makes gradient-based methods [*Craig*, 1965; *Bethan et al.*, 1996] unreliable. *Craig* [1965] suggested that the level where the lapse rate of temperature increases to -2 K km^{-1} is the best definition of the tropopause. However, with the coarse vertical resolution, this level would be at approximately 13 km, which is clearly too low compared to observations as described by *Logan* [1999] and *Ziemke et al.* [1999]. We defined the tropopause as the altitude where the temperature lapse rate becomes positive, since this is most consistent with the dynamics of the model and shows a reasonable agreement with the observations. The results are shown in Table 3.3 for stations Natal, Samoa, Brazzaville, and Ascension.

The tropical tropopause in our model seems generally too low by about 10-20 hPa. This may be due to an underestimate of the depth of convective penetration. For example, the tropical convective mass fluxes in the TM3 model reach somewhat lower heights compared to the European Centre Hamburg model version 4 (ECHAM-4) climate model [*Dentener et al.*, 1999]. The underestimate of the tropopause height by 20 hPa would lead to a 1.6 DU underestimate of TTOC, when assuming an ozone mixing ratio of 100 ppbv at the tropopause. When using other definitions of the tropopause, such as the level where the ozone mixing ratio is 100 ppbv, the thickness of the TTOCs varies slightly but it was found that this does not affect the results presented in Section 3.6.

Table 3.3: Pressure at the tropopause in the TM3 model, compared to climatological values from *Logan* [1999] for four tropical stations[a]

	Ascension		Natal		Brazzaville		Samoa	
	Model	Clim	Model	Clim	Model	Clim	Model	Clim
DJF[a]	105.3	91	105.8	94	106.7	104	105.7	92
MAM	109.0	95	110.0	95	109.4	104	110.4	94
JJA	118.0	106	118.4	104	117.8	93	118.3	98
SON	114.6	95	116.0	102	115.3	102	115.4	100

[a]Tropopause pressures reproduced from *Ziemke et al.* [1999]. Units are hectopascals.

[b] DJF denotes December-January-February; other months follow in sequence.

3.5 Tropical Ozone

Before investigating interannual variability in our 15-year model data set we assess the ability of the model to simulate the climatological tropical ozone distribution. Therefore we have compared model-calculated monthly average ozone to ozonesonde observations from the climatology compiled by *Logan* [1999] for a number of stations. In case of a partial overlap between measurements and model, we used only the model simulations from the years reported in the *Logan* [1999] climatology. In case of no overlap at all (Panama), we used all years in our model climatology.

Figure 3.1 shows the comparison for three continental stations near the Atlantic Ocean ozone maximum [*Cros et al.*, 1990; *Kirchhoff and Rasmussen*, 1990; *Diab et al.*, 1996], while Figure 3.2 shows three stations at locations in the Pacific region. Although we recognize the limited coverage over the Atlantic and Pacific Oceans by these stations, it appears to be sufficient for a first analysis. In the boundary layer (900 hPa), measurements and model simulations are in close agreement for all stations. The seasonality is captured well for all the stations, and differences are generally within the 1-σ standard deviation of the measurements. Only in months where the data coverage of the *Logan* [1999] climatology is less than 2 years do larger differences appear.

In the lower free troposphere (500 hPa), the model underestimates ozone volume mixing ratios (VMRs) throughout the year. For remote stations (Figure 3.2), this underestimate is of the order of 5-10 ppbv, while at Atlantic stations (Figure 3.1) it is even larger (10-20 ppbv). The largest discrepancies at Atlantic stations occur during the biomass burning season (July-September), when free tropospheric ozone VMRs are enhanced due to photochemical production of ozone. Although the model shows some enhancement of ozone VMRs in the early burning season, the underestimate during these months increases up to 20-40 ppbv. For stations Natal and Brazzaville, the model seems to perform best in the months of May and April, when pristine conditions occur during the wet season. These conditions resemble the situation at

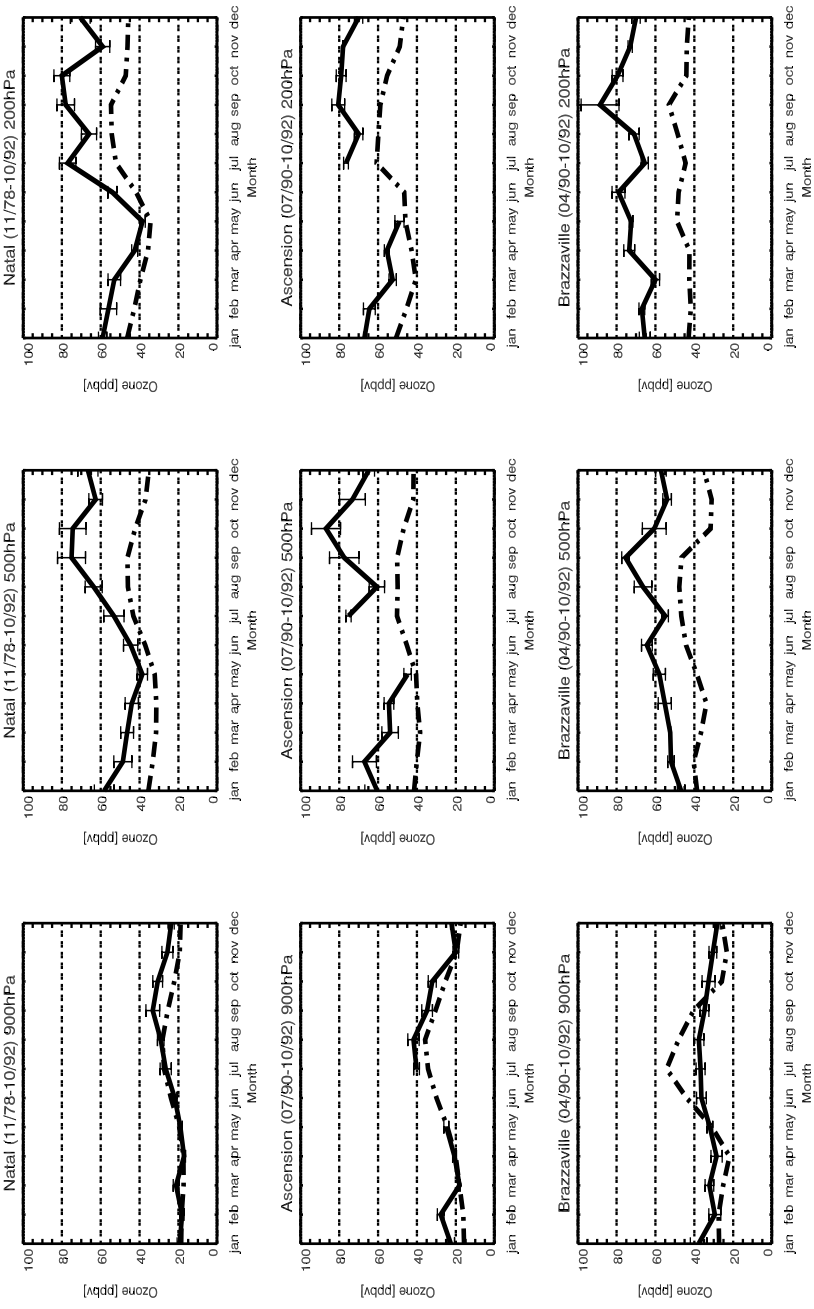

Figure 3.1: Annual cycles of ozone for stations Natal (35°W, 6°S), Ascension (14°W, 8°S) and Brazzaville (15°E, 4°S) at 900 hPa, 500 hPa, and 200 hPa. Solid lines represent the climatological values of *Logan* [1999], including the 1-σ standard deviation. Dash-dotted lines are the model-calculated values for the same stations and averaged over the same years (when possible). Standard deviations for the model are omitted for clarity.

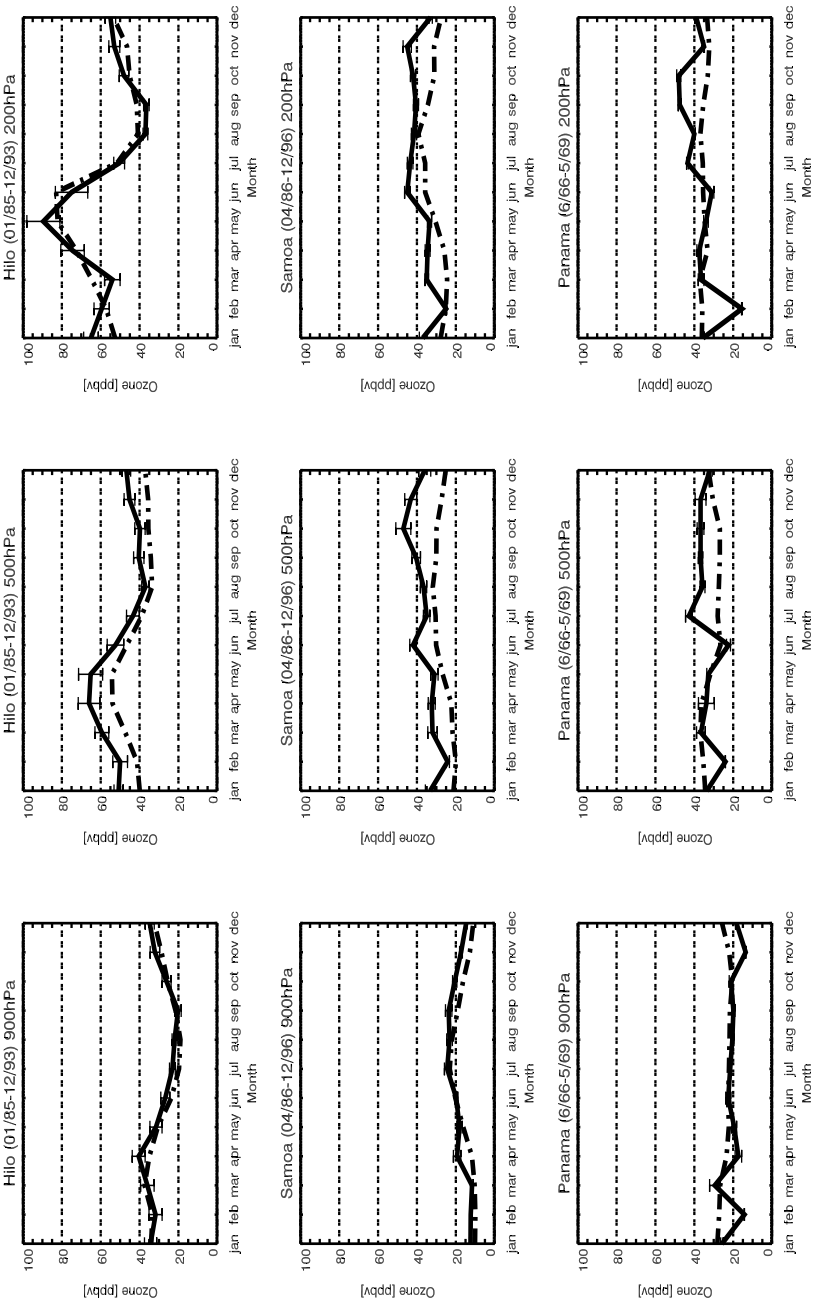

Figure 3.2: As figure 3.1, for stations Samoa (171°W, 14°S), Hilo (155°W, 19°N) and Panama (80°W, 9°N).

more remote stations, for which the model generally performs better. For the upper free troposphere (200 hPa), the model performs very well at the remote stations. The model captures both the seasonality and absolute values adequately. This contrasts with Atlantic stations, for which ozone VMRs are underestimated by 10-25 ppbv. The main differences between the Atlantic and Pacific stations at this altitude are the source region and level of photochemical processing (age) of pollutant emissions. Pacific stations are mostly influenced by upward transport of boundary layer air, which is ozone depleted and relatively pristine [*Kley et al.*, 1996]. Over the Atlantic Ocean, air masses have often resided in the upper troposphere for several weeks after being lifted over continents, and these air masses are aged before descending to lower altitudes [*Krishnamurti et al.*, 1993]. We suggest that during transport in the upper troposphere, these airmasses have become enriched with ozone. One possible mechanism for this is in situ production of ozone. Calculations with a stratospheric model indicate that O_2 photolysis can give rise to net ozone production at this altitude and latitude at an average rate of about 25 pptv/h (A. Bregman, personal communication, 2000). This corresponds to 4 ppbv per week, and since this is not incorporated in our model, it could explain part of the discrepancy in the free troposphere over the Atlantic Ocean. Other possible ozone-enhancing mechanisms in the upper troposphere are photochemical ozone production in biomass burning plumes, stratosphere-troposphere exchange (STE), and lightning. We refer to the discussion of these topics in Section 3.7.

3.6 ENSO Variability

The underestimate of free tropospheric ozone in part of the tropics is reflected in tropospheric ozone columns that are too low by about 2-10 DU compared to ozonesondes and satellite observations [*Thompson and Hudson*, 1999]. However, this underestimate is smallest over the Pacific (2-6 DU), where it is almost uniform with longitude. Therefore an analysis of interannual variability over the 15-year period should still reflect the influence of changing transport patterns during ENSO events, since it is mostly related to changing convection patterns over the Pacific. We first describe the structure of the El Niño-Southern Oscillation in TTOC, after which surface ozone variability for the Pacific station Samoa is compared to model calculations.

The modeled TTOC analyzed by means of PC analysis indicates that the most important source of interannual variability is related to ENSO. Figure 3.3 shows the first EOF in TTOC, and its corresponding PC. This EOF is responsible for approximately 22% of the interannual signal in our analysis of tropical TTOC . We have correlated the PC with the ENSO index (r=0.55, N=180) which confirms that this pattern is induced by ENSO. Similar to analysis of satellite data by *Ziemke et al.* [1999], we infer a dipole structure centered on the date line. This dipole anomaly is caused by a shift in the Walker circulation, which leads to anomalous convection over the eastern Pacific and subsidence over Indonesia.

The convective redistribution of ozone and water vapor leads to the reduced TTOC over the Pacific, while enhanced TTOC over Indonesia is related to enhanced transport from the tropopause region to lower altitudes. There is possibly a contribution of ozone production following lightning flashes in the deep convective clouds. This process would cause an increase of ozone over the Pacific and a decrease over Indonesia

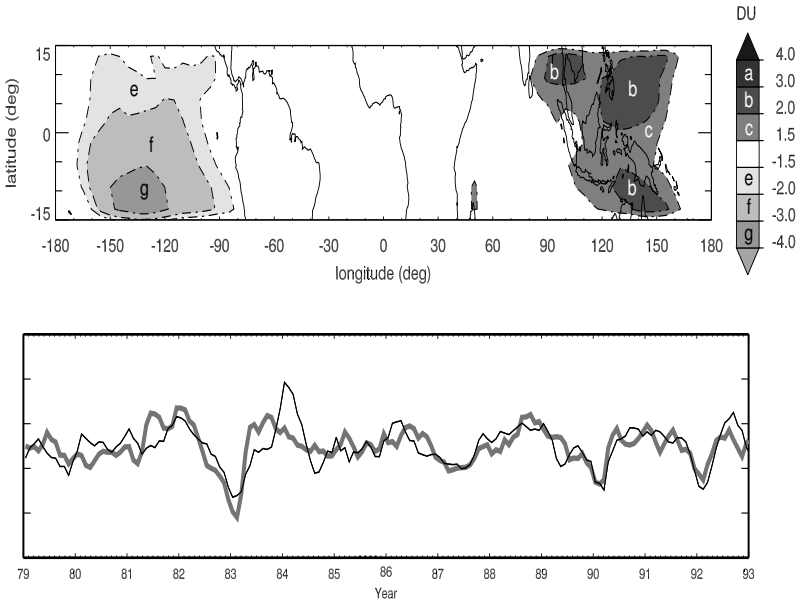

Figure 3.3: (top) Dominant interannual variability pattern from a principal component analysis (PCA) of tropical tropospheric ozone columns (TTOC). The contours represent the maximum anomaly in Dobson units for each location of the domain. (bottom) Temporal behavior of the dominant pattern and the El Niño-Southern Oscillation index (grey line). r=0.55, N=180. The bottom figure has no dimension as both lines are scaled with their standard deviation.

during ENSO, contrary to the observed signal. In our model the lightning NO_x emissions in the eastern Pacific upper troposphere increase by $\pm$10 pptv/d during ENSO. This small increase of the emissions has only very little impact on the ambient NO_x concentrations (10-40 pptv), most likely because the formation rate and scavenging efficiency of HNO_3 also increase under convective conditions. We believe that the small magnitude and intermittent character of the lightning NO_x source over the oceans, together with a slow ozone production rate at the ambient NO_x concentrations [*Jaeglé et al.*, 1999] and fast transport of ozone in the upper troposphere, cause this process to have a negligibly small effect on TTOC during ENSO.

The amplitude of the oscillation in Figure 3.3 is approximately 3-4 DU over the eastern Pacific, and 2-3 DU over Indonesia. These values agree well with the ENSO oscillation found by *Ziemke et al.* [1999], who reported TTOC anomalies of 3-4 DU during El Niño and La Niña events, based on the 20-year TOMS TTOC record. The fact that the amplitude over Indonesia in the model (without a shift in biomass burning patterns) and the satellite observations agree well, indicates that although the 1997-1998 ENSO had a great impact, the influence of biomass burning is relatively small when an analysis is made over many years (1979-1993 for the model, 1979-1998 for the satellite observations). The observed TTOC enhancement of 20 DU reported by *Chandra et al.* [1998] seems to have been unique for the 1997-1998 ENSO.

In specific locations the ENSO signal is responsible for almost 60% of interannual

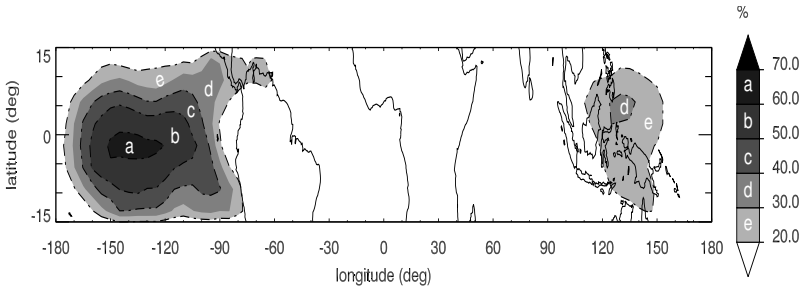

Figure 3.4: Percentage of interannual variability explained by the ENSO-related EOF.

variability. This can be seen in Figure 3.4 which shows the percentage of variability explained by the ENSO-PC at each individual model column in our analysis. The highest values are seen at the equator over the eastern Pacific, while over the western Pacific ENSO explains up to 30% of the interannual signal.

The remainder of the interannual signal is composed partly of a QBO-related signal (12%, see Section 3.7), but the other EOFs could not be related to a physical mechanism. The fact that only a relatively small fraction of the interannual signal can be explained from our analysis is related to the long lifetime of ozone relative to transport, especially in the free troposphere, and the fact that it is influenced by many different processes (e.g., lightning, STE, biomass burning, deposition). The local response of the ozone concentration to a change in these processes is nonlinear due to photochemistry. More importantly, atmospheric flow patterns provide a spatial coupling between these processes on a timescale of several days. Therefore the ozone concentration is very sensitive to changes in the meteorology, and displays relatively much high-frequency variability (noise) over the 15-year time period. Filtering out this high-frequency variability increases the variability explained by the ENSO and QBO related EOFs. However, for an interpretation of the relevance of the ENSO signal in TTOC, this ENSO signal should be interpreted relative to the meteorological variability; therefore we feel that the 'unfiltered' numbers are the most objective.

By performing the PC analysis on different vertical regions, the three-dimensional structure of the ENSO influence was obtained. Table 3.4 shows the results. The correlation with the ENSO index, as well as the variance explained by the ENSO-EOF increase with altitude, indicating that there is less noise in the ozone signal in the upper troposphere. This is related to the larger distance from precursor sources at this altitude. Remarkably, the signal of TTOC shows a higher correlation with the ENSO index than the parts separated by altitude. This means that noise at different heights in the column cancel out, giving a 'cleaner' ENSO signal for the entire vertical domain. This is also reflected in the sum of the signals at different heights, which does not equal the TTOC signal.

The signal over the eastern Pacific is quite evenly distributed with height. This suggests that the signal is rapidly transported throughout the column, as can be expected under convective conditions during El Niño. Over Indonesia the signal is clearly stronger in the free troposphere than in the boundary layer, in agreement with prevailing downward transport during El Niño. The anticorrelation between the east-

Table 3.4: The ENSO signal at different heights in the troposphere.

	PCA Statistics[a]		Signal Strength[b]			
	r (N=180)	%	Eastern Pacific		Indonesia	
			DU	DU/km	DU	DU/km
BL[c]	0.44	10	-0.31	-0.22	+0.08	0.06
LFT[c]	0.45	15	-1.28	-0.22	+1.18	0.21
UFT[c]	0.50	30	-1.53	-0.17	+1.21	0.13
TTOC	0.55	22	-2.23	-0.14	+1.98	0.12

[a]Statistics shown are the correlation of the principal component with the ENSO index and percentage of the signal explained by the ENSO related empirical orthogonal function for the entire tropics.

[b]Ozone anomalies during El Niño over the eastern Pacific (120°W, 0°N) and Indonesia (120°E, 0°N).

[c]BL =Boundary layer, LFT= Lower free troposphere, UFT= Upper free troposphere.

ern Pacific and Indonesia is strong at all altitudes, clearly connecting the two regions through the Walker circulation.

The PC analysis of both our model and of satellite data suggests that a significant fraction of interannual variability over the Pacific Ocean can be related to ENSO. Samoa (171°W, 14°S) is one of the few measurement stations located in the Pacific Ocean with a long surface ozone record. It has been shown from an analysis of surface CH_3CCl_3 concentrations [*Prinn et al.*, 1992] that interannual variability at Samoa is influenced by ENSO. Next, we address the question of whether ENSO variability is also detectable in surface ozone values.

Figure 3.5 shows the surface ozone record for Samoa (1979-1992) and the model-calculated surface ozone (1979-1993). The time series of model-calculated surface ozone for Samoa corresponds very well to observations (see also *Lelieveld and Dentener* [2000]). The deviations from the seasonal cycle in Figure 3.6 display a very noisy signal, which we ascribe to changes in local meteorology associated with the influence of synoptic systems. Nevertheless, the model seems to capture most features of this signal quite well.

A linear regression was performed on the surface ozone time series from measurements and model, using the previously mentioned linear regression model. As expected, the annual cycle contains about 80% of the variance of the data set for both time series. Apart from high-frequency variability, there is a 6% contribution from ENSO (Figure 3.6). The correlation between the modeled and measured linear regression signal is excellent (r=0.93, N=180). The signal shows an increase in surface ozone of about 2 ppbv during the 1983 ENSO. The increase in other ENSO years is smaller ($\pm$ 1 ppbv), while the decrease during the 1989 La Niña is quite pro-

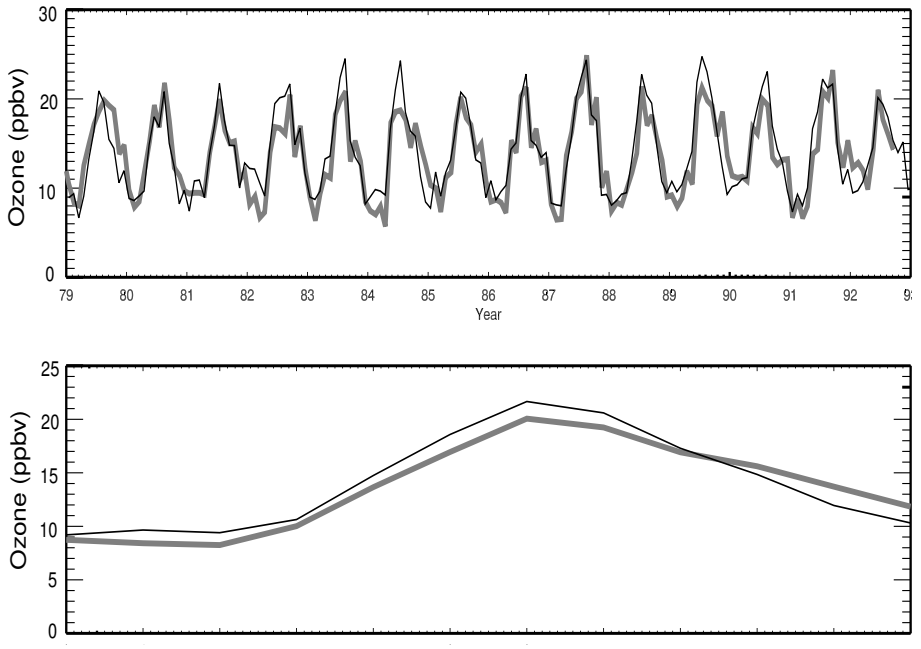

Figure 3.5: Time series and annual cycle of surface ozone at station Samoa (171°W,14°S). Grey lines represent the measurements; black lines are the model calculations. Measurements are by courtesy of the National Oceanic and Atmospheric Administration (NOAA) and S. Oltmans [*Oltmans and Levy*, 1994].

nounced. In agreement with the analysis by *Oltmans and Levy* [1994], a small but statistically significant component of variability related to QBO was obtained.

To ensure that the ENSO signal is not an artifact of the linear regression technique, we also performed a PC analysis on the surface ozone field of the model in the tropics. Although ENSO variability does not dominate the ozone field at the surface, we obtain a high correlation between the ENSO-PC and the measurements (r=0.57, N=180). However, the absolute amplitude in the PC analysis was smaller than in the linear regression because this technique has more degrees of freedom (latitude $\times$ longitude), and is based on many more concurrent time series. Yet, the fact that both statistical techniques yield an increase of surface ozone during ENSO emphasizes the robustness of the results.

The increase in surface ozone contrasts with the behavior of TTOC at Samoa, which slightly decreases during ENSO. The explanation for this is that surface ozone measured at Samoa has normally resided in the marine boundary layer for an extended period. The strong inversion at the top of the marine boundary layer isolates sampled air masses from the free troposphere where ozone mixing ratios are higher. During an El Niño, anomalous convection in the vicinity of Samoa mixes free tropospheric air to lower altitudes [*Lu et al.*, 2000], thus increasing ozone mixing ratios toward the surface. For the entire tropospheric column, however, transport of ozone-poor air and increased photochemical destruction of ozone [*Kley et al.*, 1996] domi-

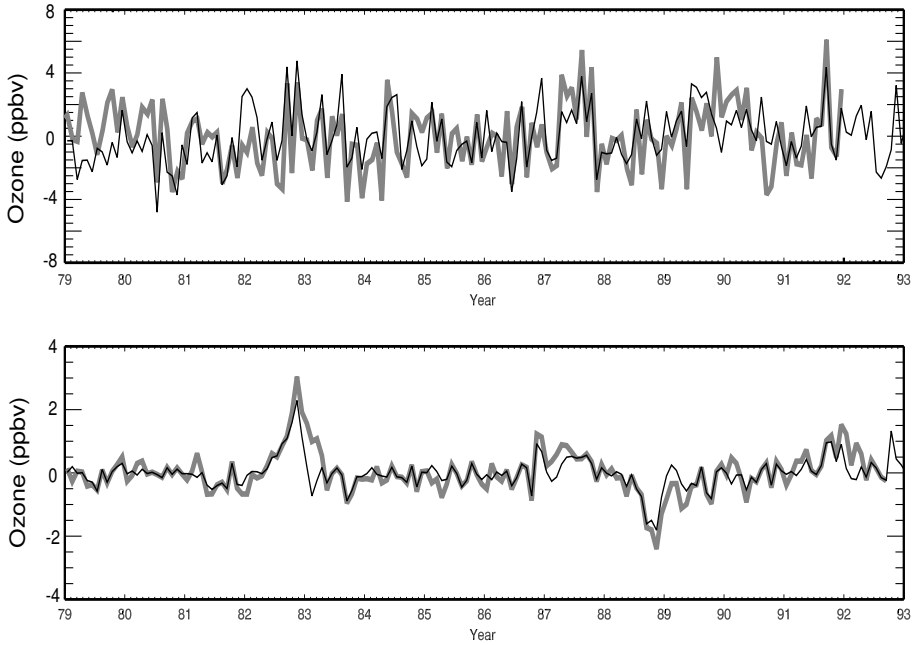

Figure 3.6: The (top) interannual variability (r=0.61, N=168) and (bottom) ENSO signal (r=0.93, N=168) in surface ozone at station Samoa (171°W,14°S) obtained by linear regression. Grey lines represent the measurements; black lines represent the model calculations.

nate over downward transport of ozone-rich air [*Lelieveld and Crutzen*, 1994], which explains the TTOC decrease during an El Niño event.

3.7 Discussion

Many processes in our model contribute to uncertainties in the simulation of ozone. Sensitivity analyses have shown that it is not possible to isolate a single process responsible for the free tropospheric ozone underestimate in the model. The comparison with observations at 500 hPa nevertheless clearly shows that the model underestimates ozone, which is likely caused by an underestimate of the effects of biomass burning in combination with convective transport and associated lightning NO_x. Owing to the relatively long lifetime of ozone in the upper troposphere, this might also explain part of the discrepancy in other months and at higher altitudes. Other possible causes for the ozone underestimate are the previously discussed omission of the O_2 photolysis, and other shortcomings of the chemistry scheme such as too low in situ lightning NO_x production, or a misrepresentation of stratosphere-troposphere exchange at low latitudes. We will briefly discuss some of these uncertainties and indicate possible directions for future research.

The CBM-IV mechanism we use was originally developed for studies of tropospheric photochemistry under polluted conditions. *Houweling et al.* [1998] have im-

proved the description of several biogenic compounds in the mechanism, as well as the performance under unpolluted (low NO_x) conditions. Nevertheless, the reaction rates and branching ratios used in the mechanism are mostly biased toward freshly polluted conditions. Although this will have an impact on the performance of the scheme at larger distances from the sources, the overall effect on the upper tropospheric ozone concentrations will probably be localized and relatively small. A similar argument can be made for the effects of trace gases that are not included in the model, such as acetone and several hydroperoxides and alkylnitrates. Sensitivity studies using more elaborate schemes indicated that the effect on ozone of using such a scheme in GCMs, was very local and less than 10% (R. von Kuhlmann and G.J. Roelofs, personal communication, 2000).

Recent discussions of the influence of tropical biomass burning on ozone, NO_x, and CO were presented by *Galanter et al.* [2000] and *Marufu et al.* [2000]. The latter authors focused on African biomass burning emissions in the same model as used in this study. However, the current work includes extended time series and covers larger regions than *Marufu et al.* [2000].

Large uncertainties exist in emission estimates of NO_x from fires, and the discussion of whether these emissions can directly influence the free troposphere has not been resolved. It is possible that biomass burning plumes are NO_x depleted before they reach the free troposphere due to rapid formation of HNO_3 or by deposition at the surface. Ozone production from this direct NO_x source would then occur close to the fires only, unless NO_x would be recycled or added to the aged plume. Conversion of HNO_3 on soot aerosols has been suggested; however, *Disselkamp et al.* [2000] showed that this process is not important under atmospheric conditions. A much more likely candidate is the NO_x produced from lightning, which has been shown to significantly influence tropospheric ozone concentrations [*Lamarque et al.*, 1996; *Martin et al.*, 2000; *Lelieveld and Dentener*, 2000]. However, the emission strength and distribution of NO_x from lightning are highly variable and poorly quantified [*Pickering et al.*, 1993; *Levy et al.*, 1996; *Price et al.*, 1997; *Pickering et al.*, 1998].

Distributions and magnitudes of NO emissions, but also of other important tropospheric compounds (CO, nonmethane hydrocarbons) are highly variable in both time and space. They often depend on many parameters, including meteorological conditions. Concerning biomass burning, arid regions can shift from one year to the next, and the onset and duration of the biomass burning season change from year to year. The model includes the biomass burning emission distribution of *Hao et al.* [1990] for the entire period, without interannual or geographical variability. This emission database was constructed on a coarse resolution ($5^\circ \times 5^\circ$), which implies that local differences in timing and magnitude of the sources are not included. A comparison of the *Hao et al.* [1990] emission data set with satellite observations showed that the timing of the burning peak is not always accurate [*Cooke et al.*, 1996]. This was confirmed by *Galanter et al.* [2000], who also mentioned the relatively long duration of the biomass burning season in the *Hao et al.* [1990] data. The overall effect is that emissions are more widespread temporally, which leads to lower peak values of ozone in the model.

To analyze emission-related uncertainties further, we performed several sensitivity studies. By varying the magnitude of NO_x emissions from biomass burning and lightning, and the emission altitude of biomass burning products, we tried to improve the comparison in Section 3.5. Although the comparison sometimes improved locally, the

situation at other stations would deteriorate, in agreement with similar experiments conducted by *Galanter et al.* [2000]. This suggests that the cause of the underestimate is a combination of several poorly modeled processes, but it also leaves open the possibility of an ozone-producing mechanism in biomass burning plumes that is not understood at the moment.

In the tropical upper troposphere, stratosphere-troposphere exchange contributes significantly to the ozone budget [*Lelieveld and Dentener*, 2000]. Besides the suggested role of O_2 photolysis, transport by STE can also be a direct source of ozone to the tropical upper troposphere [*Baray*, 1999; *Zachariasse et al.*, 2000]. The current contribution of STE to the tropical ozone budget in our model is controlled by horizontal transport from the extratropics. In our simulation the stratospheric contribution to ozone VMRs over the Atlantic is comparable to that over the tropical Pacific Ocean. This contrasts with the situation in the subtropics. *Kentarchos et al.* [2000] showed that the influence of STE is greater at Izaña (Tenerife, 3°E, 26°N) than at Hilo (155°W, 19°N) because filaments of stratospheric air can penetrate further equatorward in the gradual subsidence over the Atlantic Ocean than over the convective Pacific. It is therefore quite possible that we currently underestimate horizontal transport of filaments of ozone-rich air to the tropical Atlantic region. Based on analysis of ozonesonde data from Indonesia, *Fujiwara et al.* [2000] also suggested a stratospheric source of ozone in the tropics. Although tropopause-folding events do not occur in the tropics [*Elbern et al.*, 1996], a direct tropical source due to compensation of deep convective overshoots by downward transport of stratospheric air should be considered [*Tuck et al.*, 1997; *Lu et al.*, 2000; *Fujiwara et al.*, 2000]. For now, the underestimate of free tropospheric ozone over the Atlantic Ocean remains a problem that requires further study.

On the other hand, detection of the ENSO signal in a modeled chemical tracer is a very promising result. Other studies have suggested a possible influence of ENSO on measurements during El Niño years, while a quantification of this influence was impossible due to a lack of spatial coverage of the measurements. The results presented in this work suggest that multiyear model simulations can offer an alternative. Although the presence of the ENSO signal in our model is introduced by the off-line ECMWF reanalysis, effects of convection, changing UV fluxes, and photochemistry are calculated on-line by the model. The fact that all of these processes play an important role in the ozone abundance, and that the ENSO signal was found both in surface ozone data and in TTOC, motivates the extension of our model efforts to other trace gases.

Apart from ENSO, *Ziemke et al.* [1999] also found a contribution by the quasi-biennial oscillation to interannual variability over the Atlantic Ocean. They showed an anticorrelation between stratospheric and tropospheric ozone columns on the timescale of QBO, which they suggested to be caused by changing UV fluxes to the troposphere during QBO. An increase (decrease) in stratospheric column ozone would lead to a decrease (increase) in UV flux, causing a decrease (increase) in ozone. This implies that the photochemical regime over the Atlantic Ocean causes net ozone production. They stressed the important role that three-dimensional photochemical models could play in further study of this phenomenon. In our model the stratospheric QBO is reflected well in the wind fields, and application of the TOMS upper boundary conditions ensures that upper stratospheric ozone is modeled adequately. Our model results indicate that this introduces a 20% fluctuation in tropospheric ozone photoly-

sis rates on the timescale of QBO, which leads to a small (1-2 DU) QBO signal in the troposphere. In contrast to the results of *Ziemke et al.* [1999], this signal correlates positively with the stratospheric QBO, indicating that a net ozone destruction regime prevails in our model. This suggests that our model underprediction of free tropospheric ozone is related to underestimated in situ photochemical formation rather than transport from the stratosphere. A further analysis of the QBO signal has been planned for the future, since we first want to investigate the accuracy of our stratospheric ozone relaxation method for the tropics (see Section 3.2), as it was shown to work well for middle and high latitudes.

3.8 Summary and Conclusions

We presented model simulations of tropospheric column ozone for 1979-1993 based on 15 years of ECMWF meteorological reanalyzed data and an emission data set that accounts for the temporal development of anthropogenic emissions. From a comparison of the results with ozonesondes in the *Logan* [1999] climatology, we identify an ozone VMR underestimate, which is most pronounced over the Atlantic Ocean at higher altitudes in the troposphere and during the biomass burning season. The model captures surface ozone values and seasonal cycles of ozone in the tropics well. Owing to the underestimate of free tropospheric ozone and an underestimate of tropopause heights, TTOC is underestimated by 2-10 DU. This does not affect interannual variability, and the model reproduces observed signals of ENSO in the 15-year TTOC record. The ENSO signal in model-calculated tropospheric ozone columns is very similar in structure and amplitude (3-4 DU) to that observed in tropospheric ozone retrieved from satellites. Furthermore, an analysis of the ENSO signal in surface ozone at station Samoa showed excellent agreement between measurements and model. This consistency of the model-calculated ENSO signal with two independent data sets lends credibility to the ability of the model to capture effects of ENSO on the ozone concentration, and the underlying processes, that is convective redistribution of ozone within the troposphere. Besides improvement of the simulation of tropical ozone over the Atlantic Ocean, future work will focus on the three-dimensional structure of the ENSO signal, as well as the ENSO signal in other important trace gases (CO and hydrocarbons, including CH_4). The quantification of this variability will be an important consideration when analyzing tropical trace gas measurements.

Acknowledgments. We are grateful to J. Logan and S. Oltmans for making ozone data available through the internet. We also want to acknowledge R. Scheele for his help in preprocessing the data. We thank two anonymous reviewers for their constructive comments that improved this manuscript.

Chapter 4

Chemistry-transport modeling of the satellite observed distribution of tropical tropospheric ozone columns

[1]Published in *Atmospheric Chemistry and Physics*, **2**, 103–120, with F. J. Dentener, M. C. Krol, A. M. Thompson and J. Lelieveld as co-authors.

Abstract

We have compared the 14-year record of satellite derived tropical tropospheric ozone columns (TTOC) from NIMBUS–7 Total Ozone Mapping Spectrometer (TOMS) to TTOC calculated by a chemistry-transport model (CTM). An objective measure of error, based on the zonal distribution of TTOC in the tropics, is applied to perform this comparison systematically. In addition, the sensitivity of the model to several key processes in the tropics is quantified to select directions for future improvements. The comparisons indicate a widespread, systematic (20%) discrepancy over the tropical Atlantic Ocean, which maximizes during austral Spring. Although independent evidence from ozonesondes shows that some of the disagreement is due to satellite overestimate of TTOC, the Atlantic mismatch is largely due to a misrepresentation of seasonally recurring processes in the model. Only minor differences between the model and observations over the Pacific occur, mostly due to interannual variability not captured by the model. Although chemical processes determine the TTOC extent, dynamical processes dominate the TTOC distribution, as the use of actual meteorology pertaining to the year of observations always leads to a better agreement with TTOC observations than using a random year or a climatology. The modeled TTOC is remarkably insensitive to many model parameters due to efficient feedbacks in the ozone budget. Nevertheless, the simulations would profit from an improved biomass burning calendar, as well as from an increase in NO_x abundances in free tropospheric biomass burning plumes. The model showed the largest response to lightning NO_x emissions, but systematic improvements could not be found. The use of multi-year satellite derived tropospheric data to systematically test and improve a CTM is a promising new addition to existing methods of model validation, and is a first step to integrating tropospheric satellite observations into global ozone modeling studies. Conversely, the CTM may suggest improvements to evolving satellite retrievals for tropospheric ozone.

4.1 Introduction

The availability of trace gas measurements in the tropics has increased considerably by a large number of intensive campaigns (LBA, PEM, TRACE, INDOEX, SAFARI) and the expansion of the number of measurement stations in the tropics. The interest in the tropics is based on the active photochemistry, rapid convective mixing along with lightning discharge, high humidity, widespread biomass burning, and growing industrial emissions. All these processes influence the concentration of oxidants such as ozone and the hydroxyl radical. The latter plays a crucial role in the removal of biogenic emissions and anthropogenic pollution from the atmosphere.

Observations from satellites play an increasingly important role in monitoring of the chemical composition of the troposphere. The Total Ozone Mapping Spectrometer (TOMS) instrument aboard the NIMBUS–7 and Earth Probe (EP) Satellites [*McPeters and Labow*, 1996] has been used to retrieve tropospheric column ozone (TTOC) [*Fishman and Larsen*, 1987; *Kim et al.*, 1996; *Ziemke et al.*, 1998; *Hudson and Thompson*, 1998], while the GOME instrument aboard ERS–2 has been used to retrieve columns of tropospheric NO_2, SO_2 [*Eisinger and Burrows*, 1998; *Burrows et al.*, 1999], and BrO [*Richter et al.*, 1998]. In the near future, SCIAMACHY [*Burrows and Chance*, 1992] will expand this suite of trace gases with N_2O, CO_2, CO and CH_4. These last two trace gases are also the focal point of the MOPITT instrument [*Pan et al.*, 1998] aboard the EOS-TERRA satellite, launched in 2000. The most important advantages of satellite observations are the global coverage and the continuous monitoring on time scales from days to years, and sometimes even decades. For historically data sparse regions such as the tropics, this will contribute significantly to our understanding of atmospheric processes and help detect changes.

In addition, satellite measurements can easily be combined with chemistry-transport models (CTM) and global circulation models (GCM), since spatial and temporal scales are often comparable. There are several ways in which these properties can be exploited in a quantitative way. This includes for instance assimilation of satellite measurements into models to constrain chemistry calculations [e.g. *Jeuken et al.*, 1999] and provide boundary conditions. Also, satellite measurements can be used as additional constraints in inversion problems, where the global distribution of a tracer is used to infer the distribution and magnitude of its sources and sinks [e.g. *Houweling et al.*, 1999]. Vice versa, model calculations can be used in satellite retrieval algorithms to provide a 'first guess' field or to provide missing parameters needed in the retrieval [e.g. *Chance et al.*, 2000]. The growing amount of satellite observations and expansion of remotely sensed trace species will intensify the use of these observations in modeling studies.

From the several tropospheric satellite observations available at the moment, the TTOC record derived from the NIMBUS–7 observations is the most extensive. It spans the complete NIMBUS–7 observational period (1979–1992) on a high spatial (2×1 degrees) and temporal (twice monthly) resolution. This has enabled analysis of seasonal cycles [*Martin et al.*, 2000], trends [*Thompson and Hudson*, 1999] and interannual variability [*Ziemke et al.*, 1999] in tropical ozone. Moreover, this dataset has shown to be very useful in studying both local scale features such as the effect of El Niño-Southern Oscillation (ENSO) related fires over Indonesia [*Chandra et al.*, 1998; *Thompson et al.*, 2001], as well as large scale phenomena such as the evolution of the South Atlantic ozone maximum [*Thompson and Hudson*, 1999] and the changing

Walker circulation during ENSO [*Ziemke et al.*, 1999]. Neverthless, most modeling studies have only used the TTOC data for a qualitative comparison, while ozone sondes [*Logan*, 1999] were used for a quantitative comparison. Here, we explore how satellite derived TTOC can be used to validate and improve our CTM.

Previously, we have tested our model against in situ data from sondes and ground-based stations [*Lelieveld and Dentener*, 2000; *Marufu et al.*, 2000; *Peters et al.*, 2001]. Comparison to the climatology of *Logan* [1999] revealed an apparent problem in the representation of the zonal ozone distribution in the tropics, which shows a maximum of TTOC over the Atlantic Ocean and a minimum over the Pacific Ocean. This distribution is often called the 'zonal wave one pattern' [*Kim et al.*, 1996], and is a typical example of a large scale feature in tropical ozone that can be well studied with a combination of global models and satellite observations. Therefore, we present a quantitative comparison with TTOC derived with the Modified Residual (MR) algorithm of *Hudson and Thompson* [1998]. We have developed a measure of error to consistently perform this comparison. This measure of error allows us to recognize systematic shortcomings in our model on seasonal and interannual time scales, and study the influence of meteorology and photochemistry on our model results. Moreover, it helps to identify processes that should be considered for improvement and allows us to quantify the sensitivity of our model results to several processes such as biomass burning and lightning NO_x emissions. It is important to stress that these techniques are not used to 'tune' the model to observations. The processes that are most likely to cause the observed differences should be carefully studied in future work, preferably in a three dimensional perspective using ozone sondes. Our work presented here should be seen as an exploration of model sensitivities providing guidance to actual improvements.

We start in Section 4.2 with an introduction of the CTM that was used in this study, and a discussion of the photochemistry, biomass burning and lightning NO_x emissions. Next, we give some basic information on the TTOC data used (Section 4.3). In order to compare model and measurements, we introduce a measure of error in Section 4.4, which will be the basis for the results in this paper. We apply this measure of error to firstly identify the magnitude, location, and seasonality of the discrepancy between model and data (Section 4.5), after which we will look at the roles of meteorology (Section 4.6) and photochemistry (Section 4.7) in our model. The latter is done by looking at the spatial and temporal distribution of photochemically marked ozone tracers. The processes that are identified as most likely candidates to explain the discrepancy are further studied in Section 4.8, through a series of sensitivity experiments in which changes in emission magnitude and distributions are applied. The results from these experiments are illustrated with several ozone sondes in Section 4.9. Finally, we discuss our results in Section 4.10, and give a short summary in Section 4.11.

4.2 Model Description

We use the chemical tracer transport model version 3 (TM3) to simulate transport and photochemistry of 48 trace gases within a global domain. The TM3 model has a horizontal resolution of 5° longitude $\times$ 3.75° latitude and uses 19 layers with a hybrid of sigma-pressure coordinates in the vertical, with the model top at 10 hPa. Approx-

imately five layers constitute the boundary layer, nine the free troposphere, and five the lower and middle stratosphere. Transport in the off-line model is prescribed using ECMWF data [*Gibson et al.*, 1997].
The model uses six-hourly, 3-dimensional fields of geopotential height, horizontal mass-fluxes, temperature, specific humidity and cloud information (liquid water and ice water content), as well as 2D information on cloud cover and precipitation (large-scale and convective). The subgrid scale transport by turbulence and convection is calculated from archived diffusion and entrainment/detrainment coefficients from the ECMWF model using a modified scheme by *Louis* [1979] and *Tiedtke* [1989] respectively.
All the input fields are extrapolated from the ECMWF archived resolution (spectral, T106) to the TM3 model resolution. The results presented in Section 4.5 and 4.6 were obtained using the multi-year (1979–1993) simulation by *Lelieveld and Dentener* [2000], which was also used in Chapter 3. The configuration of the TM3 model in the sensitivity studies (Section 4.8) is identical, and pertain to the year 1992. However, the model currently runs on a new SGI-3800 massive parallel system from the Dutch National Supercomputing Facility (NCF) (see also the Appendix at page 113).
A short list of processes in the model and references to more elaborate discussion of these processes is given in Table 3.1 (page 45). We will limit ourselves to a description of the processes explicitly relevant for this study, being the emissions from biomass burning, the photochemistry of ozone and its precursors, and the lightning NO_x parameterization.

Biomass burning emissions

The emissions of biomass burning in the model were originally constructed from two datasets. The EDGAR emission database [*Olivier et al.*, 1996] prescribes the total amount of CO, HCHO, NO_x, and NMHC emitted yearly from anthropogenic and natural sources. This database is based on estimates for the year 1990 that were obtained from various sources on a resolution of 1° longitude $\times$ 1° latitude. For the temporal distribution of these emissions, the model relies on the *Hao and Liu* [1994] fire calendar, which contains monthly fractions of annual amounts of biomass burned on a 5° longitude $\times$ 5° latitude resolution. For the sensitivity studies presented in Section 4.8, we have replaced the fire calendar of *Hao and Liu* [1994] with one based on fire counts from the AVHRR satellite [*Dwyer et al.*, 1999], which contains 10-day composites of global fire activity for 1992–1993. The observations were used to construct a time distribution function for each gridbox, by scaling the monthly total of counts by the yearly total of counts, yielding a fraction of fires occurring each month. Thus, the yearly totals remain the same, but the emissions maximize in the month with the largest number of fires.

It is important to note that this approach is meant to provide a simple alternative to the use of the *Hao and Liu* [1994] database, suitable for a model sensitivity analysis. In our algorithm, we do not account for the size of the fires that were observed; large fires and small fires contribute equally to our calendar, while in reality the amount of trace gases released to the atmosphere can differ strongly. Our algorithm will therefore overestimate the influence of these small fires and, since the total emissions are constant, underestimate the influence of large fires. Also, our algorithm does not include the smoldering phase of the fires, which can continue for

several weeks especially after forest fires [*Andreae and Merlet*, 2001]. Due to the neglect of the smoldering phase, the timing of smoldering-related emissions (such as CO, NH_3) is biased towards the moment of detection of the fire, i.e. the flaming phase. Nevertheless, our alternative fire calendar suffices for a sensitivity analysis, whereas real satellite derived emission estimates require a more sophisticated approach [*Pinty et al.*, 2000; *Duncan et al.*, 2002]

Photochemistry of ozone

Photochemistry in the TM3 model is based on the CBM-4 mechanism of *Gery et al.* [1989]. It includes 38 trace gases and 110 gas phase reactions. The CBM-4 mechanism was initially intended to simulate ozone photochemistry over urban areas with high NO_x abundances. Therefore, *Houweling et al.* [1998] modified the scheme such that low NO_x conditions are better represented. This has improved ozone photochemistry over more remote areas, where NO_x concentrations are much lower. To reduce the number of reactions and species, the CBM-4 mechanism uses a form of structural lumping, where trace gases of common origin with similar structures, lifetimes and reactive properties are treated as one species, which has the common characteristics of all the species it is meant to represent. This concept and the consequences for the photochemistry are described in more detail in the work of *Gery et al.* [1989], *Duncan and Chameides* [1998], *Houweling et al.* [1998] and *Pöschl et al.* [2000].

Precursors for ozone production that are emitted from biomass burning include NO_x, CO, formaldehyde and acetaldehyde. Other NMHC compounds that are known to originate from biomass burning (e.g. acetone, acetonitrile, ethene) are represented through the emissions of several lumped species (parafinic and olefinic NMHC's, methylglyoxal). The scheme includes the photochemistry of peroxy-acetyl nitrate (PAN), which is an important secondary product from the oxidation of acetaldehyde and contributes significantly to the free tropospheric nitrogen budget [*Singh et al.*, 1995]. Dry deposition is an important sink for NO_x, HNO_3, PAN, formaldehyde and acetaldehyde, while wet deposition through scavenging by clouds removes predominantly HNO_3, formaldehyde and H_2O_2. The chemical mechanism includes the heterogeneous conversion of NO_x to HNO_3 on sulfate aerosols according to *Dentener and Crutzen* [1993], as well as a description of sulfur chemistry [*Jeuken*, 2000].

Lightning NO_x emissions

The lightning NO_x emissions in the model are based on the widely used parameterization of *Price and Rind* [1992]. The spatial distribution of lightning, as well as the intensity, is calculated using the heights of cloud tops in systems of deep convection. To discriminate between the efficiency of lightning NO_x production over the oceans relative to land, we have assumed a ratio of 1:10 in production efficiency, following *Levy et al.* [1996]. The lightning NO_x production efficiency in cloud-to-ground discharges has been scaled to account for the higher efficiency in high latitudes [*Mackerras and Darveniza*, 1994]. The NO_x emissions are uniformly distributed between cloud base and cloud top, proportional to air-density. By scaling the lightning NO_x emissions with meteorological parameters, interannual variability in the model meteorology is also reflected in interannual variability in the lightning NO_x emissions. The

total annual simulated lightning NO_x emissions over the period 1979–1993 are 4.6 $\pm$ 0.3 $TgN\,yr^{-1}$.

In our sensitivity experiments, we have used the vertical lightning NO_x distribution profiles as given in *Pickering et al.* [1998]. In this work, the vertical distribution depends on the location (tropics or extra-tropics), and surface characteristics (land or sea). Also, we have implemented a lightning NO_x parameterization developed by *Meijer et al.* [2001]. This follows the principles of *Price and Rind* [1992], however, the occurrence and intensity of lightning NO_x emissions is coupled to the convective precipitation in the model. This was shown to correlate well with space-based observations of lightning flash rates over Europe, and was tested against NO_x observations in the extra-tropics. The main difference between the two approaches is the fraction of the emissions occurring in the tropics. In the new parameterization, this fraction decreases from 80% to 70%, which agrees better with independent estimates [*Levy et al.*, 1996; *Price and Rind*, 1992].

Labeled tracers

To attribute photochemically produced ozone to the different processes in our model, we applied a tracer labeling technique. The assumption that ozone formation in the troposphere is NO_x-controlled [*Crutzen*, 1988] implies that NO-to-NO_2 conversion by peroxy-radicals can be used to diagnose ozone formation. Thereto, we have introduced labeled tracers of NO_x, the most important NO_y species, and ozone. The NO_x tracers are labeled according to their source category, representing emissions from lightning, biomass burning, nonagricultural soils, and industrial sources. When a labeled NO molecule is converted to NO_2 by a peroxy radical, the subsequent photolysis of NO_2 yields an ozone molecule labeled accordingly. Furthermore, tropospheric ozone introduced through stratosphere-troposphere exchange (STE) is labeled by tagging molecules once they pass the 100 hPa level. The labeled tracers participate in all other processes open to their regular, non-labeled counterparts. This approach was tested and discussed in *Lelieveld and Dentener* [2000].

The sum of all the labeled tracers represents $\sim$90% of the total ozone concentration in the tropical troposphere. The residual of $\sim$10% that we cannot reproduce in the tracer labeling is simply a result of the chosen approach. The labeled ozone tracers in the model are a diagnostic tool, and not an exact solution of the differential equations governing ozone photochemistry. Although many reaction pathways, including cycling of NO_x through several reservoir species, are labeled, not all possible routes and recombinations are taken into account. For instance, cycling of NO_2 and NO_3 through N_2O_5 can yield back the original products, or HNO_3. The many combinations in which this is possible given five marked tracers (plus one unmarked) is large, and had to be simplified. Also, the production of marked ozone from $NO+RO_2$ reactions is calculated simply from the reaction fluxes, which can also lead to errors as was discussed extensively in the original work of *Johnston and Kinnison* [1998], and comments on that work [*Pöschl et al.*, 2000]. For the purposes in this paper the labeled tracer approach, although clearly not exact, gives very useful information and the ability to diagnose the ozone budget qualitatively.

In the calculations presented in the next sections, the local tropopause height is calculated in the same way as in Chapter 3. We define the tropical tropopause as the level where the temperature lapse rate changes sign. This gave better agreement

with the observed tropopause heights (see Chapter 3) than gradient based methods such as *Craig* [1965]. Due to the coarse vertical resolution, our model underestimates tropopause heights in the tropics by about 20 hPa, which translates to a 1.6 DU underestimate of tropospheric ozone columns assuming a mixing ratio of 100 hPa at the tropopause.

4.3 Observations

We use the NIMBUS–7 TTOC record (1979–1992) to detect systematic flaws in our model and to gain more insight in the sensitivity of our model calculated ozone. The observations were derived from the TOMS total ozone observations with the Modified-Residual (MR) method [*Hudson and Thompson*, 1998].

The TTOC record provides twice monthly fields of TTOC, covering all the tropical latitudes where a zonal wave one pattern in total column ozone is observed. The horizontal resolution of the dataset is 2° longitude $\times$ 1° latitude (230x115 km at the equator), and through averaging over several orbital passes of the satellite, a picture of the full zonal distribution of TTOC is obtained in several days. Through averaging the observations over 13–15 day periods, errors associated with the scan angle, as well as instrument noise are filtered out. Thus, the product is not suited to study day-to-day variability. The data is available on the internet through http://metosrv2.umd.edu/-$\sim$tropo/.

Uncertainties in the observations of TTOC are related to the assumed tropopause height as well as the insensitivity of the TOMS instrument to tropospheric ozone near the surface. The instrument is progressively insensitive to the signal of ozone originating from altitudes below the stratospheric ozone maximum. The algorithms that were developed to circumvent these problems are explained in detail in *Hudson and Thompson* [1998]. In the MR retrieval algorithm (also see Chapter 2), sonde observations from selected stations in the SH are used to obtain a-priori information on the zonal distribution of tropospheric ozone, which is thereafter projected onto each grid point of the total column ozone observations to yield the TTOC. The averaging of several sondes to obtain a half-month average leads to a standard deviation of $\pm$5.3 DU. Therefore, the a-priori zonal ozone distribution cannot be fixed more accurately than this sonde standard deviation, and 5.3 DU is thus the lower limit for the precision in TTOC. This value is comparable to the TOMS instrument accuracy. An independent comparison of TTOC with four ozone sonde stations in the tropics revealed a RMS deviation of 5.1 DU between TTOC and sondes [*Thompson and Hudson*, 1999]. This value is expected to increase with distance from the sonde stations used in the algorithm, and is probably larger in the NH than in the SH, since the underlying zonal wave one pattern used in the retrieval was based on SH ozone sondes. However, since there is no objective way to define the deviations at other locations, the overall standard deviation of the TTOC product is given by σ=5.3 DU over the whole domain.

The Nimbus–7 TTOC record (1979–1992) has been evaluated in two ways with ozonesonde data. Note that these comparisons are mostly performed in the Southern Hemisphere tropics [*Thompson et al.*, 2002b], since the available Northern Hemisphere tropical data are restricted to campaign data [*Thompson et al.*, 2000] and to stations at Suriname (6N, 55W) and Malaysia [*Yonemura et al.*, 2002b]. First, the

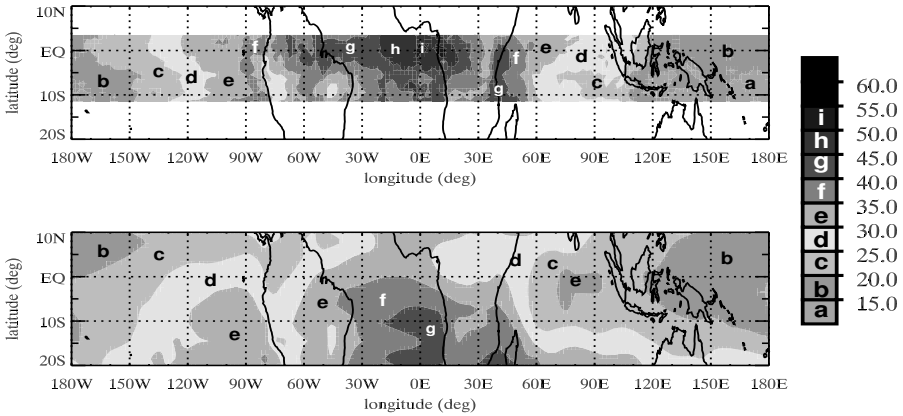

Figure 4.1: Observed (top) and model calculated (bottom) distribution of TTOC in September 1992. Note the widespread underestimate of TTOC over the tropical Atlantic Ocean and adjacent continents.

limited ozonesonde data for the 1979–1992 period agreed with the TTOC satellite product within 6–7 DU on average [*Thompson and Hudson*, 1999]. Second, a statistically averaged annual dataset was prepared from Nimbus–7 TTOC and compared to the 1998–2000 SHADOZ ozonesonde record in four regions: tropical Atlantic, central Pacific, eastern Pacific and Indonesian maritime continent. Excellent agreement in TTOC magnitude and seasonality was found in the central Pacific TTOC compared to sondes at Samoa (14S, 171W). The TTOC seasonality over the eastern Pacific and Indonesian maritime continent compared well to ozonesonde seasonal patterns at San Cristobal (1S, 89.6W) and Watukosek, Java (7.5S, 113E), respectively, but tended to be too high in magnitude. Over the Atlantic, comparison of the TTOC annual mean with ozonesondes over Ascension Island (6S, 15W) suggests an overestimate of 5–8 DU on average during the period from July–October 1998–2000.

It should be noted that differences among several retrieval algorithms of TTOC (e.g. *Ziemke et al.* [1999], *Fishman and Larsen* [1987]) can be quite large, also compared to the reported standard deviation of 5.3 DU. No comprehensive intercomparison has been published so far, although *Martin et al.* [2002] have noted a tendency for tropical Atlantic ozone from TOMS-based data to run high relative to in-situ measurements, particularly in the second half of the year. Our experiences with working with the *Ziemke et al.* [1999] data suggest that the MR method generally gives higher values of TTOC, and several regions are suspected to experience unwanted aerosol influences in the MR method (*A. Frolov, personal communication*). A detailed quantification of the uncertainties of individual locations in the MR method is beyond the scope of this study, as is an intercomparison between the different TTOC datasets. More insight in the value and representivity of these datasets can be obtained through actively using them, as we do in this study. For now, we therefore take the MR-TTOC data 'as is', and are cautious not to overinterpret our results.

Alternatively, ozone sondes and in situ measurements from campaigns such as TRACE-A, PEM, NOXAR, or MOZAIC could be used to test our models performance in

the tropics. The data acquired in these campaigns generally include detailed vertical information on several trace species and meteorological parameters. However, there is an important trade off to consider that can be seen as a choice between the amount of detail of information and the areal and temporal coverage. The individual campaigns usually cover periods of several weeks in a specific year, and focus on a limited geographical region. Especially near the surface, they are often influenced by local pollution or particular small scale meteorological conditions (e.g. sea-breeze, orographic flows). This is especially disadvantageous when comparing to global models that generally apply coarse resolutions and parameterizations not designed to capture these small scales. Ozone sondes and in situ measurements are much better suited to study smaller temporal and spatial scales, or the effect of a single process (e.g. biomass burning or convection). These data would therefore form an ideal basis to improve possible model shortcomings, which is the next step in our research. However, in this work we take advantage of the global, multi-year TTOC record to firstly isolate the regions, seasons, and processes that require improvement.

4.4 Measure of error

Figure 4.1 (top) shows the observed TTOC distribution in September 1992, when biomass burning emissions were particularly strong. The TOMS-based TTOC is in excellent agreement with in-situ observations [*Thompson et al.*, 1996; *Thompson and Hudson*, 1999]. Ozonesondes at Ascension Island and the near-coast locations of Brazzaville (4S, 15W) and Natal (6S, 35W), averaged 50 DU in September 1992. On aircraft flights out of Ascension during October 1992, TTOC from lidar measurements ranged from 45–55 DU [*Browell et al.*, 1996].

The South Atlantic ozone maximum clearly stands out with values $>$50DU, gradually decreasing with distance from the Atlantic, reaching minimum values between 10 and 20 DU over the Pacific Ocean. The comparison with model simulation of TTOC for the same year and month in Figure 4.1 (bottom) shows distinct differences. The absolute values of the TTOC often differ by more than the one sigma (5.3 DU) standard deviation of the measurements, and many smaller scale features are not reproduced. The discrepancies are largest over the Atlantic Ocean, where a systematic mismatch is seen between observations and model calculations. In contrast, the model reproduces the TOMS observations quite well over the Pacific Ocean. This is consistent with earlier results (Chapter 3), based on a comparison with ozone sondes from Samoa, Ascension and Natal.

Beside this 'Atlantic mismatch', there are two other important features that appear from Figure 4.1. Firstly, the amount of detail in the observations is larger. This can be partly attributed to the higher resolution of the observations, but it is also caused by a lack of variation in the model's monthly emission data. To account for the different resolutions of the datasets, we interpolated the model results to the 2°x1° degree resolution of the TTOC observations and we applied a zonal running average to the TTOC observations, with a window size equal to the zonal model grid-size (5° latitude). This filters out strong local features in the observations at resolutions smaller than the model grid, which cannot be reproduced by the model.

Secondly, it is important to note that variations in the meridional direction are small compared to the large zonal variation. Since the area depicted in Figure 4.1

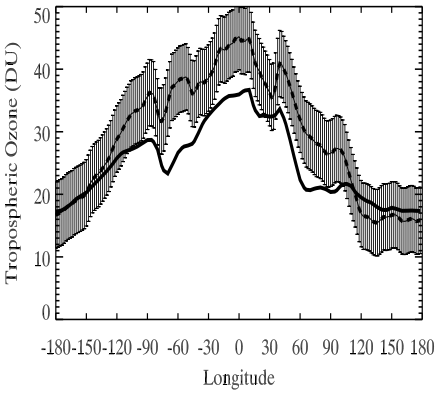

Figure 4.2: The meridionally averaged zonal TTOC distribution in model calculated (blue) and satellite retrieved (red) TTOC for September 1992. This distribution is used to define a measure of error according to equation (4.1). The shaded lines denote one-sigma standard deviation (5.3 DU). Atlantic ozonesonde and aircraft ozone data (taken within longitudes 35W to 15E) during September and October 1992 fall within the shaded region.

encompasses only 5–6 model grid boxes in the meridional direction ($\approx 19°$), the model can not reproduce fine scale structures in the meridional direction. Moreover, the zonal TTOC distribution is typically a feature on large (planetary) scale, while meriodional variations within the tropics are on a much smaller, almost local scale. Therefore, the next step in our comparison is to take the meridional average of the respective datasets at each longitude, which yields the zonal distribution of TTOC.

Zonal TTOC distribution

Figure 4.2 shows the derived zonal TTOC distribution in September 1992 for both datasets. It has already been pointed out that the MR-TTOC for September 1992 agrees well with the available sonde data near the Atlantic (location of peak in zonal maximum, Figure 2). More comprehensive ozonesonde data, collected in 1998–2000 from 10 stations across the entire tropical zone, confirm the wave-one pattern [*Thompson et al.*, 2002a]. A longitudinal cross-section of those observations, shows the wave to be associated with elevated ozone (> 45 ppbv) concentrated in the free troposphere between 50W and 50E [*Thompson et al.*, 2002b]. The distribution and intensity of the higher-ozone feature, hence the magnitude of the wave, varies with time of year, but it is always present. The regions of enhanced ozone correspond to locations where ozonesondes and other observations implicate biomass burning, lightning [*Thompson et al.*, 1996], large-scale subsidence [*Krishnamurti et al.*, 1996] and stratospheric intrusions [*Baray et al.*, 2000] as possible ozone sources.

The figure clearly shows the zonal extent of the Atlantic mismatch, characterized by model calculated TTOC values that are consistently lower than the observations over the 90W to 90E region. Although this mismatch maximizes each year in Septem-

ber, other months show a similar problem. The TTOC distribution depicted in Figure 4.2 is chosen as the focal point of our comparison. Conveniently, the TTOC retrieval algorithm uses the meridional extent of the zonal wave one pattern to distinguish tropical air masses from extra-tropical air masses. Thus, this pattern is always present in the satellite observations, and points that do not qualify as 'tropical' in the retrieval algorithm are not included in the comparison to our model calculations.

To make an objective comparison between the observed and modeled zonal TTOC distributions, a mathematical measure of error is introduced, which consists of two components. First, we define ε_1, which is simply the correlation (r) between the observed and modeled zonal wave one pattern in Figure 4.2. The parameter ε_1 indicates how well the horizontal gradients in the zonal TTOC distribution are reproduced, and how well transitions in TTOC induced by the land-sea distribution for instance are captured. The shape of this pattern is influenced amongst other factors by the location of the Inter Tropical Convergence Zone (ITCZ), the presence of biomass burning plumes, or the occurrence of large scale convection and associated lightning. Increasing values of ε_1 denote a better representation of these zonal gradients. It is important to note that ε_1 is not influenced by the absolute value of TTOC, and its value will increase only when the zonal gradients in the model calculations better fit the observations. This is advantageous because it excludes the errors in the measurements and model that are introduced through uncertainties in the tropopause height. On the other hand, the parameter ε_1 cannot be used to assess the absolute fit between the observations and the calculations.

Therefore, we also introduce a second parameter, ε_2, that is defined as the absolute deviation between observations and measurements, scaled by the standard deviation of the observations:

$$\varepsilon_2(t) \quad = \quad \frac{1}{N_{lon}} \sum_{lon} \frac{\left| \overline{TOMS(t)} - \overline{TM3(t)} \right|}{\sigma_{TOMS}} \tag{4.1}$$

Where $\overline{TOMS(t)}$ is the observed zonal distribution of TTOC for each month (t), and $\overline{TM3(t)}$ is the model calculated zonal distribution of TTOC for each month. The value of ε_2 will decrease as the discrepancy between observations and calculations decreases.

The number of longitudes used in the summation can vary depending on the scale we want to look at. For instance, in the analysis of the variability (Section 4.5), we analyze 14-year time series of ε_2 at each location (N_{lon}=1, t=168), while for the analysis of our sensitivity runs (Section 4.8) we subdivide the zonal domain into only two regions; a Pacific region (N_{lon}=90, t=168) and an Atlantic region (N_{lon}=90, t=168). Together, ε_1 and ε_2 enable us to quickly and objectively quantify the agreement with the TTOC observations, and intercompare the results of different model simulations.

Algorithm test

In order to assess the robustness of our algorithm, and to get an indication of the sensitivity of ε_1 and ε_2, we have applied our measure of error to a series of test distributions of ozone in a Monte-Carlo like approach. Thereto, an ensemble of one hundred 3-dimensional ozone distributions was created, in which each gridpoint of

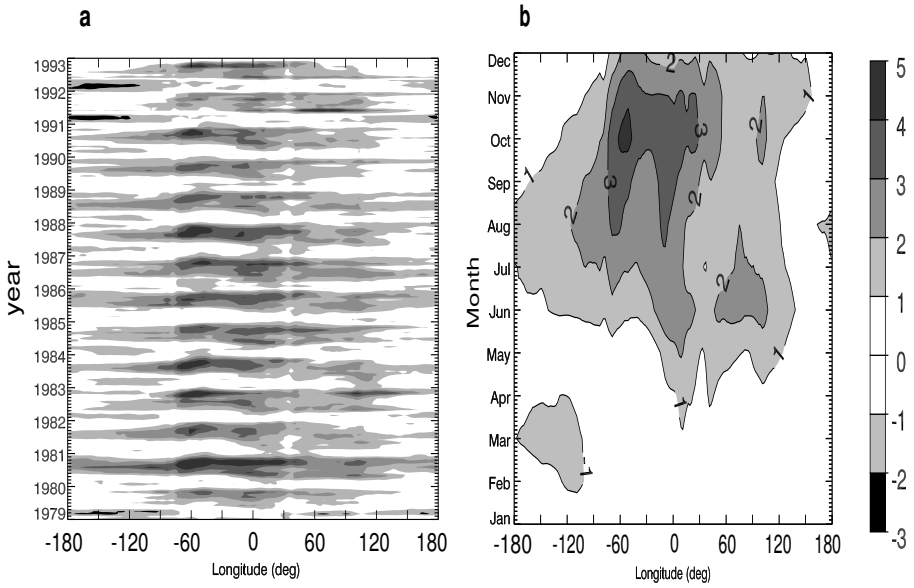

Figure 4.3: (a) Hövmoller plot of ε_2 as a function of longitude for the period 1979–1992. (b) 14-Year average seasonal cycle of ε_2 as a function of longitude. A value of 1 denotes a difference of 5.3 DU ($1\times\sigma$) between model and observations. The +/– signs were added to the colorbar to signify model underestimates or overestimates repectively.

an actual model calculated ozone distribution was randomly perturbed by an average of $\pm$ 10 %. These random perturbations represent the effects of for instance anomalous winds, convective venting, or unexpected emissions of ozone precursors that could disturb the ozone concentration within a gridbox in a non-systematic way, that is nevertheless substantial in magnitude. Next, we have integrated the columns, averaged to make the zonal pattern, and then calculated the yearly values of ε_1 and ε_2 for each of the one hundred perturbed distributions. The distribution of ε_1 and ε_2 in this ensemble reveals the spread that can be expected from relatively large, but random perturbations. Any change in ε_1 and ε_2 that is significantly larger (more than 1σ) than this, should then be seen as a systematical change of our model calculated ozone field.

From our one hundred member ensemble, we have derived a one-sigma standard deviation of $\pm$ 0.001 for ε_1, and $\pm$ 0.01 for ε_2. We can thus say that the small differences we report in Section 4.6 and Table 4.1 represent a systematic difference between the calculated ozone fields from different years, and under different scenarios.

4.5 Comparison of TTOC

As a first step, we calculate the values of ε_2 for each longitude and each month (t=168) of our multi-year simulation. The result is shown in Figure 4.3a, where a negative sign indicates that the model calculated values are higher than the observations. It shows that the values of ε_2 range from 0–2 σ ($\sim$ 0–10 DU) over the tropical Pacific, to more than 3–σ ($\sim$16 DU) over the tropical Atlantic. The largest underestimates occur during August through November. The model calculated values of TTOC are generally lower than the observations. The only time the model overpredicts the TTOC values is in Dec-Jan-Feb over the Pacific Ocean.

It is clear from Figure 4.3a that the Atlantic mismatch is the most serious problem in our comparison, and that it is an annually recurring feature. In contrast, high values of ε_2 over the Pacific Ocean appear for several years, but not in all. To separate these systematic differences from the ones that occur occasionally, we have decomposed each time series of ε_2 into a seasonal cycle, and a component of interannual variability. For a discussion of the interannual variability in TTOC we refer to Chapter 3. The seasonal cycle of ε_2 is shown in Figure 4.3b. The figure confirms that most of the Atlantic mismatch is caused by seasonal differences. On average, the seasonal cycle contains 75% of the variance of the ε_2 time series over this region. In contrast, the seasonal cycle of ε_2 over the Pacific Ocean explains less than 50% of the original variance. If we consider the relative errors, both deviations translate to ca 30% of the observed TTOC. From this, we can conclude that the most important model improvements should focus on the seasonality of TTOC over the Atlantic Ocean. Possibly, the Pacific region would profit from such improvements as well, since the two regions are coupled through transport.

4.6 Influence of transport

The coupling between the regions through transport is not the same in each year due to the occurrence of anomalous meteorological conditions such as those induced by ENSO. Through the use of ECMWF wind fields for each year, we have included this transport variability, and in Chapter 3 we showed that the effect of ENSO on TTOC is present in our multi-year simulation. In this section, we will apply our measure of error to quantify the influence of transport on our results.

We compare each year of TTOC observations with each year of our multi-year simulation. In our multi-year simulation, we have 15 years of calculated TTOC, which differ in meteorology (including lightning), stratospheric upper boundary conditions for ozone, and the anthropogenic emissions which include trends over the 1979–1993 period. In this section, we use yearly averaged values for 1979–1992 of the monthly calculated ε_1 to assess the performance of our model. Since ε_1 is independent of the absolute values of TTOC, the influence of increasing emissions in the multi-year simulation is largely excluded in this comparison. Thus, any year-to-year difference in ε_1 is due to changes in meteorology (including changing lightning patterns).

For each year of the TOMS observations (1979–1992, n=14), we have calculated 14 values of ε_1; one value for each year of simulations (1979–1992, m=14). These individual values of ε_1 denote the success in simulating the observed zonal distribution of TTOC, given the specific meteorological conditions of each of the 14 simulated

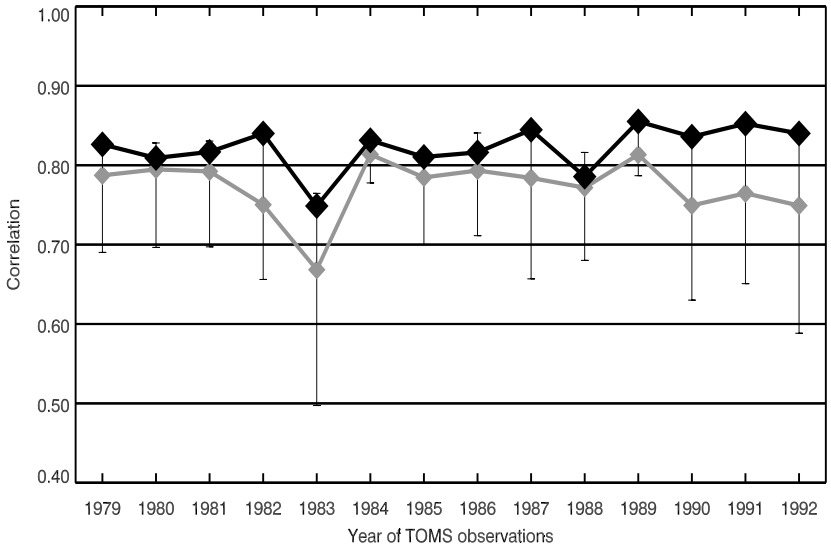

Figure 4.4: Correlation coefficient (ε_1) between the zonal TTOC distribution in observations and simulations. For each year of TTOC observations (1979–1992) correlations were calculated with each year of a multi-year simulation with our CTM (1979–1992). The bars denote the range of correlations, the red diamonds are the averages. This value is representative for a simulation with 'climatological' meteorology. The green diamonds signify the correlation when the correct meteorology of the year of observations is applied to the model.

years. The average ε_1 of these individual years would represent the value when a random year of meteorology is applied, while there is one value of ε_1 that corresponds to the correct meteorology matching the year of TTOC observations.

Figure 4.4 shows the multi-year average value (grey diamonds) and range of interannual variation (bars) for each of the 14 years TTOC observations, as well as the values of ε_1 for the model year corresponding to the year of observations (filled diamonds). The simulations with actual meteorology consistently perform better than average. In fact, the simulation with actual meteorology generally ranks higher than any other year. This is due to the fact that meteorological conditions determine to a large extent the location of local ozone maxima, as well as the zonal gradients in TTOC. Although the differences between a correlation of 0.7 and 0.84 might seem small, the fact that these differences show up in a yearly and meridionally averaged TTOC distribution indicates that the individual differences are in fact quite large, and certainly significant given the sensitivity of ε_1 (Section 4.4).

From the figure one can also see that the 14-year average value of ε_1 varies from year-to-year, as does the range. This shows that some years of observations are more difficult to model than others presumably because their specific conditions are more difficult to capture. This is obvious for 1982/83, when El Niño conditions prevailed. While the simulation with actual meteorology performs well, some other years show

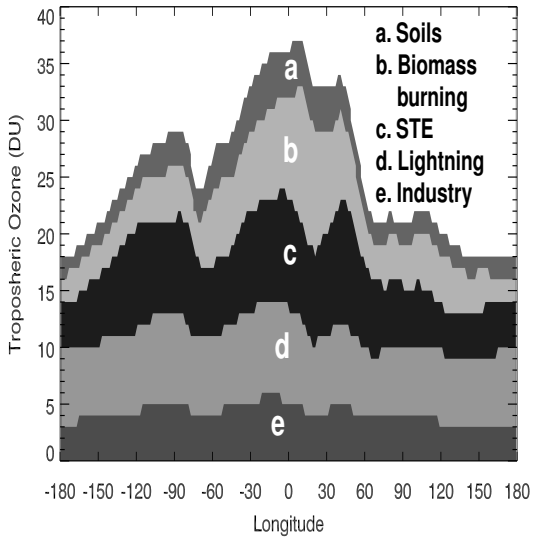

Figure 4.5: Absolute contribution of several processes to the modeled TTOC distribution. Processes include photochemical production of ozone following NO_x emissions from soils, lightning, biomass burning and industrial sources, as well as ozone from stratosphere-troposphere exchange. Values for September 1992.

a poor correlation. This indicates that in such a year, the zonal TTOC distribution can not be modeled very well if one does not consider the specific meteorological conditions during ENSO. The fact that the maximum of ε_1 for 1983 is the lowest in the whole series shows that other processes than transport that change during ENSO also influence the shape of the zonal TTOC distribution. Such processes include the occurrence of wildfires following anomalous droughts. Although this was shown to have a large impact on TTOC [*Chandra et al.*, 1998; *Thompson et al.*, 2001], it was not included in our multi-year model simulations. Adding this variability in emissions to the model is a difficult challenge, for which tools are currently being developed [*Duncan et al.*, 2002].

4.7 Role of photochemistry

Beside the previously mentioned wildfires, other sources contribute to the photochemical production of ozone in the troposphere, and thus partly determine the zonal distribution of TTOC as depicted in Figure 4.2. By using the labeled tracers (see Section 4.2), we have calculated the contribution of several tropospheric ozone sources to the modeled TTOC distribution. The processes that were thus separated are photochemical ozone production from lightning, industrial, biomass burning, and soil NO_x emissions, as well as the contribution from the stratospheric influx of ozone. Figure 4.5 shows the contribution of these processes to the modeled zonal TTOC distribution

Table 4.1: Experiments conducted and their values of the parameter ε_1 or ε_2. Experiments that meet the criteria described in Section 4.8 are preceeded by a →, and discussed in the text. Improvements in ε_1 are achieved from a more than 0.001 increase in value, and improvements in ε_2 from a 0.01 decrease.

Experiment	ε_1	$\varepsilon_{2,Pac}$	$\varepsilon_{2,Atl}$
Base	0.842	0.77	1.80
	Biomass burning		
→2× NO_x	0.848	0.71	1.58
→2× CO	0.843	0.73	1.71
→2× NMHC	0.844	0.76	1.77
2× J(HNO_3)	0.702	0.82	1.79
→Injection height	0.853	0.72	1.52
→Alternative calendar	0.852	0.76	1.74
	Lightning		
→2× NO_x lightning	0.848	0.52	1.08
5× NO_x oceans	0.723	0.62	1.26
Pickering profiles	0.797	0.69	1.67
Coupling to conv. prec.	0.814	0.82	1.81
land/ocean ratio 2:1	0.762	0.70	1.85
	Other		
→5 DU offset	0.842	0.57	1.01

in September 1992.

Ozone production from industrial NO_x emissions contributes several DU to the modeled ozone concentration. There is only very little difference in zonal direction, because the most important source is located in the NH extra-tropics. Transport in longitudinal direction by the powerful jet streams of the NH and SH occurs more rapidly than meridional transport to the tropics and across the ITCZ, leading to a largely zonally invariant distribution in the tropics.

Lightning NO_x emissions in the tropics are stronger over the continents than over the oceans. Yet, the distribution of TTOC from lightning NO_x does not show much structure in zonal direction, because the NO_x enriched air is brought into the middle and upper free troposphere, where transport is fast, and the lifetime of ozone relatively long. The monthly mean signal of ozone from lightning NO_x is therefore seen throughout the tropics, adding 5–8 DU of ozone to most columns. The strongest influence is seen over the Atlantic Ocean and South American continent.

An almost equal contribution to TTOC comes from stratosphere-troposphere exchange. However, most of this ozone is located at the edges of the domain in our analysis, where the subtropical jet sometimes penetrates far equatorwards. This happens at locations where the jetstream is disturbed most frequently: near surface orography and land-sea barriers. Thus, most of the stratospheric ozone encountered in the tropical troposphere in our model has crossed the tropopause in the sub-tropics, and is subsequently transported equatorwards from these locations where disturbances in

the jetstream occur.

The strongest contributors to the 'wave one' character of tropical TTOC are soil NO_x emissions and biomass burning NO_x emissions. Both these sources are terrestrial surface sources (50% of soil emissions occur in the tropics), which maximize over South America and Africa. The ozone produced from these NO_x emissions is transported more slowly in the lower free troposphere, and has a shorter lifetime there. It therefore slowly accumulates over the Atlantic, but exerts only little influence on the more distant tropical Pacific region.

The seasonality of ozone from biomass burning (not shown) is very similar to the seasonality of ε_2 in Figure 4.3. In contrast, ozone produced from lightning NO_x emissions displays its maximum in April-May-June, while ozone produced from soil emissions is almost constant throughout the year. This again suggests that biomass burning could be partly responsible for the observed Atlantic mismatch. To see which part of our treatment of biomass burning could be the cause of the seasonal ozone underestimate, we have performed a sensitivity analysis.

4.8 Sensitivity analysis

Beside our treatment of biomass burning emissions, the sensitivity analysis includes simulations to investigate uncertainties in the lightning NO_x emission parameterization. These two processes occur predominantly in the tropics, in contrast to industrial emissions, soil emissions and STE. Although the seasonality and zonal distribution of lightning NO_x emissions do not match the pattern of ε_2 (Fig 4.3), its large contribution to the ozone budget and large uncertainties in magnitude and distribution justifies a more detailed look at its parameterization.

Strategy

To ensure an objective intercomparison between different model simulations, we now define ε_2 for two different regions. The first region encompasses all longitudes between 90W and 90E (N_{lon}=90, 'Atlantic'), and the other region encompasses the longitudes outside this area (180W–90W and 90E–180E, N_{lon}=90, 'Pacific'). Since the good performance of the model over the Pacific Ocean was determined independently by comparison with ozone sondes (Chapter 3), our strategy to determine whether a simulation constitutes an improvement over our base run is: 1) ensure that ε_2 for the Pacific fit does not increase; 2) achieve a decrease of ε_2 for the Atlantic mismatch, and 3) increase or maintain the value of ε_1. Only when these three criteria are met, a systematic improvement of modeled TTOC has been achieved. This has turned out to be a very strict constraint due to the large number of observations and the scale of the phenomenon. All the sensitivity simulations pertain to the year 1992.

Table 4.1 presents an overview of all the sensitivity simulations that were performed, and their yearly average values of ε_1 and ε_2. The base simulation is the model as used in Chapter 3 as well as in the previous sections of this work. The simulations that meet the criteria described above are highlighted in boldface. These simulations are discussed briefly in this section. We repeat that the aim of these simulations was to prioritize directions for further research. Therefore, the analysis and

Table 4.2: Budgets of ozone in the base run, and in a simulation with double NO_x emissions from biomass burning. The last column shows the difference between both simulations . Numbers are tropospheric integrals over the tropical Atlantic region and adjacent continents [80W–40E,12S–12N][a] for the year 1992.

	BASE (A)	double NO_x (B)	B-A
Chem. production	+1095	+1200	+105
$NO+HO_2$ (%)	62	62	0
$NO+CH_3O_2$ (%)	16	16	0
$NO+XO_2$ (%)	17	17	0
$NO+CH_3COO_2$ (%)	5	5	0
Chem. destruction	-951	-1019	-68
O_3 + hv (%)	59	58	-1
O_3 + OH (%)	10	10	0
O_3 + HO_2 (%)	25	26	+1
O_3 + HC[b](%)[b]	6	6	0
Net chemistry	+144	+181	+37
Advection	+26	+7	-19
Dry deposition	-166	-182	-16
STE[c]	0	0	0
Total	+4	+6	+2
Tropospheric burden	40	42	+2

[a]Units are $TgO_3\,yr^{-1}$.
[b]HC denotes isoprene, ethylene and olefinic hydrocarbons.
[c]direct STE in this region is negligible.

discussion of these simulations will be only brief, and simulations that did not qualify as improvements will not be addressed.

Three of the possible improvements are related to biomass burning. Simulations were performed with an increased injection height of biomass burning products, double NO_x emissions from biomass burning, and an alternative fire calendar, respectively. These experiments increase the amount of NO_x in the free troposphere over the tropical Atlantic, and thereby increase the photochemical production of ozone. The amount of NO_x reaching the free troposphere is determined by the complex interaction between emissions, deposition to the surface, oxidation by OH, and convective venting from the planetary boundary layer (PBL).

The efficiency by which an NO_x molecule contributes to ozone formation depends to a large extent on its lifetime, i.e., its ability to reach the free troposphere and avoid dry deposition or oxidation to HNO_3. Due to the dry conditions prevailing during

biomass burning events, strong convective systems can be assumed to be absent near large fires. Moreover, NO_x has a lifetime of only several days in the PBL, and in its oxidized form (HNO_3) surface deposition is even faster and rainout during convective transport occurs quickly. Therefore, the interaction between meteorology and emissions largely determines whether a NO_x molecule will reach the free troposphere, or will be oxidized and/or deposited in the PBL. Our three successful experiments influence this interaction in three different ways.

Firstly, we reduce rapid deposition of NO_x in the PBL and increase the concentration in the free troposphere by distributing the biomass burning NO_x emissions over the lower 6 km of the troposphere. Obviously this is arbitrary, but it shows that an improvement would be realized if more biomass burning NO_x were transported to the free troposphere in our model. This could indicate a lack of transport of biomass burning products from the planetary boundary layer (PBL), which is plausible since this parameterization depends on 6-hourly updated diffusion parameters, that can not adequately capture the diurnal growth and decline of the PBL. Using Rn^{222}, *Dentener et al.* [1999] already noticed that our model appears to underestimate convective venting of the PBL over the African continent. It could also indicate that biomass burning smoke plumes may reach the free troposphere on their own buoyancy, which is not included in our model. Finally, *Yienger and Levy* [1995] suggested that post-burning soil emissions of NO_x could contribute to the emission budget. These emissions could easily reach the free troposphere under unstable or convective conditions occuring after the fire activity has ceased.

In addition, the interaction between transport and biomass burning in the model could be improved through implementation of a more realistic fire calendar. As a result, the location and occurrence of convection would become more consistent with the emissions. The convective vertical exchange of NO_x decreases in July and August, and increases by 15% in September and October. This leads to more ozone production in the free troposphere during these months. This agrees well with the findings of *Cooke et al.* [1996] and *Galanter et al.* [2000], who applied more detailed alternative fire calendars to point out shortcomings in the inventory of *Hao and Liu* [1994]. The fact that ε_1 increases significantly indicates that the interaction between biomass burning and convection has a strong influence on the zonal TTOC gradients.

The third important parameter in the description of biomass burning is the emission magnitude. A doubling of the emissions of NO_x from biomass burning also increases the flux of NO_x from the planetary boundary layer. Table 4.2 shows the consequences for the tropospheric ozone budget. The increase in production of ozone is largely balanced by an increase in destruction, as well as by an increase in deposition and an increase in advection of ozone out of the Atlantic region. The net effect of a doubling of the NO_x emissions is therefore a 2 Tg increase in ozone, which is only 5% of the tropospheric burden. The effect on the TTOC columns is similar (appr. 2 DU). The effect of increased emissions is more pronounced when it is coupled to the alternative fire calendar. In fact, this simulation shows the highest sensitivity. This suggests that the correct representation of the occurrence and magnitude of biomass burning is an important prerequisite to model TTOC, in agreement with *Galanter et al.* [2000].

An alternative method to increase the concentration of NO_x in the free troposphere is through lightning NO_x emissions. Our current emission magnitude of 4.6 $\mathrm{TgN\,yr^{-1}}$ is in the lower part of the range of Inter Governmental Panel on Climate

Change (IPCC) estimates (4–20 $TgN\,yr^{-1}$ [*IPCC-TAR*, 2001]), and a doubling would still be within the uncertainty limits (although at the high end of currently used values in global models). Table 4.1 shows that this would yield an improvement in our comparison to TTOC. Clearly, the impact of this parameter is very large, and an increase in tropical lightning NO_x emissions would give better agreement with TTOC observations. However, this would also strongly affect the concentrations of ozone in the extra-tropics where ∼20% of the emissions occur in our model. This would lead to a large overestimate of ozone over Europe, the United States, and Asia, where ozone concentrations were previously modeled well [*Lelieveld and Dentener*, 2000]. Although this good agreement could be a fortuitious result of several uncertain processes, we cannot neglect this important side effect of an increase in lightning NO_x emissions. In the alternative parameterization of *Meijer et al.* [2001], the percentage of extra-tropical emissions would be even higher (30%), and the sensitivity in the extra-tropics even larger. Alternatively, we adjusted the lightning NO_x emissions through changing the land/sea emission ratio, the emission magnitude over the oceans, and through inclusion of vertical distribution profiles of emissions according to *Pickering et al.* [1998]. However, none of these simulations met the criteria of a systematic improvement. For now, we will therefore only state that TTOC in the tropics is very sensitive to lightning NO_x emissions, and further studies are urgently called for.

4.9 Vertical ozone profiles

To illustrate the results of our sensitivity experiments we present a comparison with selected vertical ozone profiles from several tropical stations. These stations are part of the SHADOZ program, which encompasses 11 ozone sonde stations throughout the tropics. The details of the different stations and a comparison to TOMS data and ground-based measurements can be found in *Thompson et al.* [2002a, b].

Figure 4.6 shows six observed (black solid lines) vertical ozone profiles from selected stations and dates from the year 1998, as well as several model calculated profiles for the same day in 1998. These modeled profiles show results from a standard model simulation (grey dotted lines), a simulation with the meteorology of 1997 applied (long dashed), and a simulation with doubled biomass burning NO_x emissions and an alternative fire calendar (solid grey lines).

In many cases, the base simulation captures the general shape of the vertical ozone profile quite well (a,b,c,d,f), while the simulation with wrong meteorology does not (a,b,d,f). This again illustrates the importance of large-scale transport in modeling tropospheric ozone, which we also concluded from our comparison to TTOC in Section 4.6. As expected, adjusting the emission parameterization most strongly influences the stations over the Atlantic Ocean and African continent (c,d,e,f). What is most important to note from the comparison however, is that many features of the individual sonde profiles are not reproduced by the model. Adjusting the biomass burning emission parameterization, or any of the other parameters we tested, does not appear to lead to systematic improvements.

There are several reasons for this. First of all, we mention the difference in vertical resolution, which strongly limits the amount of detail our model can produce. Secondly, we mention the strong damping present in the ozone production, which is

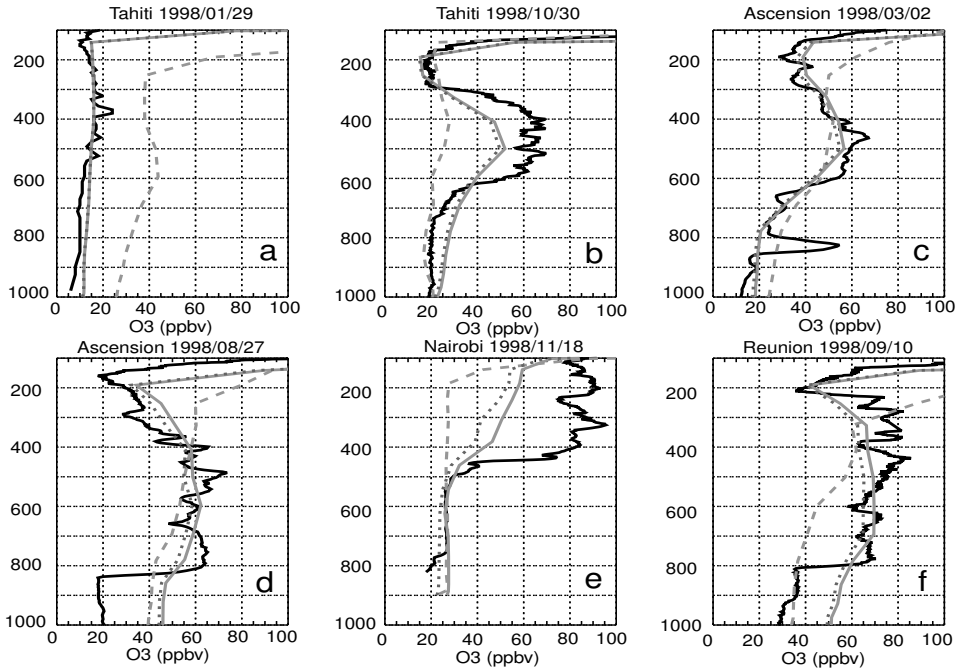

Figure 4.6: Selected sondes from six SHADOZ stations in 1998. The profiles show observations (black), a standard model run for 1998 (short dashed), a model run with meteorology from 1997 (long dashed), and a model run with additional NO_x emissions and a new fire calendar (grey solid).

obvious from the small differences between the short dashed and solid grey lines in Figure 4.6 and from Table 4.2. Generally, the ozone mixing ratios increase by approximately 0–5 ppbv at all altitudes, leading to an increase of several Dobson Units when vertically integrated. This difference is small compared to the observed underestimate of TTOC. Finally, the comparison presented is obviously hampered by the representation of different spatial scales. When we try to improve our model through changes in the parameterizations, the response seems to be strongest on the large scales which are dominated by transport in our model, while the smaller scales remain largely unaffected. Since these smaller scales are dominant in the ozone sondes, intercomparing the different model runs does not convey much information on the performance of the models parameterizations. In fact, it is impossible to judge from Figure 4.6 which simulation performs better; grey solid or short dashed?

The comparison illustrates that individual sondes are not the best product to use when testing a CTM. As was recognized previously by *Logan* [1999], climatologies of ozone observations are more useful in this respect (see also Chapter 3), even though they lack interannual variability and the density of the measurement network is quite low. We show that the use of TTOC offers a suitable alternative, where the lack of vertical information is 'compensated' by the geographical coverage, the frequency of observations, and the length of the observational record.

4.10 Discussion

Our model evaluation depends to some extent on the accuracy of the TTOC data as well as their assumed standard deviations. The meteorological variability in the model and in the satellite TTOC dataset is very similar, which provides some confidence in the retrieval algorithm applied to produce this dataset. Even though the MR retrieval applies sonde observations from two specific years (1990–1991) to produce the entire 1979–1992 record, the details of individual years seem to have been retained well. Nevertheless, the accuracy and the standard deviations of the TTOC observations are not yet well quantified because the ozone sondes did not provide an absolute reference due to the limited spatial and temporal coverage [*Thompson and Hudson*, 1999].

To illustrate possible effects, we calculated the values of ε_1 and ε_2 after applying a uniform negative 5 DU offset to the TTOC measurements. This brought model and measurements almost within one-sigma, and was an even more effective way to reduce the underestimate of TTOC than any of our sensitivity simulations. However, a 5 DU offset in TTOC cannot be justified, and the dependence of ε_2 on the accuracy of the measured TTOC columns does not invalidate our approach. If the TTOC measurements change, for instance due to an update in the retrieval algorithm, ε_2 can easily be re-defined to focus on regions that consequently appear most problematic, and then applied to the sensitivity runs to isolate possible solutions. Nevertheless, a thorough validation of the retrieved TTOC data using ozone sondes, as well as a more detailed quantification of the uncertainties would add to the usefulness of these data in global modeling studies.

The fact that a 5 DU reduction in the observations would have greater impact than any of our sensitivity simulations further illustrates the robustness of ozone to perturbations. This is also obvious from the small ranges in ε_1 and ε_2 in Table 4.1. Although the change in boundary conditions is often quite extreme (factor of two), the response of ozone is only small. Table 4.2 illustrates that this nonlinear, damped response is mostly due to strong feedbacks in the NO_x–HO_X chemistry, as well as in the deposition working against any change in the concentrations of ozone, NO_x, and HNO_3. These feedbacks are especially important in the tropics, since both photochemistry and uptake of trace gases by vegetation depend strongly on the sunlight intensity. It is also the non-linearity of the system that requires CTMs to use sophisticated mathematical solvers for the chemistry with small time steps to solve the system of partial differential equations (PDE's), which generally consumes a large amount of computer resources.

An effective way to reduce the demand of computer resources is by pre-calculating the solution of the system of PDE's for many different boundary conditions and initial conditions. The solution of the system at each time step is then retrieved from an archive of solutions matching the forcing. *Klonecki and Levy* [1997] have shown that this can be done in a way that retains many of the feedbacks, and their model performs well in simulating tropical ozone, CO and NO_x. However, the interaction between NO_x and HO_x was not included in their simulations, which removes part of the nonlinear response of ozone. Therefore, the method of *Klonecki and Levy* [1997] produces more ozone over the tropical Atlantic and displays greater sensitivity to forcing (see also *Galanter et al.* [2000]). We speculate that the sensitivity of such models will usually be larger than in models that calculate the solution of the PDE's

at each time step.

Our results show that the meteorology particularly strongly influences the distribution of ozone. It is striking that the range of values of ε_1 in Figure 4.4 is much larger than the range in Table 4.1. Apparently, zonal gradients in TTOC are largely determined by transport, and the location of lightning NO_x emissions that are coupled to transport. Using actual meteorology has clear advantages over 'climatological' meteorology, because the interannual variability is large, also addressed in Chapter 3. Although the differences in correlation might seem quite low, we have shown that they are much greater than can be expected from random perturbations. The fact that improvements can be achieved indicates that the differences associated with transport are an important aspect of the models performance. Nevertheless, many models still rely on climatological wind fields, or apply one year of meteorological analyses to simulate any year of interest. This approach will yield results that are best compared to climatologies of observations, and are much less suited to study multi-year time series, or instantaneous distributions of species with lifetimes that are smaller than, or comparable to, the time scale of transport.

The requirements of the model concerning meteorology are very demanding. Not only does large scale transport determine the shape of the zonal TTOC distribution, meteorology also introduces interannual variability, and its interaction with biomass burning emissions is one of the most sensitive model parameters. However, meteorological conditions in the tropics are complex, and their representation in numerical weather prediction models such as the ECMWF model suffers from a lack of in-situ measurements that are used as constraints. Especially subgrid scale vertical mixing processes are difficult to model. This includes the vertical transport of biomass burning plumes. *Mauzerall et al.* [1998] estimated that the majority of ozone production takes place in these plumes. It thus seems obvious that besides improvements of our knowledge on the occurrence and intensity of fires, further improvements should focus on the sub-grid representation of turbulent and convective transport of biomass burning plumes, as well as the chemistry in these plumes.

Our study shows most convincingly that it is very unlikely that a single factor affecting ozone is responsible for the observed differences between model and observations. Given the serious disagreement, and the sensitivities as presented in Table 4.1, a combination of processes would be required to bring observations and model within one-sigma. This fact, together with the strongly damped response of ozone to the applied forcing strongly complicates attempts to infer information on model parameters (e.g. lightning NO_x and biomass burning emissions) from the tropical distribution of TTOC. The simultaneous use of global CO and NO_x observations, for instance, could be useful in this respect, as these could help to constrain the emissions. Ongoing developments in remote sensing might make these products available on spatial and temporal scales suitable for the approach presented in this work.

4.11 Conclusions

We have combined satellite observations of TTOC with model calculations to test the performance of our model and prioritize directions for improvement. Such a systematic comparison of model calculations with satellite observations has not been performed before, and it yields interesting insights in problems and possibilities asso-

ciated with the use of increasingly available space-borne tropospheric observations. Through a large number of simulations, we were able to quantify the influence of meteorology, as well as biomass burning and lightning NO_x emissions on the simulation of TTOC. Our most important conclusions are:

- With a standard set of emissions such as in *Houweling et al.* [1998]; *Lelieveld and Dentener* [2000]; *Peters et al.* [2001] the Atlantic TTOC maximum is not sufficiently captured, whereas the interannual variability over the Pacific Ocean is represented quite well.
- Using actual meteorology in a model is the most important prerequisite in reproducing the horizontal and vertical distribution of tropical tropospheric ozone.
- Efficient feedbacks in the tropical ozone budget strongly dampen the response of ozone to changes in precursor emissions.
- Systematic improvements in our model can be achieved through a better representation of the biomass burning timing and magnitude, including their interannual variability. Further studies should focus on these processes, as well as the parameterization of lightning NO_x emissions.
- Quantitative use of satellite derived TTOC to test a global model is a promising approach, that would strongly profit from a more detailed quantification of the uncertainties in TTOC data.

Acknowledgments. We would like to thank Dr. Simon Pinnock of JRC for providing the fire counts and Rinus Scheele of the KNMI for his help in processing the ECMWF meteorological data. We also thank Dr. Jennifer Logan of Harvard University, and the National Oceanic and Atmospheric Administration (NOAA), the Climate Monitoring and Diagnostics Laboratory (CMDL), and the Carbon Cycle Group for making their data available through the internet. Finally, we thank the reviewers for their elaborate comments and helpful remarks.

Chapter 5

Stability of tropospheric hydroxyl chemistry

[1]Based on a publication in *Journal of Geophysical Research*, with J. Lelieveld as first author, and W. Peters, M.C. Krol, and F.J. Dentener as co-authors.

Abstract

Tropospheric hydroxyl (OH) is the cleaning agent of the atmosphere since most oxidation processes are initiated by OH. If the OH chemical system were unstable, runaway growth of oxidants (autocatalytic conditions) or of reduced gases (catastrophic conditions) might occur, especially since the atmospheric composition is changing rapidly. We present simulations with a global chemistry-transport model, indicating that during the past century global mean OH has nevertheless remained nearly constant. This constancy is remarkable because CH_4 and CO, the main OH sinks, have increased strongly. We studied the system sensitivity to perturbations using the OH recycling probability, calculated from primary OH formation and OH recycling. We conclude that the constancy of global mean OH does not imply that regional OH has not changed or that the system is insensitive to perturbations. Over the tropical oceans, where OH concentrations are highest, the system stability is relatively low. During the past century the OH concentration decreased substantially in the marine troposphere, however, on a global scale it has been compensated by an increase over the continents associated with strong pollution emissions of nitrogen oxides. Our results suggest that the changing atmospheric composition during industrialization has been accompanied with a 60% increase of the tropospheric oxidation power (i.e. gross OH production).

5.1 Introduction

Atmospheric oxidation processes largely proceed along reaction chains that are initiated by hydroxyl radicals (OH) [*Levy II*, 1971]. Although other oxidants can also initiate such reactions, OH is by far dominant so that we focus on this molecule. The primary formation of OH is mediated by ozone (O_3), which, in the stratosphere, is produced from O_2 photodissociation. A small fraction of stratospheric O_3 is transported to the troposphere, which constitutes a baseline OH source. Additionally and most importantly, OH is formed from O_3 that is produced by in-situ photochemistry within the troposphere. The reactions are initiated by ultraviolet (UV) sunlight. Figure 5.1 shows that primary OH formation is controlled by ozone, UV radiation and water vapor in reactions R1-R4. UV radiation fluxes, in turn, are strongly dependent on the solar zenith angle and the overhead O_3 column. Therefore OH levels are highest in the tropics where the stratospheric ozone layer is thinnest and the absolute humidity is highest. For a historical overview of the global scale processes involved we refer to *Logan et al.* [1981]; *Perner et al.* [1987]; *Spivakovsky et al.* [1990, 2000]; *Ehhalt et al.* [1991]; *Thompson* [1992]. The tropospheric lifetime of OH is very short, a few seconds, because it rapidly reacts with carbon monoxide (CO) and hydrocarbons, in the background troposphere notably methane (CH_4) [*McConnell et al.*, 1971; *Crutzen*, 1973; *Chameides and Walker*, 1973]. Although CH_4 and CO constitute efficient OH sinks, these reactions do not necessarily deplete OH because part of the radicals can be recycled, e.g. by the action of nitrogen oxides (NO_x = NO + NO_2). Figure 5.1 shows that in the presence of NO, O_3 is produced and OH is reformed through reaction R7 (Cycle 1).

NO_x is removed within a few days, i.e. close to the sources, by the formation of nitric acid (HNO_3), predominantly by reaction with OH, and also through heterogeneous conversion on aerosols and clouds at night. The lifetime of CO, on the other hand, is much longer, about two months, so that it can be transported over thousands of kilometers. The lifetime of CH_4 is about eight years so that it is globally well mixed. In NO_x depleted air far downwind of pollution sources reaction R7 between NO and HO_2 is insignificant and the alternative Cycle 2 prevails (Figure 5.1). In this case O_3 is destroyed and the HO_2 radicals can recombine into hydrogen peroxide (H_2O_2). This terminates the radical reaction chain because a large part of the H_2O_2 is removed by dry and wet deposition, being a definitive sink of HO_x radicals (HO_x = OH + HO_2).

The stability of the OH chemical system, as affected by emissions of NO_x, CO and CH_4, has been extensively studied with photochemical box models [*Guthrie*, 1989; *Kleinman*, 1994; *Prather*, 1994; *Stewart*, 1995; *Krol and Poppe*, 1998; *Poppe and Lustfeld*, 1996; *Hess and Madronich*, 1997]. It appears that under NO_x depleted conditions OH recycling is inefficient and HO_2 recombination into H_2O_2 predominates. When concentrations of CO and CH_4 are very high and growing rapidly, such conditions can become catastrophic. Conversely, under conditions where OH recycling is very efficient, the system can become autocatalytic, leading to a runaway of oxidants. At high NO_x levels OH recycling is quite efficient, however, the reaction between NO_2 and OH gains importance as a sink of HO_x. At very high NO_x mixing ratios (> 10 nmol/mol) NO_2 can deplete OH to very low levels. The previously mentioned box model studies have shown that the high NO_x system can become unstable, and that short periods with high (initially autocatalytic) OH formation are followed by long periods of OH suppression. However, in the atmosphere such conditions are rare and

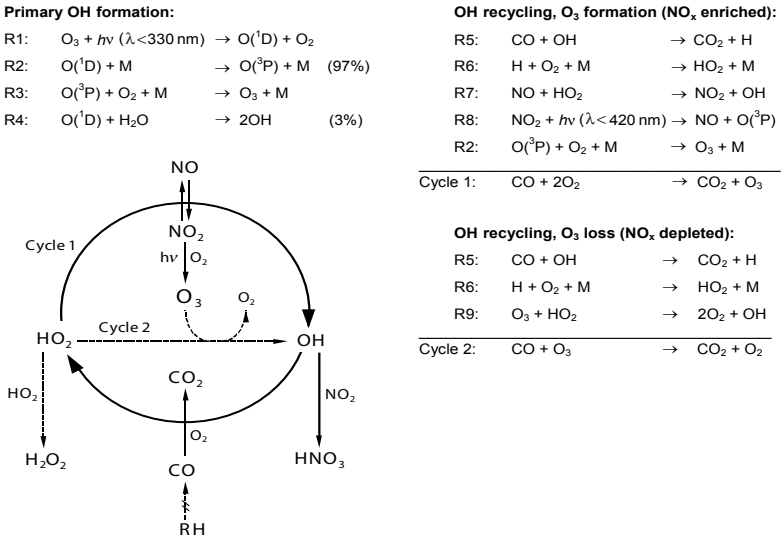

Figure 5.1: Reaction cycles of OH and HO_2 as determined by reactions with CO and NO_x. RH represents hydrocarbons (on a global scale dominated by CH_4). In reactions R2,3,6 collisions with air molecules (M) dissipate excess energy. About 3% of the $O(^1D)$ atoms formed in the troposphere through reaction R1 produces OH. Cycle 1 regenerates OH and produces O_3, while Cycle 2 (dashed) destroys O_3 hence reduces primary OH formation. H_2O_2 and HNO_3 are important sinks of HO_x at NO_x depleted and highly NO_x enriched conditions, respectively

spatially confined since transport and mixing processes lead to rapid dilution.

We have investigated global OH in view of paradoxical reports about historical OH variations. On the one hand, analyses of multi-year methyl chloroform measurements (MCF: 1,1,1-trichloroethane), a man-made trace gas that is removed by OH, and of which sources and atmospheric concentrations are well quantified, suggest large OH changes of 5-15% per decade since 1979 [*Krol et al.*, 1998; *Prinn et al.*, 2001]. Re-analysis of the MCF measurements, based on modified MCF emission data, has moderated this conclusion [*Krol et al.*, 2002; *Krol and Lelieveld*, 2002]. On the other hand, model simulations constrained by ice core measurements have shown that global OH changes during the past century have probably been small, in spite of CH_4 and CO increases in excess of a factor of two [*Pinto and Khalil*, 1991; *Lelieveld and van Dorland*, 1995; *Wang et al.*, 1998].

Here we present simulations with a global chemistry-transport model to study changes in the concentration and distribution of OH in the troposphere during the past century. We introduce several concepts to help analyze these changes. The oxidation power of the troposphere, for example, is defined as the global gross OH formation (the concept is also applied to smaller scales). We avoid using the term oxidation efficiency because it is often related to specific compound to be oxidized, and therefore difficult to determine [*Lawrence et al.*, 2001]. We furthermore study the

sensitivity of the OH chemical system to perturbations, for which we define the OH recycling probability (a diagnostic of the instantaneous stability). We differentiate between the instantaneous stability, being the sensitivity to small perturbations in the present or pre-industrial atmosphere, and long-term changes. The latter are the result of forcings (e.g. changing emissions) as well as the stability (how does the system respond to a forcing). The first does not account for potentially non-linear feedbacks on long timescales, while the second takes these into account.

In the next section we describe our model and the emission scenarios. In Section 5.3 we define the OH recycling probability, and first apply it on a single box, representing global mean conditions. Since the system stability depends on the type of perturbation exerted and the ambient conditions, we subsequently analyze all grid boxes of the global model to refine the concept to regional scales. We have performed sensitivity simulations based on NO_x and CH_4 perturbations, which have opposite effects on OH, to explore to what extent the stability analysis can be generalized. In Section 5.4 we discuss OH distribution changes in the past century, and argue that statements about global mean OH changes need to be extended with a regional view. In Section 5.5 we address the role of oxidant transport in maintaining the stability of OH chemistry in the background troposphere. Section 5.6 presents the conclusions.

5.2 Model description

The global chemistry-transport model used has a spatial resolution of 5° longitude, 3.75° latitude and 19 levels up to 10 hPa, and has been tested by comparison with in situ and remote sensing data [*Houweling et al.*, 1998; *Dentener et al.*, 1999; *Lelieveld and Dentener*, 2000; *Peters et al.*, 2001, 2002]. Tracer transport, cloud properties, precipitation, temperature and other physical parameters have been derived from six-hourly mean meteorological fields from the European Centre for Medium-range Weather Forecasts (ECMWF) re-analyses, available for the period 1979-1993 [*Gibson et al.*, 1997]. All model simulations have been performed with a one-year spin-up period.

Stratospheric O_3 above 10 hPa has been prescribed based on Halogen Occultation Experiment (HALOE) satellite measurements. Between 10 and 50 hPa ozone is relaxed towards zonal mean mixing ratios based on measurements by the Total Ozone Mapping Spectrometer (TOMS) and ozone sondes, whereas the 3D ozone variability arises from simulated transports [*Lelieveld and Dentener*, 2000]. Below 50 hPa ozone is calculated without fixed boundary conditions. Methane is prescribed at the surface on the basis of observations, model interpolation and comparison with ice core analyses [*Houweling et al.*, 2000].

The chemical scheme accounts for 48 species that describe CH_4-CO-NMHC-NO_x-SO_x chemistry of which 32 are transported (including marked tracers) (NMHC is Non-Methane Hydrocarbons). The model accounts for 24 photodissociation and 67 thermal reactions and heterogeneous processes. The chemistry calculations are performed with a time resolution of 15 minutes. Photodissociation frequencies are calculated with the routine of *Landgraf and Crutzen* [1998]. The chemistry scheme includes peroxyacetyl nitrate (PAN), which represents the sum of all PAN-like components, as described and evaluated by *Houweling et al.* [1998]. Dry deposition of trace gases is simulated according to *Ganzeveld et al.* [1998] and wet deposition is

based on the method of *Guelle et al.* [1998]. Dry deposition is an important sink for NO_2, HNO_3, PAN, formaldehyde and acetaldehyde, and wet deposition is important for HNO_3, H_2O_2 and formaldehyde. The chemical mechanism includes the heterogeneous conversion of NO_x to HNO_3 on aerosols according to *Dentener and Crutzen* [1993].

Trace gas emissions are from the Emission Database for Global Atmospheric Research (EDGAR) [*Olivier et al.*, 1999]. Information about EDGAR is available through *http://www.rivm.nl/env/int/coredata/edgar/intro.html*. The simulations of pre-industrial conditions have been based on the emission data of *van Aardenne et al.* [2001]. Present-day emissions of CO amount to 585 TgC/yr (of which 424 TgC/yr are anthropogenic); for the pre-industrial conditions this is 303 TgC/yr (and 98 TgC/yr). Present-day emissions of NMHC are 597 Tg/yr (190 Tg/yr anthropogenic); pre-industrial NMHC emissions are 430 Tg/yr (20 Tg/yr anthropogenic). Present-day NO_x emissions are 45.7 TgN/yr (36.3 TgN/yr anthropogenic); pre-industrial NO_x emissions are 12.9 TgN/yr (2.7 TgN/yr anthropogenic). These emission estimates have been described in more detail by *Lelieveld and Dentener* [2000]. Biomass burning emissions have been described and evaluated by *Marufu et al.* [2000], and further discussed by *Peters et al.* [2002].

5.3 OH recycling probability

The results of our global model simulations for the present-day troposphere indicate that in total about 92 Tmol/yr primary OH formation takes place through the photodissociation of O_3 (R1) followed by reaction of $O(^1D)+H_2O$ (R4) (Tmol is 10^{12} mol). Figure 5.2 presents normalized global mean production and destruction rates of OH and HO_2 in the troposphere (the results from the pre-industrial scenario will be discussed in Section 5.4. We calculate that nearly half the OH initially lost in the oxidation of CH_4 and CO is recycled by NO in reaction R7. In the absence of NO regeneration of OH by the reaction with O_3 (R9) is important. Furthermore, many hydrocarbon oxidation pathways lead to OH through the formation and breakdown of oxygenated intermediates such as aldehydes, notably formaldehyde (CH_2O). The OH yield from these intermediates can even overcompensate the OH loss from the initial hydrocarbon attack. The total secondary OH formation, defined as the yield from OH recycling in Cycle 1, 2 and photodissociation of peroxides, is about 96 Tmol/yr.

Next we define the oxidation power, G, being the time rate at which OH is produced (gross OH formation). G is the sum of primary (P) and total secondary (S) OH formation. For the whole troposphere G is expressed as a global annual rate (Tmol/year). The OH recycling probability (r) is defined by r = 1-P/G. G is related to P and r by

$$G = P + S = P + rP + r^2P + r^3P + ... = \frac{P}{1-r} \tag{5.1}$$

From our model calculations we infer that globally, G = 188 Tmol/yr and P = 92 Tmol/yr, yielding a mean r of about 0.5. By considering the global troposphere as a well-mixed reaction vessel, it would follow that the system could become autocatalytic if r approaches 1. The result that $r \approx 0.5$ implies that tropospheric OH formation is quite efficient but not autocatalytic. The global OH chemical system may thus appear to be stable so that perturbations by CH_4 and CO are expected to cause

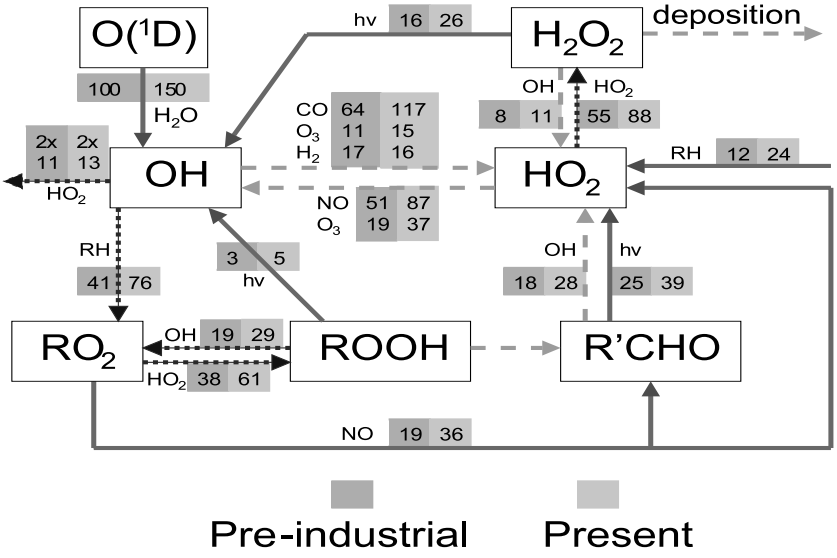

Figure 5.2: Model calculated global, annual mean HO_x reaction cycle in the troposphere. The numbers represent fractional contributions in percent, scaled to primary OH formation by the reactions R1,4; 100% represents 62 Tmol/yr (reaction $O(^1D)+H_2O$ in the pre-industrial troposphere). During industrialisation primary OH formation has increased by about 50% and gross OH formation by about 60%. Solid arrows refer to a gain of HO_x, short-dashed to a loss of HO_x, and long-dashed arrows are HO_x neutral. Minor pathways have been accounted for through the major ones.

only small or moderate OH changes, depending on the system forcing. At low r OH concentrations could become very sensitive to CH_4 and CO changes. Under low-r conditions OH production strongly depends on primary production, so that it is most sensitive to changes in O_3 photolysis rates (UV radiation), ozone and water vapor. Under high-r conditions the system is insensitive against perturbations of primary OH formation, however, at $r \rightarrow 1$ runaway oxidant build-up may result from secondary OH formation.

In addition to global mean values of r in a box-model approach, this quantity can also be evaluated for much smaller scales using local OH production and recycling rates. This is viable because OH is entirely determined by local chemical conditions. Figure 5.3 presents model calculated annual mean OH in the boundary layer, showing that OH can vary up to an order of magnitude over single latitudes, which illustrates the geographical OH dependence and the importance of local conditions. Note that in this article we focus on the middle and low latitudes, limiting ourselves to the model domain in which annual average primary OH formation exceeds 0.55 nmol/mol s^{-1}. This appears to encompass 74% of the Earth's surface. In the discussion we thus exclude conditions that only marginally affect the tropospheric oxidation power. The latter typically applies to high latitudes (higher than about 50-60° latitude), where annual mean OH concentrations are below 10^5 molecules cm^{-3} (Figure 5.3). Most

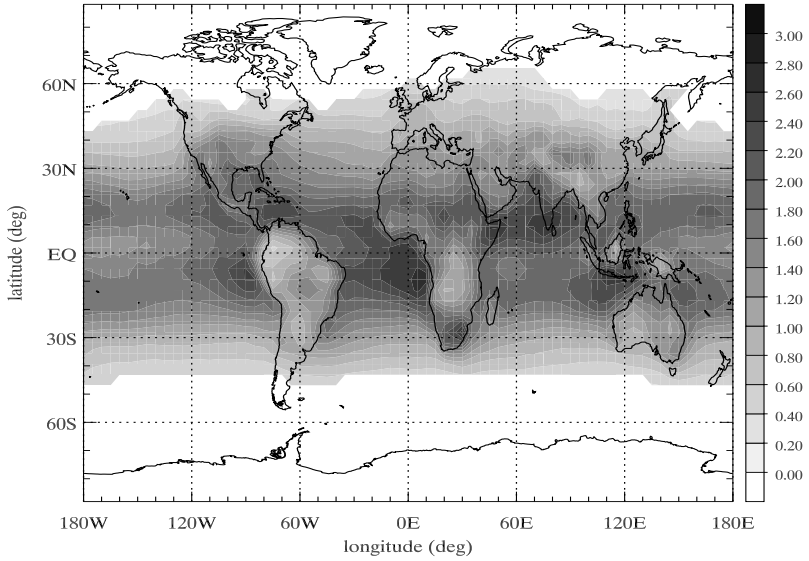

Figure 5.3: Model calculated annual mean OH in the present-day boundary layer in units of 10^6 molecules cm^{-3}, showing the domain in which primary OH production is most significant. In the white areas, i.e. outside the model domain discussed here, mean OH is less than 10^5 molecules cm^{-3}. Highest OH concentrations generally occur in regions where primary OH formation is strongest (controlled by O_3, UV and H_2O), and where OH sinks (e.g. by reactive carbon) are relatively small.

examples used in this article pertain to the boundary layer because the contrasts between polluted and clean air and the sensitivity to trace gas emissions appear to be largest near the surface.

Figure 5.4 shows model results for r as a function of NO_x for all boundary layer grid boxes. First we focus on the present-day atmosphere (black dots). The NO_x range apparent from Figure 5.4 includes very low mixing ratios of a few pmol/mol, typically over the remote oceans, up to about 10 nmol/mol in polluted locations. At very low NO_x r asymptotes to about 0.15, reflecting OH recycling through the Cycle 2 mechanism (R9). At an r-value of about 0.6 there is a discontinuity toward the polluted regime where OH becomes almost insensitive to the NO_x perturbation. At even higher NO_x r levels off at about 0.95. Note that in very polluted areas measured NO_x mixing ratios can sometimes exceed 10 nmol/mol. These concentrations do not occur in our model since emissions are released into relatively large grid boxes so that locally very high levels are artificially diluted. This means that in reality local r-values might even exceed 0.95, approaching 1, so that locally the system may become unstable, as mentioned above, although dilution is also a natural factor that limits such instabilities. Figure 5.5 presents the mean boundary layer OH recycling probability as a function of geographical location, showing that r is generally lowest in the marine troposphere ($r < 0.4$), while over the continents r is typically > 0.5. Figure 5.5 also shows that the highest mean r-values occur over Europe and N-America,

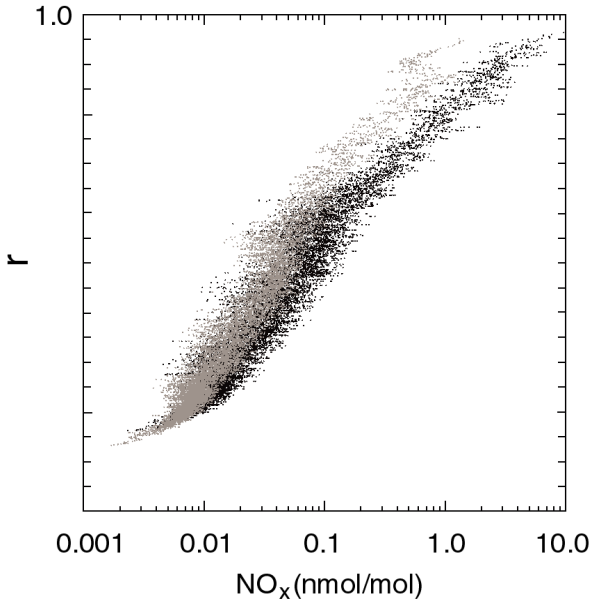

Figure 5.4: Model calculated annual average OH recycling probability (r) as a function of the ambient NO_x mixing ratio for all boundary layer grid boxes from one year of simulation. Black dots represent model results for present-day, grey for pre-industrial conditions.

associated with strong NO_x emissions. Since primary OH formation is lower in Europe than in N-America (higher latitude; lower UV, T and H_2O) and the NO_x source density is highest in W-Europe, mean r in this region is highest in the world. From Figure 5.4 it is furthermore evident that r is a strong function of NO_x. For the free troposphere we obtain similar results although on average r is higher and the range is smaller, $0.35 < r < 0.85$, because the spread in NO_x is less.

To investigate in which regions OH levels are most sensitive to perturbations we performed several sensitivity experiments. The objective was to approximate the total derivative dOH/dX for each grid box, thus extending the box model studies to the entire range of atmospheric conditions represented by our global model. For species X we selected CH_4 and NO_x since they have opposite effects, and because it is known that their sources have increased substantially. Figures 5.6a and 5.6b present results from two simulations, in which we perturbed the CH_4 and NO_x fields (separately). dCH_4 represents a 1% increase in the CH_4 mixing ratio at the surface. dNO_x has been simulated by adding a small NO source (of 0.014 molecules/cm^3/s) to each grid box. Additionally the NO emissions have been increased by 10^{-7} percent per time step because in polluted grid boxes the small fixed NO source is insignificant, hence we simultaneously applied both constant and proportional perturbations. Transport effects of the short-lived NO_x perturbations were thus minimized, and the perturbations were chosen such that we expect only marginal effects on the overall chemistry. The difference terms $\Delta OH/\Delta CH_4$ and $\Delta OH/\Delta NO_x$ as presented in Figures 5.6, have been calculated from the yearly average concentrations from the perturbed and un-

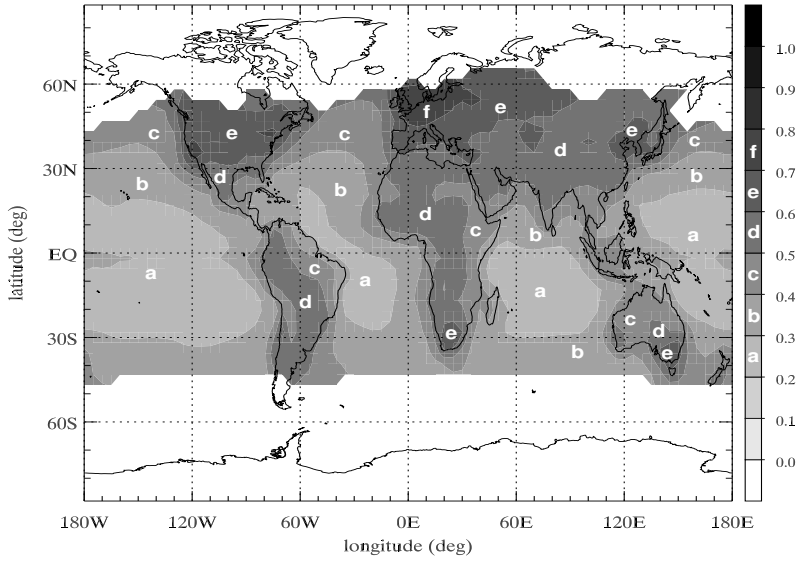

Figure 5.5: Model calculated annual mean OH recycling probability r in the boundary layer for the present-day simulation.

perturbed simulations.

The system appears to be relatively insensitive to perturbations at r-values above about 0.6. At $r < 0.6$ the system is quite sensitive depending on ambient conditions. The system is most sensitive at about $r < 0.4$, mostly in low latitude marine locations, in particular in the southern tropics. Although the OH response to CH_4 and NO_x perturbations is not identical because of highly variable conditions from one location to the other, the comparison of $\Delta OH/\Delta CH_4$ and $\Delta OH/\Delta NO_x$ in Figures 5.7 and 5.8 with the mean OH field in Figure 5.3 clearly shows that the system is generally most sensitive in regions in which OH concentrations are highest. In some continental regions with high NMHC concentrations, on the other hand, CH_4 perturbations have little effect. Figure 5.7 shows that over Amazonia, for example, isoprene levels are relatively high so that the small CH_4 perturbation applied only has a minor local influence on OH. Hence $\Delta OH/\Delta CH_4$ is small, also over other forested regions such as those in Africa and Indonesia (Figure 5.7).

The sensitivity to NO_x perturbations is highest in the NO_x depleted regions over the tropical oceans where OH concentrations are nonetheless high. The most sensitive region is over the eastern Pacific Ocean at 10-20° S (Figure 5.8). In the subtropics the highest OH values are found in regions with strong NO_x emissions, high concentrations of O_3 and water vapor, or high photodissociation rates. One example is the Tibetan Plateau, where OH is also relatively sensitive to perturbations by CH_4 (Figure 5.7). The least sensitive regions are found over the polluted continents and high latitudes where OH recycling exceeds primary OH formation. An important implication of these results is that in NO_x depleted parts of the troposphere, i.e. far downwind of pollution sources, growing levels of reduced gases such as CH_4 and CO have the

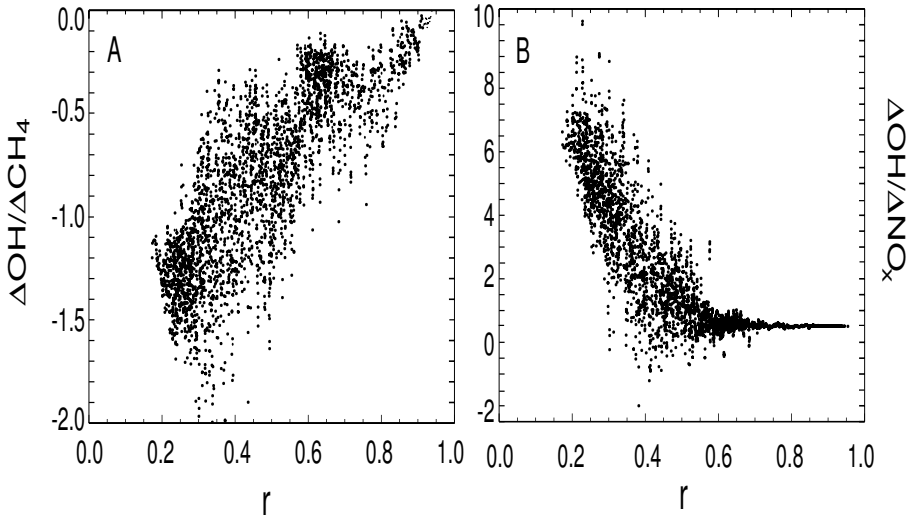

Figure 5.6: Model calculated OH changes caused by increases of (a) CH_4 (mol/mol$\times 10^8$) and of (b) NO_x (mol/mol$\times 10^3$) as a function of r. These results pertain to present-day conditions.

largest OH decreasing effect.

5.4 OH distribution changes

Figure 5.2 shows the global mean HO_x cycles for both the pre-industrial and present-day emission scenarios. Table 5.1 summarizes the global OH production rates, distinguishing the boundary layer from the free troposphere. We also differentiate between primary and secondary OH formation. By comparing these scenarios, it appears that global primary OH production has increased by about 50% from 62 to 92 Tmol/yr. Gross OH production increased even more strongly by more than 60% from 116 to 188 Tmol/yr. Hence increasing pollution has been accompanied by a 60% growth of the tropospheric oxidation power (defined as gross OH production). The global, diurnal mean OH abundance (volume weighted 1.1×10^6 molecules/cm^3), on the other hand, decreased merely about five percent. This relatively small OH change, considering that CH_4 and CO emissions have more than doubled, may suggest that global mean OH is not sensitive to perturbations. We argue, however, that global OH constancy should not be confused with OH stability.

Previous modeling results have also indicated that mean OH has decreased less than 10% during the past century [*Lelieveld and van Dorland*, 1995; *Wang et al.*, 1998]. Even studies of the pre-industrial holocene indicated that OH has remained within about 20% of its present value [*Pinto and Khalil*, 1991; *Crutzen and Brühl*, 1993; *Martinerie et al.*, 1995]. These modeling studies inferred that the relative constancy of mean OH during industrialization is associated with the correlation between the sources of NO_x and of CH_4 and CO. The concurrent growth of CH_4 CO and NO_x

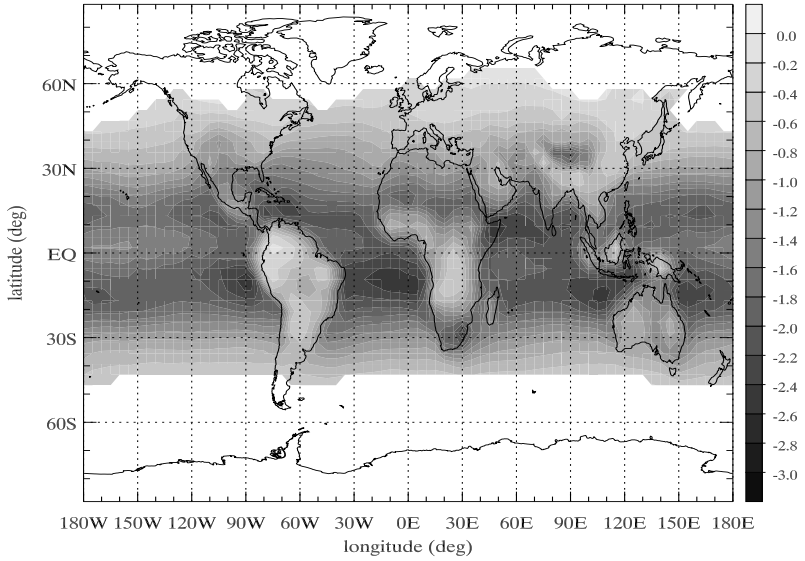

Figure 5.7: Model calculated OH changes caused by increases of CH_4 (mol/mol$\times 10^8$) in the present-day boundary layer.

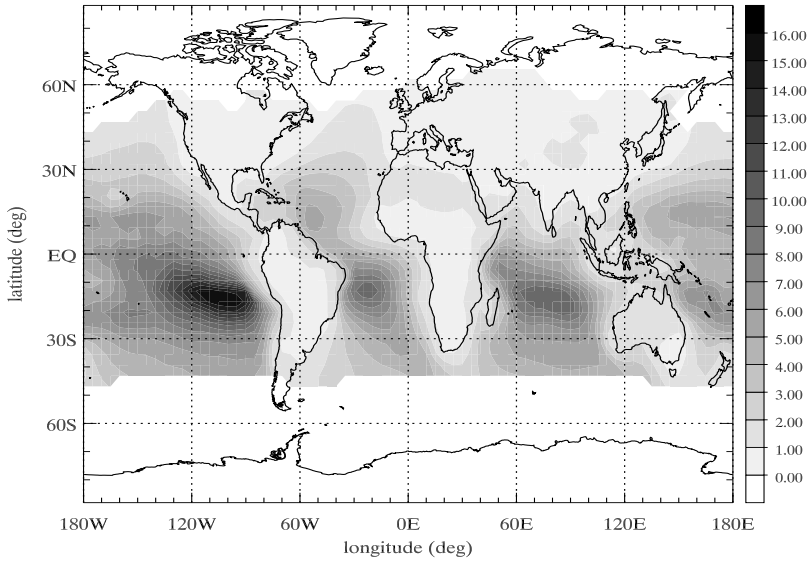

Figure 5.8: Model calculated OH changes caused by increases of NO_x (mol/mol$\times 10^3$) in the present-day boundary layer.

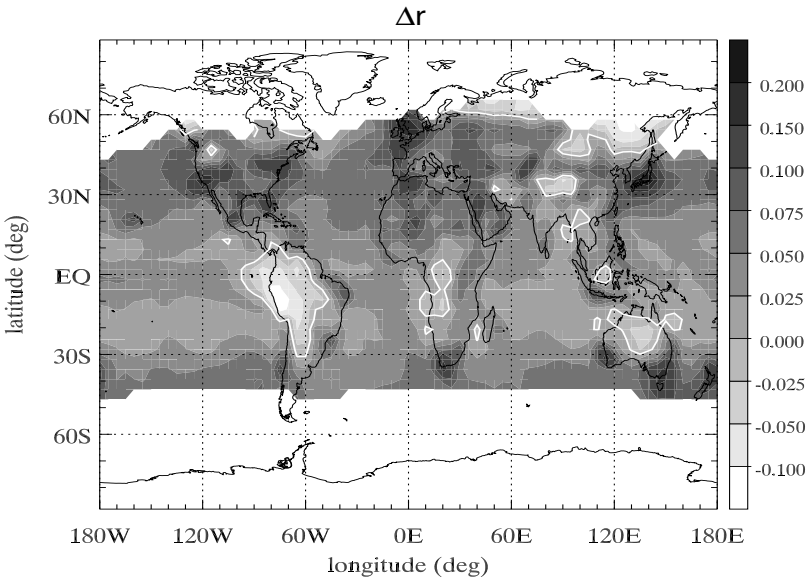

Figure 5.9: Model calculated annual mean change of the OH recycling probability r in the boundary layer, comparing the present-day with the pre-industrial troposphere (r present minus r pre-industrial). The white lines highlight the zero-contours.

emissions has intensified OH recycling and O_3 formation in the troposphere, while increasing CH_4 and CO alone would have reduced global OH by at least a third [*Isaksen and Hov*, 1987; *Lelieveld and van Dorland*, 1995; *Wang et al.*, 1998]. At present-day CH_4 and CO levels NO_x is quite efficient in recycling OH, in particular in the background troposphere (also because in low-r regions the NO_x lifetime has increased). Furthermore, the OH recycling probability r has increased over polluted regions, especially in the northern hemisphere, while changes of r over the remote oceans have merely been small. Figure 5.9 presents annual mean changes of r in the boundary layer, showing that these have been largest in the northern hemisphere in regions with strong NO_x emissions. Interestingly, Figure 5.9 suggests that the OH recycling probability decreased relatively strongly over the Amazon basin. Although primary OH production has increased owing to pollutant ozone formation, OH recycling is suppressed by the high isoprene concentrations so that r is substantially reduced.

Although the global mean recycling probability has increased during the past century, on average from 0.47 to 0.51 (Table 5.1), Figure 5.4 shows that r-values as a function of NO_x have nevertheless decreased. The global increase of r results from the overall increased NO_x abundance. Globally, OH recycling has grown even more strongly than primary formation. Primary formation increased by nearly 50%, whereas OH recycling (i.e. secondary OH formation) increased by 75%, indicating a stability increase, at least globally averaged. The reduction of the recycling probability per NO_x molecule during industrialization is further illustrated by Figure 5.10, which shows the mean OH concentration as a function of NO_x sampled from all boundary layer grid boxes. Figure 5.10 suggests that presently the OH optimum is

reached at higher NO_x concentrations than in the pre-industrial atmosphere. If an air mass contains more reactive carbon, more NO_x is required to attain the OH optimum and prevent radical-radical termination reactions. The decrease in OH sensitivity to NO_x in the 0.05-0.5 nmol/mol NO_x range, apparent from Figure 5.10, represents the reduced sensitivity of the system to perturbations, which is also seen in Figure 5.4 (notably for $r > 0.5$). Figure 5.10 furthermore shows that at low NO_x concentrations OH levels have decreased whereas under high NO_x conditions they have increased. The latter is a consequence of intensified primary OH formation associated with increasing O_3, while r has also increased because OH recycling has grown even more strongly.

Figure 5.11 aditionally presents OH changes between the present-day and pre-industrial scenarios. Note that Figure 5.3 shows model calculated annual mean OH in the present-day boundary layer, and Figure 5.11 the fractional changes between pre-industrial and present (ratio present/pre-industrial OH). It illustrates the relatively large OH increases over the polluted continents, even though they are the most stable regions with the highest values of r. In these regions chemical perturbations are huge, associated with high photochemical O_3 production rates. In the background troposphere, in particular over the tropical oceans, CH_4 and CO have increased substantially during the past century, whereas the concurrent increase of NO_x has been limited by its short lifetime. In these regions, therefore, the enhanced OH loss by reactions with CH_4 and CO predominates. On a global scale the positive and negative OH effects, over the continents and over the oceans, respectively, nearly cancel.

From a long-term perspective global mean OH thus appears quite constant in time despite large-scale redistribution. The "unintentional" human practice to simultaneously emit nitrogen oxides and reactive carbon compounds from combustion processes has helped maintaining mean OH during industrialization. The global mean OH recycling probability has even slightly increased (Table 5.1). It should be emphasized, however, that global mean r cannot unequivocally characterize the system stability. The atmosphere is not an instantaneously mixed reservoir, in particular regarding slow inter-hemispheric exchange with a time constant of about a year. Moreover, in the background marine troposphere r has stayed approximately constant so that these regions have remained particularly sensitive to perturbations. In fact, increasing r in the polluted troposphere only moderately influences the system sensitivity, since r-values above about 0.6 are within a stable regime anyway (unless r would approach 1). Perturbations in the background troposphere, on the other hand, have a relatively larger influence, so that even small changes in reactive carbon concentrations have a relatively strong negative effect on OH.

Table 5.1: Primary (P) and Secondary (S) hydroxyl formation for regions with low r (r<0.47) and high r (r>0.47), calculated for pre-industrial and present day emissions. FT is the free troposphere, BL is the boundary layer.

	P (Tmol/yr)		S (Tmol/yr)									
	$O(^1D)+H_2O$		$NO + HO_2$		$O_3 + HO_2$		$H_2O_2 + h\nu$		$ROOH + h\nu$		Total S	
	BL	FT	BL	FT	BL	BL	FT	BL	FT	BL	FT	BL
Low-r												
pre-ind	18.4	27.4	3.0	16.8	2.3	6.1	1.9	4.9	0.4	0.9	7.6	28.7
present	27.2	39.9	5.8	25.5	4.6	11.5	3.0	8.7	0.7	1.8	14.1	47.5
High-r												
pre-ind	6.2	9.7	4.0	7.7	1.2	2.2	1.1	1.9	0.1	0.2	6.4	12.0
present	10.5	14.3	10.7	11.9	2.7	4.3	1.5	2.9	0.2	0.4	15.1	19.5
Global												
pre-ind	24.6	37.1	7.0	24.5	3.5	8.3	3.0	6.8	0.5	1.1	14.0	40.7
present	37.7	54.2	16.5	37.4	7.3	15.8	4.5	11.6	0.9	2.2	29.2	67.0

Table 5.2: Primary (P) and Secondary (S) hydroxyl formation.

	Global P (Tmol/yr)	Global S (Tmol/yr)	Total G (Tmol/yr)	recycling probability (r)
Pre-industrial				
FT	37.1	40.7	77.8	0.52
BL	24.6	14.0	38.6	0.36
total	61.7	54.7	116.4	0.47
Present				
FT	54.2	67.0	121.2	0.55
BL	37.7	29.2	66.9	0.44
total	91.9	96.2	188.1	0.51

5.5 Role of transport

In this section we use our scenario simulations to study to what extent the advection of OH precursors may have played a role in OH distribution changes. Though globally averaged r $\approx$ 0.5, much lower r-values can occur in large areas, especially over the (sub)tropical oceans. The geographical distribution of r indicates that the system can be subdivided into the marine troposphere with values below about 0.45-0.5 and the continental troposphere with higher r-values (Figure 5.5). We therefore selected the global mean OH recycling probability of the pre-industrial troposphere, r = 0.47, to serve as a threshold value between the high- and low-r regions (Table 5.2). This choice seems reasonable, bearing in mind that Δr is a measure of $\Delta \ln[NO_x]$, and that the principal NO_x increases in the past century have occurred over the continents. We have used the same area definition for the pre-industrial and present troposphere so that the chemical budget calculations can be directly compared. The low-r area covers 67% and the high-r area 33% of the model domain considered, which encompasses 74% of the Earth's surface (where primary OH formation exceeds 0.55 nmol/mol s^{-1}). Note also that this partitioning is applied both to the boundary layer and the free troposphere although the transitions between the low and high-r regimes in the free troposphere are more diffuse owing to fast zonal transport. Table 5.2 presents the chemical budget terms for the low- and high-r regimes, for the boundary layer and the free troposphere, and for the present and pre-industrial troposphere. The sum of these terms matches the total primary and secondary OH formation as listed in Table 5.1.

As argued in Section 5.4, the low r-values over the oceans indicate that CH_4 and CO increases in this part of the troposphere have a relatively large impact on OH. At low r the system is strongly dependent on primary OH formation. This is particularly the case in the marine boundary layer where primary OH formation typically exceeds secondary formation by a factor of two or more. For the NO_x depleted regions, where in situ photochemical O_3 loss dominates O_3 formation [*de Laat and Lelieveld*, 2000], transport of ozone appears to be very important. Our model calculations show that

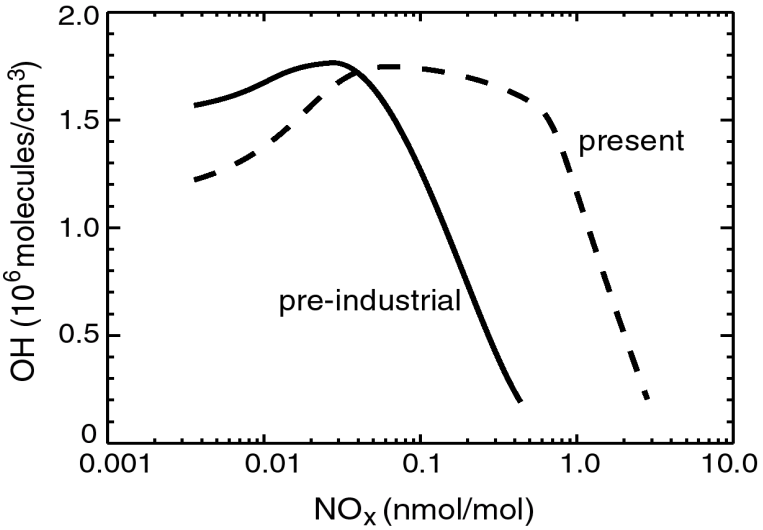

Figure 5.10: Average OH concentration as a function of ambient NO_x calculated for the lower atmosphere. For NO_x depleted conditions (< 40 pmol/mol; left of the curve crossing) the OH recycling efficiency has decreased during industrialization, whereas it has increased for NO_x enriched conditions.

under pre-industrial conditions the low-r troposphere received a net amount of 12.7 Tmol/yr O_3 through advection. A fraction of 80% was from the stratosphere, highlighting the importance of stratosphere-troposphere exchange for the oxidation power of the background troposphere. The high-r troposphere imported as much ozone as it exported under pre-industrial conditions. In the present-day troposphere, on the other hand, the high-r regions have become a net O_3 advection source, so that the low-r troposphere now receives 16.4 Tmol/yr O_3, an increase of about 30%. Note that under the low-r conditions the direct quantum yield from chemical O_3 loss is typically 1.8 OH (mostly through $O(^1D)+H_2O \rightarrow 2OH$). Moreover, the additional OH enhances O_3 formation and thus primary OH production and recycling.

The 30% increase of O_3 advection to the low-r troposphere in the past century helps to compensate the OH depletion caused by increasing CH_4 and CO, thus maintaining the oxidation power of the background troposphere. Ozone has a mean lifetime of several weeks so that rapid zonal transport leads to redistribution from polluted areas that are oxidant-enriched to remote areas that are oxidant-depleted. Ozone lives long enough to transfer the NO_x effect on a scale of thousands of kilometers while NO_x itself is rapidly removed in the vicinity of its sources. In Section 5.4 we showed that OH has strongly increased in the high NO_x regions, thus limiting the NO_x lifetime and transport. Our model calculations nevertheless indicate that in the past century NO_x advection from high- to low-r regions increased from 42 to 127 Gmol/yr, being the result of a large NO_x emission increase by a factor of 3.5 (Gmol is 10^9 mol). Several other compounds also have an oxidant transport potential, for example, peroxy acetyl nitrate (PAN) and other nitrates that act as reservoir species of NO_x [*Crutzen*, 1979; *Singh and Salas*, 1983; *Atlas*, 1988; *Atherton*, 1989]. PAN

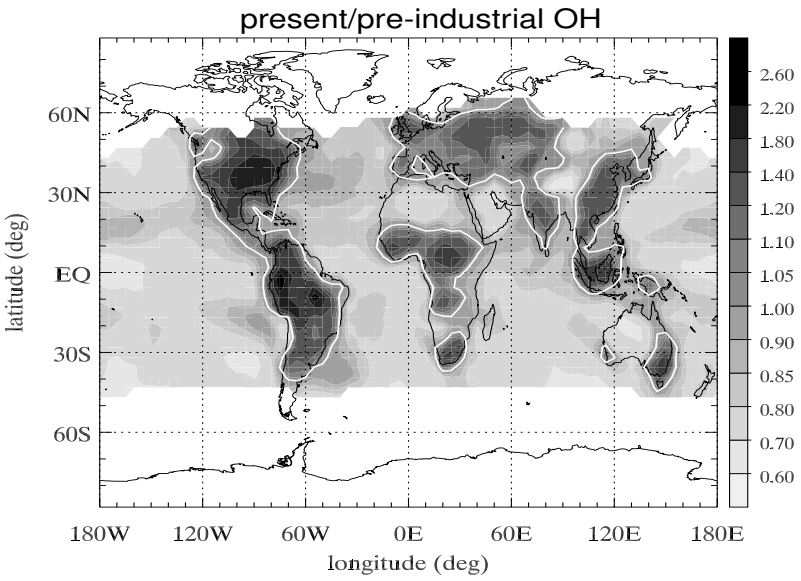

Figure 5.11: Model calculated fractional change of mean OH in the boundary layer, comparing the present-day with the pre-industrial troposphere (OH present/pre-industrial). OH has decreased over the oceans while it increased over the part of the continents where anthropogenic influences are strongest. The white lines highlight the 1.0-contours.

mostly releases NO_x in the relatively warm lower troposphere since it is thermally labile. Our model simulations suggest that PAN advection to the low-r regions increased from 111 to 231 Gmol/yr. Nitric acid is another NO_x reservoir species, which is more important for the upper troposphere (in the lower troposphere HNO_3 removal by deposition is very efficient). Advection of HNO_3 to low-r regions increased from 30 to 200 Gmol/yr.

In the past century both primary and secondary OH production in the low-r troposphere have increased substantially (from 46 to 67 Tmol/yr and from 36 to 62 Tmol/yr, respectively). A significant fraction of the increased primary OH formation has been caused by enhanced ozone advection, about 7 Tmol/yr. Locally produced ozone increased by about 20 Tmol/yr, being compensated by increased chemical O_3 loss. The O_3 chemistry increase has also been caused by the growth of NO_x emissions within the region, from 171 to 398 Gmol/yr, in addition to the increase of NO_y advection by 375 Gmol/yr and of other O_3 precursors such as CH_4 and CO. As a consequence, the O_3 burden increased by 30% from 6 to 7.8 Tmol. The comparison of the present and pre-industrial scenarios nevertheless shows that this O_3 increase, accompanied by enhanced primary and secondary OH formation, was not sufficient to prevent substantial OH depletion in the background troposphere.

5.6 Conclusions

According to our modeling results and sensitivity studies, the global and long-term mean OH has remained close to about 10^6 molecules/cm^3 during the past century, however, the OH distribution has changed substantially. Over the polluted continents oxidant levels have increased strongly, associated with a decrease in air quality. Large-scale air pollution in the past century has been accompanied by a $\sim$60% increase of the tropospheric oxidation power. Since global mean OH has remained approximately constant, this implies that the average OH lifetime has decreased by $\sim$60%. In a previous study we have argued that, on a global scale, tropospheric ozone is controlled by in situ formation rather than by transport from the stratosphere, both in the present and pre-industrial troposphere [*Lelieveld and Dentener*, 2000]. Globally, this exerts a stabilizing influence on OH, because an O_3 transport driven system would be strongly dependent on primary OH production, whereas in the chemistry dominated system OH recycling is equally important. Based on MCF analyses it has been suggested that OH changes during the past two decades may have been quite large. *Krol et al.* [1998] derived a positive global mean OH trend of nearly 0.5%/yr between 1978 and 1994. *Prinn et al.* [2001] inferred an even larger upward trend during the 1980s and a steep decline during the 1990s. Recent re-analysis of the MCF measurements, however, suggests that the large presumed OH changes, in particular the strong negative OH trend during the 1990s have been overestimated [*Krol et al.*, 2002; *Krol and Lelieveld*, 2002]. It is actually more likely that global mean OH has been rather constant over the period considered (1978-2000). This does not necessarily mean, however, that the system is stable and that OH changes have been small. We must consider compensating effects of anthropogenic perturbations by reactive carbon and NO_x emissions, and redistribution of OH, which are hard to detect from MCF analyses. Hence global mean OH constancy is not the same as system stability. To determine the latter we also need to focus on smaller scales, associated with the limited lifetime of many substances that are not globally mixed. We have thus characterized the sensitivity of the OH chemical system through the OH recycling probability (r), a diagnostic calculated from primary and secondary OH formation. Although global mean r has slightly increased during the past century, we calculate large regional differences.

Our modeling results indicate that the low latitude marine boundary layer is the most sensitive environment, characterized by a low OH recycling probability (low r). Increases of CH_4 and CO have therefore strongly reduced OH here in the past century. In this part of the troposphere the system is increasingly dependent on oxidant advection to sustain OH formation. It appears that transport of O_3 and its precursors, notably reactive nitrogen species, plays an increasingly important role in the oxidation power of the background troposphere (i.e. the low-r troposphere). In the present troposphere long-range transport redistributes oxidant from photochemically polluted regions, being OH enriched, to OH depleted regions. This is not only important to supply oxidant for primary OH formation, it also contributes to OH recycling. Hence oxidant transport to the marine troposphere has thus prevented even larger OH depletion by increasing CH_4 and CO during the past century.

In fact, oxidant transport away from the pollution sources is also important to maintain the stability of OH chemistry over the continents. Although these regions are characterized by a relatively high OH recycling probability, the huge perturbations

by NO_x emissions have nevertheless caused strong OH increases. Without advective dilution, OH formation could locally even become autocatalytic, leading to oxidant outbreaks, as predicted by box model studies and sometimes observed in very polluted conditions during summer [e.g. *Kleinman* [1994]]. It should be emphasized that even though the OH chemical system in the continental troposphere is more stable than over the oceans, regional perturbations e.g. in Europe and the USA during the past century have been so large that OH could still change substantially. If the reactive carbon and NO_x emissions would not have taken place simultaneously, the OH changes might have been dramatic. Therefore, one should not conclude that in the most stable environments OH changes are small. Rather, if the system stability were low in these environments, OH changes would have been even much larger.

Although our study has concentrated on the low and middle latitude troposphere where OH levels are highest, we note that the high latitude troposphere ($> 50^\circ$ latitude), where primary OH formation is slow, is characterized by relatively high values of r, suggestive of a low sensitivity to perturbations (both pre-industrial and present). We conclude that in regions where both the OH recycling probability is low and OH concentrations are high the system is sensitive to perturbations, i.e. in the low latitude marine troposphere. Moreover, the OH chemistry over the tropical rainforests in the Amazon has become more sensitive to perturbations. This underscores the importance of the tropics where future atmospheric changes will probably be largest, and where observations are particularly scarce (and thus urgently needed). Finally we emphasize that efforts by environmental protection agencies to limit NO_x emissions (to control smog, photochemical O_3, acid rain and eutrophication) contribute to a reduction of both OH and system stability unless CH_4 and CO emissions are reduced simultaneously. The latter should be pursued for many reasons, for example, to limit climate change.

Chapter 6

General conclusions and future perspectives

The studies presented in Chapters 2–5 have led to many insights into physical and chemical processes in the atmosphere, as well as into shortcomings in the models and datasets used. In this chapter, we briefly repeat the most important conclusions from the previous chapters, and highlight the most important insights from this work. These insights are grouped by subject, while the research that led to these conclusions is referenced by chapter (in **boldface**).

Transport in the tropical Atlantic region

Through the use of new ozone sonde data from station Paramaribo, it was found that the division between the Atlantic and Pacific regime in tropospheric ozone (and relative humidity) can be placed west of Paramaribo (55W), and east of San Cristobal (90W), making the natural barrier of the Andes mountains the region where the strongest zonal gradients occur (**Chapter 2**). Paramaribo is thus part of the more polluted Atlantic basin, just like Ascension (14W, 8S) and Natal (35W, 6S). Although the seasonality of ozone at Paramaribo resembles that at these SH stations, the occurrence of the short dry season (Feb-March) distinguishes it from all SH stations in the SHADOZ network (**Chapter 2**). Enhanced ozone VMR's during this period (60-80 ppbv) are due to advection of polluted air from the northern hemisphere at low altitudes, and subsidence of ozone-rich air from the upper troposphere at higher altitudes (**Chapter 2**).

The Paramaribo ozone sonde record also shows layers of high ozone (80-100 ppbv) that most likely originate from biomass burning sources. Although this process was known to pollute large parts of the southern hemisphere Atlantic basin [*Fishman et al.*, 1990; *Roelofs et al.*, 1997; *Thompson et al.*, 2001], simple modeling techniques applied in **Chapter 2** show that also NH station Paramaribo can be reached by biomass burning plumes during the long dry season (August-November). Interestingly, Africa is a more important source region than nearby South America in this respect, because mean wind directions favor westerly transport over the NH equatorial Atlantic basin.

Quantitative modeling of these plumes remains a problem (**Chapter 3, 4**). Ozone

concentrations over the equatorial Atlantic in our CTM are too low compared to seasonal cycles apparent from sondes (**Chapter 3**), satellite observations (**Chapter 4**), and individual profiles (**Chapter 2, 4**). The seasonal recurrence of this underestimate suggests an important role for biomass burning emissions. The dispersion of these emissions over the Atlantic basin depends strongly on transport mechanisms that are currently sub-grid scale in our model, notably convection and turbulent exchange. *Dentener et al.* [1999] already described a lack of exchange between the boundary layer and the free troposphere over parts of the African continent from ^{222}Rn studies. Sensitivity studies in **Chapter 4** suggest that the same lack of exchange partly cause the observed underestimate of ozone concentrations.

The importance of correctly describing meteorology in a CTM was demonstrated quantitatively in **Chapter 4**. It was found that the zonal gradients in satellite observed ozone (MR-TTOC) were reproduced significantly better by the model when meteorology from the year corresponding to the observations was used. Such a quantitative assessment was not reported previously in literature. These model results were supported by our analysis of the Paramaribo ozone record (**Chapter 2**), where we also concluded that the ozone changes over Paramaribo are largely controlled by meteorological variability, which is strongly linked to the annual migration of the ITCZ.

Finally, it was shown in **Chapter 5** that transport of ozone and its precursors have played an important role in maintaining the oxidation power of the troposphere as it changed composition since pre-industrial times. Long-range transport redistributes oxidants from photochemically polluted regions, being OH enriched, to OH depleted regions. This is not only important to supply ozone for primary OH formation (92 Tmol/yr), it also contributes to OH recycling (96 Tmol/yr). Our results suggest that oxidant transport to the marine troposphere has thus prevented large OH depletion by increasing CH_4 and CO during the past century.

Photo-chemistry in the tropics

The breakdown of the zonal wave one pattern of ozone using marked tracers in **Chapter 4** brings out an interesting aspect of the tropical ozone distribution: NO_x precursors for photo-chemical ozone production originate from four different sources (lightning, biomass burning, soils, industry) that contribute in almost equal amounts. Besides the previously described transport patterns, all four of these sources (and also the fifth: stratosphere-troposphere exchange) therefore need to be modeled correctly to reproduce measurements.

We found that ozone is only weakly dependent on the magnitude of these sources (**Chapter 4**). Factor of two increases in emissions did often not alter ozone concentrations in the tropics significantly. This is due to efficient chemical feedbacks in the control of ozone, that tend to dampen the response. This effect is strongest in the tropics because photo-chemistry there is most active. As a consequence of the remarkable stability of ozone, it is very difficult to extract information on the individual processes and sources that govern its concentration, by studying the ozone distribution.

Although methyl-chloroform (MCF) studies suggest that OH variations over the past decades have been substantial [*Krol et al.*, 1998; *Prinn et al.*, 2001], our modeling study (**Chapter 5**) shows that global average OH has remained close to 10^6 molecules cm^{-3} since pre-industrial times. Using the novel concept of recycling probability, we

have shown that increased levels of ozone and NO_x have increased the likeliness of OH to be reformed after an initial oxidation reaction has occurred (from 47% to 51% globally averaged). Together with increased levels of photo-chemically produced ozone available for primary production of OH this has led to a global 60% increase in oxidizing power (**Chapter 5**).

Our analysis indicates that although the global mean recycling probability has increased only slightly during the past century, large regional changes (mostly coupled to NO_x emissions) have occurred. The low latitude marine boundary layer appears to be the least stable environment (**Chapter 5**), characterized by a low OH recycling. OH levels in these regions have decreased substantially (>20%) since pre-industrial times. In this part of the troposphere, the system is increasingly dependent on oxidant advection to sustain OH formation.

Although runaway growth of oxidants or OH-catastrophes are unlikely to occur due to the stabilizing effect of transport in the troposphere (**Chapter 5**), the (increased) sensitivity of the tropics to changes is worrisome. We emphasize that efforts by environmental protection agencies to limit NO_x emissions (to control smog, photochemical ozone, acid rain and eutrophication) contribute to a reduction of both OH and system stability unless CH_4 and CO emissions are reduced simultaneously.

Variability in ozone

The record of ozone at five tropical monitoring stations showed that the annual migration of the ITCZ determines to a large extent the seasonal cycle of ozone, and interannual variability therein (**Chapter 2**). Over the Pacific station Samoa, interannual variability in the surface ozone record (20% of total signal) is reproduced by a 15-year model simulation with ECMWF analyzed meteorology. In **Chapter 3**, an EOF-analysis applied to this 15-year simulation showed that the most important component of interannual variability (25% averaged over the tropical domain) is related to the El Niño-Southern Oscillation (**Chapter 3**). This is mostly due to shifting convection patterns during alternate phases of ENSO, while changes in lightning NO_x distribution and wet removal of ozone precursors appear to be of minor importance. Locally, ENSO variability explains up to 60% of the interannual variations in ozone, suggesting that this variability should be incorporated in analysis of trace gases from both models and measurement campaigns.

Modeling and remote sensing

We have shown that satellite observed tropospheric ozone columns (MR-TTOC) do not reproduce the observed seasonality at Paramaribo correctly. Underestimates occur during the first months of the year, and overestimates during the second half. Analysis suggests that this is due to an assumption on background ozone over the Pacific in the MR-method, which is based solely on SH ozone sondes (**Chapter 2**). Even in the NH, this background value has a distinctly SH seasonality in the MR-method, while the Paramaribo data and chemistry-transport model results suggest that this seasonality reverses for the NH, as would be expected based on the migration of the ITCZ. This leads to an underestimate of satellite retrieved MR-TTOC compared to sonde measured TTOC in February-March, and an overestimate in August-November.

The reversed seasonal cycle alone explains a substantial part (8 DU) of the observed discrepancy at Paramaribo, and moreover suggests that Paramaribo can be used to improve the MR-retrieval algorithm.

Quantitative use of satellite derived TTOC to test a global model is a promising approach, that would strongly profit from a more detailed quantification of the uncertainties in TTOC data (**Chapter 4**).

With a standard set of emissions, such as in *Houweling et al.* [1998]; *Lelieveld and Dentener* [2000]; *Peters et al.* [2001], the Atlantic TTOC maximum is not sufficiently well captured, whereas the interannual variability over the Pacific Ocean is represented quite well (**Chapter 4**). Using actual meteorology in a model is the most important prerequisite in reproducing the horizontal and vertical distribution of tropical tropospheric ozone (**Chapter 4**).

Future research

Based on the work presented in this thesis, the following steps would be recommended in future research:

- Increase the use of satellite measurements in atmospheric chemistry research. Our study in Chapter 4 has shown the potential of these data in chemistry-transport modeling, including possible ways to use them quantitatively. Chapter 2 has shown the potential for mutual benefit in the combination of models and satellite data.

- Continue and possibly expand the tropical ozone measurement network. The Paramaribo data have been very useful, and led to new insights on transport in the tropical Atlantic even from a straightforward analysis. Moreover, ozone sondes help to validate satellite measurements, which are of much greater value when their (spatial) uncertainties are known in detail.

- Improve the description of biomass burning emissions in CTM's, to include interannual variability and preferably make it interactive with meteorology. In this respect, the composition and chemistry of biomass burning plumes needs to quantified in more detail, as it is likely to be much larger than resolved in our model. The dispersion of biomass burning plumes might have to be included in a separate parameterization to capture rapid ozone formation on sub-grid model scales.

- Increase our knowledge on lightning NO_x emissions. The model parameterization of this process is very simple, but we were unable to indicate possible improvements due to the limited knowledge on the occurrence, and effects of lightning discharges.

- Increase cooperation with meteorological research groups. All our analysis have shown the importance of transport in determining large-scale distributions of trace species, as well as in controlling photo-chemistry. The application of transport schemes to chemical tracers has led to new insights, that would not have surfaced from studies of moisture and temperature alone.

- Prepare to run higher resolution CTM's (such as the new TM5 model) with the upcoming ERA-40 re-analysis. Studies of the 15-year TM3 simulation have yielded new insights on ozone photo-chemistry [*Lelieveld and Dentener*, 2000], OH-stability [*Lelieveld et al.*, 2002], ozone variability [*Peters et al.*, 2001], methane sources [*Dentener et al.*, 2002a], and the role of transport [*Peters et al.*, 2002]. The opportunity to repeat this simulation with improved meteorology for a longer period should have a high priority.

Appendix A: Paralellization of the TM3 model

A-1 Introduction

Similar to many other fields of research, the use of computer models has rapidly become an important tool in atmospheric science. The increased interest in this area was stimulated by the possibilities offered by computer systems, as they grew faster, larger, and more reliable over the past decades. This has advanced research in many areas including weather prediction, radiative transfer, and urban pollution.

In the area of global chemistry-transport modeling, which is the subject of this thesis, the models applied cover the entire globe, and often extend vertically up to the stratosphere. This domain is subdivided into a horizontal grid, and several vertical layers on which Eulerian transport of trace gases is prescribed. The number of tracers, vertical layers and the density of the horizontal grid largely determine the demand of computer resources. In the earlier work of for instance *Langner and Rodhe* [1991], the MOGUNTIA model was applied to simulate 20 trace gases on a resolution of 10×10 degrees and 10 vertical layers, while more recent model studies use a grid of 1×1 degrees with 33 vertical layers to transport more than 50 tracers [*Krol et al.*, 2001]. This means that the workload, and memory demands of these models has increased by more than three orders of magnitude.

The computer resources needed to answer these demands are found in specialized supercomputers, which usually possess a large amount of disk capacity, memory, and processor speed. In the Netherlands, the Stichting Academisch Rekencentrum Amsterdam (SARA) hosts the national supercomputer available to the Dutch Scientific community. Previously, this was a CRAY C90 computer, but this machine was discontinued in December 2000. In April 2001, the CRAY was replaced by a Silicon Graphics International (SGI) model 3800 computer. The SGI-3800 is based on a completely different concept than the old CRAY-C90. Whereas the CRAY-C90 used one very fast, specialized processor (called vector processor) to perform computations, the SGI-3800 uses multiple regular processors (called parallel processors) at a time. If these multiple processors equally share the amount of work in a computation, the required time will decrease with an increasing number of processors. We will discuss some more differences between the two computers in later sections.

To optimally use the power of the multiple processors on the SGI-3800, changes in the structure and source code of the TM3 model were required. In this appendix, we briefly discuss the approach chosen and results of the porting of our computer code to the new supercomputer. We start with a description of the infrastructure of the SGI-3800, and the software available to optimally use the architecture of this system. After that, we will introduce the approach for parallelization we opted for, and describe the technical consequences for our model. We will introduce concepts used in assessing model performance, and finally show the results of the parallelization process, that has led to a faster, better portable model.

A-2 Methods

The national supercomputer 'TERAS' is a 1024-CPU system consisting of two 512-CPU SGI Origin 3800 systems. This computer has a peak performance of 1 TFlops (1012 floating point operations) per second. The machine is fitted with 500MHz R14000 CPUs that each have 1Mb of associated cache memory, adding up to a total of 1 Tb

of memory. The memory is thus distributed throughout the machine, but memory management is performed by the system (e.g. invisible to users).

The previous national supercomputer, a CRAY-C90, was a so-called vector-machine. It was equipped with a large amount of memory that was accessed by a single, very fast processor, which could perform operations on small blocks (vectors) of data at a time. One logical next step would have been to equip such computers with multiple processors (so called Parallel Vector Processing or PVP machines). However, the scalibility (time gained/extra processor) of such systems is limited because of the large amount of data exchange between processors and memory that has to occur over one line (the so-called bus).

The processors of TERAS have their own private memory and therefore each processor possesses only part of the data. When data from another processor is needed, communication between processors takes place. As long as the computation to communication ratio of the program is high, the scaling factor of the TERAS can be very large. This architecture can be seen as the best of both worlds (distributed workload/ fast memory access). The operating system of TERAS includes compilers that automatically evaluate programs and ensure parallel operation when necessary. However, parallelization is achieved only for small parts of the code, and the memory architecture of the SGI-3800 is not exploited efficiently. For that, more rigorous redesign of the code is necessary, to include data distribution over the processors and adapt for explicit communication. This can be done through parallelization with the message passing interface (MPI).

Message Passing Interface (MPI)

MPI is the widely used standard that provides software guided communication between processors [*Pacheco*, 1996], allowing a full distribution of the workload over the processors. It consists of a series of commands that can be integrated into regular computer code, telling individual or groups of processors to send and/or receive data. When to invoke such commands and which command to execute is decided by the programmer. At the start of each program, MPI establishes a grid of processors, numbered consecutively. Each processor can thus be referenced by a number, and tasks can be assigned to specific processors. An example of such a 'grid' is seen in Figure 1. The most important operations performed by MPI include:

- monitoring and synchronizing progress on multiple processors.
- sending (blocks of) data from one processor to another, or to multiple processors.
- receiving (blocks of) data from a processor, or from multiple processors.
- manipulating (blocks of) data from one processor, or multiple processors.

MPI works on many platforms, including clusters of PCs. A program designed to use MPI is thus easily portable to other platforms. As an example of an MPI directive, consider the following line taken from the TM3 source code:

```
CALL MPI_BCAST(timestep,1,MPI_INTEGER,0,com_crt,i_err)
```

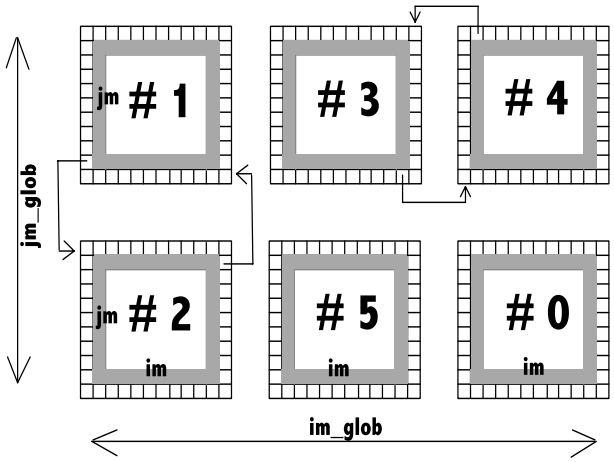

Figure 1: Example of a grid of six processors that encompass the global model domain (im_glob×jm_glob). Local arrays have dimensions im×jm, with im=im_glob/n_pcx and jm=jm_glob/n_pcy. Arrays used in advection have (im+2)×(jm+2) cells, in order to exchange information with neighboring processors, as indicated by the arrows. Numbering of processors is random, from zero to five.

This line would call the MPI routine MPI_BCAST, which broadcasts (blocks of) data from one processor, to all others. In this case, it will send one (1) integer (MPI_INTEGER) named timestep, from processor zero (0), to all other processors included in the group (called com_crt). An error flag (i_err) indicates the success or failure of the requested operation. The new TM3 code is packed with such specific calls, which has not helped the readability and transparency of the source code. This is a disadvantage of MPI based parallelization.

Approach

There are several ways to divide the workload over all processors. For instance, each processor can do the calculations needed for one tracer. Each processor can then easily handle advection and sources and sinks, and only when there is interaction between species (i.e. chemistry), communication would be necessary. Likewise, we could split the domain vertically, so that chemistry and horizontal transport can be done per processor, while communication would be needed when there is interaction between vertical layers (i.e. convection and turbulent transport). The approach that was chosen here is to divide the horizontal domain over the processors, so that each processor can solve chemistry and convection for a smaller subsystem, and communication is necessary during horizontal transport (i.e. advection).

The grid of processors for an example with 6 processors is shown in Figure 1. The global domain (im_glob×jm_glob) is subdivided into 6 equal parts (im×jm, with im=im_glob/3 and jm=jm_glob/2). MPI defines this grid, and manages communications. Note that the numbering in the processor grid runs from zero to five, and that there is no specific order in the numbering. Definition of the grid is controlled by the user defined TM3 variables n_pcx (=3 here) and n_pcy (=2 here), which govern the

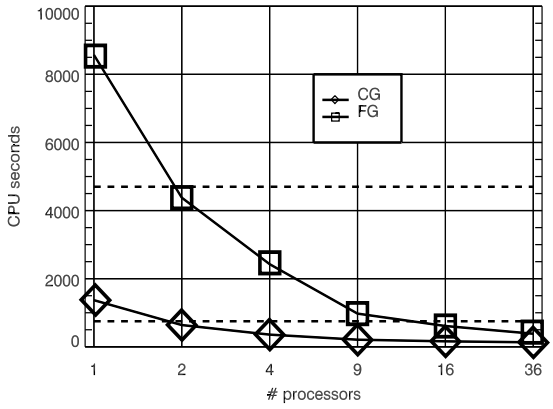

Figure 2: Turnover time of TM3 on a CG (36×24×19) and FG (72×48×19) resolution, for several numbers of processors. The turnover time of the old CRAY C90 computer is indicated by the dashed horizontal line. Note that the x-axis is not linear.

number of processors used in x- and y-direction respectively. Together, they determine the total number of processors n_pcs (=n_pcx×n_pcy).

The approach chosen has forced us to make several adjustments in the code, and redesign certain algorithms. The most important changes that were necessary pertained to the advection algorithm and Input/Output routines. Advection in the TM3 scheme is handled by a first order advection scheme [*Russel and Lerner*, 1981]. This scheme uses the local trace gas concentration and gradient to calculate the mass flux from one grid-box to the next. This gradient can easily be calculated everywhere, except on the edges of the sub-domains of a processor, since information from a neighboring processor is needed. This requires a substantial amount of communication between different processors each time an edge of a processor is encountered in advection.

Similar processor-to-processor communication is required in the Input/Output routines of the model. The TM3 model on Fine Grid resolution (5×3.75 degrees) uses 270 MB of input data per month, of which most is read at 6-hourly intervals. In parallel operation, only one processor handles the opening, reading and closing of a file, and distributes the information to the other processors afterward. Likewise, writing of data starts with one processor gathering information and then writing it to a file.

Although many other calculations (for instance solar zenith angles, zonal averages, area aggregated values) require MPI-guided communications, these were usually minor changes in the TM3-code.

Performance tests

Many software packages and routines are available on the SGI-3800 to test programs and to assess the success of parallelization. We have firstly chosen the most pragmatic approach to assess our model, by answering the questions: How much time does a

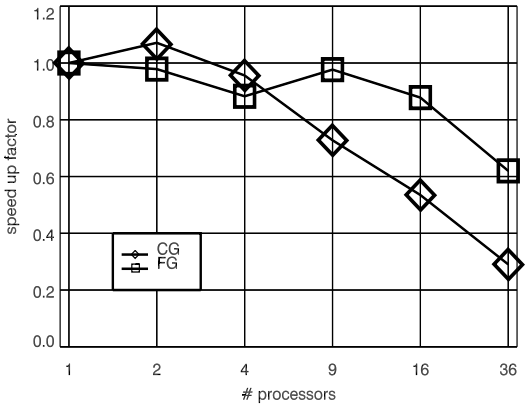

Figure 3: Speed up of TM3 on a CG (36×24×19) and FG (72×48×19) resolution, for several numbers of processors. Note that for two processors on a CG resolution, a superlinear speed up is achieved. Note that the x-axis is not linear.

standard model simulation take on the new SGI-3800 versus the old CRAY C90? A standard model simulation in this case is defined as a simulation covering one month on a predefined resolution of either 10°×7.5° (Coarse Grid or CG) or 5°×3.75° (Fine Grid or FG) degrees (lon×lat) with 19 vertical layers and 38 trace species, of which 24 are transported. This configuration is similar to that used in chapters 3,4, and 5. Time spent waiting idle or in the system queue is not counted. In the next section, we will use the following definitions:

- Turnover time: The time needed to complete a one month simulation, not counting idle time and queue time.
- Speed up: Fractional decrease in turnover time on n processors (t_n) compared to one processor (t_1) : ($\frac{t_1/t_n}{n}$).
- Cost: Total amount of CPU seconds used by all processors, multiplied by the price per CPU second.

A-3 Results

Figure 2 shows the turnover time of TM3 on the SGI-3800 (curve), and on the CRAY C90 (dotted line). Obviously, one processor of the SGI-3800 is slower than the vector processor of the CRAY C90, as the turnover time for one processor almost doubles on the new computer. This illustrates the need for parallel computing on the new machine. When two processors are used on the SGI-3800, both the CG and FG simulations perform slightly faster than on the CRAY, and each added processor decreases the turnover time further. When 36 processors are employed, the CG simulation is finished in 1/6th of the time needed on the CRAY, while the FG simulations are done

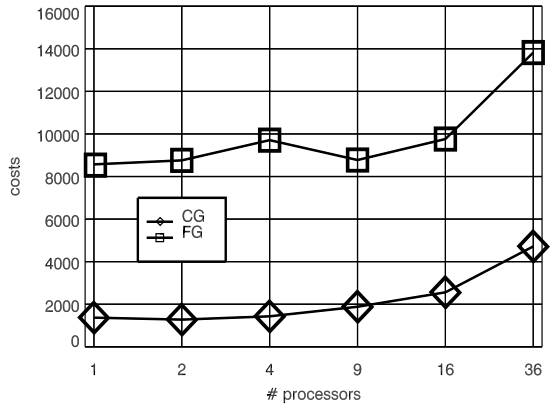

Figure 4: Costs of TM3 on a CG (36×24×19) and FG (72×48×19) resolution, for several numbers of processors. The costs are defined as the total number of CPU seconds used by all processors. Note that the x-axis is not linear.

in 1/12th of the time previously needed. Compared to the performance on one SGI-3800 processor, these numbers are 1/11th, and 1/22th, respectively.

Interestingly, the turnover times on both resolutions converge for increasing number of processors. While for one processor the ratio CG/FG is 1:6, it is near 1:3 when 36 processors are applied. This is caused by the relatively higher ratio of calculations/communications on the FG resolution. While the number of calculations increases with more grid boxes, the frequency of communications remains constant (note that more data needs to be shared per communication, this is not a limiting step however). Thus, more (parallel) calculations can be done before communication is necessary, rendering the parallelization of 'calculation intensive' projects more effective. This is an important result, which suggests that most can be gained from parallelization of high resolution configurations, and that the differences in turnover time between resolutions is no longer linear (as on the CRAY), but minimizes when more processors are used. This can potentially be an important argument in choosing a (higher!) resolution for future model studies.

Figure 3 shows the speed up of the model. Clearly, the FG resolution retains a high speed up factor for more processors than a CG resolution. Highest speed up can be seen at low processor numbers, while the speed up decreases quickly for higher numbers of processors. Note that with two processors, the CG resolution shows super-linear speed-up (the model runs more than twice as fast on two processors), probably due to a more efficient use of cache memory in this configuration. When the speed up reaches zero, the turnover time will no longer decrease through the use of more processors. The CG and FG curves in Figure 2 will converge to this value. Most likely, adding more processors beyond this point will even increase the turnover time, leading to a negative speed up. From a computational point of view, the optimum number of processors is reached when the speed up factor changes sign. This point is not included in our graphs, since other factors also play a role in the choice of number of processors.

Table A.1: Relative time spent per model process on the CRAY C90 and SGI–3800 computers.

CRAY C90		SGI-3800	
Process	Load	Process	Load
Chemistry	60%	Advection	40%
Advection	18%	Chemistry	23%
Convection	9%	Convection	9%
I/O	3%	I/O	12%
Other	10%	Other[a]	16%

[a]Includes overhead from MPI routines.

As an example, see Figure 4. It shows the costs (in CPU seconds) of running the model for each configuration. Since the total costs of a model run are calculated as the sum of all time used on each processor (multiplied by an amount of money/CPU second), adding more processors will normally increase the costs. Only when a speed up of one or more is achieved, the costs do not increase. It can be seen in the figure that the costs start to increase seriously when the speed up factor decreases. Using more than 9 or 16 processors for a CG or FG run respectively will strongly increase the costs while yielding only little gain in turnover time.

Another result of parallelization is shown in Table A.1. When we compare the breakdown of turnover time per process for the old and new computers, it is obvious that a large shift has occurred. Where the CRAY C90 spent most time in the chemistry solver (EBI), the SGI-3800 spends most of its time in the advection algorithm. This is due to the good scalability of chemistry relative to advection. The workload of the chemistry solver can be distributed fully over all the processors, since no communication is necessary between grid boxes. In contrast, the advection routine on a distributed grid requires frequent communication between processors to share boundary conditions and exchange concentrations on the edge of the processor domain. Therefore, this algorithm is the most time intensive on the SGI-3800. Such shifts in the order of most time consuming algorithms is interesting from an optimization point of view, and suggests that efforts to speed up the model code should no longer focus on chemistry, but on advection instead.

A-4 Conclusions

Although the porting of the TM3 code to the new SGI-3800 infrastructure demanded considerable effort and time, the results presented show that in terms of model performance the parallelization was a success. A 22 times faster model was achieved on multiple processors, compared to one processor on the new computer. Relative to the old computer, a gain of a factor of 12 in turnover time was achieved. Moreover,

a high resolution (FG) run can now be applied in the same time a coarse resolution (CG) required on the old computer.

Based on a small study of the performance for different configurations of the model, and different configurations of processors, it can be concluded that TM3 parallelization works best when the simulation is calculation intensive, as opposed to communication intensive. Therefore, higher model resolutions will scale better, and the difference between coarse and finer resolutions is smaller on the new SGI–3800. This makes modeling on higher resolutions more attractive, lowering the threshold to apply these higher resolutions also in longer studies. Currently, a 16 processor simulation represents the optimum in costs/time for the FG resolution.

The different approach on the new computer has changed the order of most time consuming processes, putting advection before chemistry on the SGI–3800. Future improvements in model performance should therefore focus on this algorithms first, while the heavy calculations in the chemistry solver are now of lesser importance. This renders expansion of the chemical scheme to include more reactions and (non-transported) hydrocarbon intermediates feasible.

Bibliography

Andreae, M. O., The influence of tropical biomass burning on climate and the atmospheric environment, in *Biogeochemistry of Global Change: Radiatively Active Trace Gases*, pp. 113–150, Chapman and Hill, New York, 1993.

Andreae, M. O., and P. Merlet, Emission of trace gases and aerosols from biomass burning, *Glob. Biogeochem. Cyc.*, *15*, 955–966, 2001.

Arino, O., and J.-M. Melinotte, Fire Index Atlas, *Earth Observation Quarterly*, *50*, 1995.

Atherton, C., Organic nitrates in remote marine environments: Evidence for long-range transport, *Geophys. Res. Lett.*, *16*, 1289–1292, 1989.

Atlas, E., Evidence for $\leq$ C3 alkyl nitrates in rural and remote atmospheres, *Nature*, *331*, 426–428, 1988.

Baray, J. L., Tropical cyclone Marlene and stratosphere-troposphere exchange, *J. Geophys. Res.*, *104*, 13,953–13,970, 1999.

Baray, J.-L., V. Daniel, G. Ancellet, and B. Legras, Planetary-scale tropopause folds in the Southern subtropics, *Geophys. Res. Lett.*, *27*, 353–356, 2000.

Benkert, A. (Ed.), *Northern Hemisphere Biome and Process Specific Forest Areas and Gross Merchantable Volumes: 1880-1890*, Carbon Dioxide Information and Analysis Centre (CDIAC), Oak Ridge Natl. Lab., Oak Ridge, Tenn., 1997.

Bethan, S., G. Vaughan, and S. J. Reid, A comparison of ozone and thermal tropopause heights and the impact of tropopause definition on quantifying the ozone content of the troposphere, *Q. J. R. Meteorol. Soc.*, *122*, 929–944, 1996.

Brasseur, G. P., J. T. Kiehl, J.-F. Müller, T. Schneider, C. Granier, X. Tie, and D. Hauglustaine, Past and future changes in global tropospheric ozone: Impact on radiative forcing, *Geophys. Res. Lett.*, *25*, 3807–3810, 1998.

Bregman, A., M. C. Krol, H. Tyssedre, W. A. Norton, A. Iwi, M. Chipperfield, G. Pitari, J. K. Sundet, and J. Lelieveld, Chemistry-transport model comparison with ozone observations in the midlatitude lowermost stratosphere, *J. Geophys. Res.*, *106*, 17,479–17,496, 2001.

Bretherton, C. S., C. Smith, and J. M. Wallace, An intercomparison of methods for finding coupled patterns in climate data, *J. Clim.*, *5*, 541–560, 1992.

Browell, E. V., G. L. Gregory, R. C. Harris, and V. W. J. H. Kirchhoff, Ozone and aerosol distributions over the Amazon basin during the wet season, *J. Geophys. Res.*, *95*, 16,887–16,901, 1990.

Browell, E. V., et al., Ozone and aerosol distributions and air mass characteristics over the South Atlantic basin during the burning season, *J. Geophys. Res.*, *101*, 24,043–24,068, 1996.

Burrows, J. P., and K. V. Chance, SCIAMACHY and GOME: The scientific objectives, *Optical Methods in Atmospheric Chemistry*, *1715*, 151–175, 1992.

Burrows, J. P., A. Richter, F. Wittrock, M. Eisinger, and J. P. Burrows, The Global Ozone Monitoring Experiment (GOME): Mission Concept and First Scientific Results, *J. Atmos. Sci.*, *56*, 151–175, 1999.

Chameides, W. L., and J. C. G. Walker, A photochemical theory of tropospheric ozone, *J. Geophys. Res.*, *1973*, 8751–8760, 1973.

Chance, K. V., P. Palmer, R. J. D. Spurr, M. V. Randall, T. P. Kurosu, and D. J. Jacob, Satellite observations of formaldehyde over North America from GOME, *Geophys. Res. Lett.*, *27*, 3461–3464, 2000.

Chandra, S., J. R. Ziemke, W. Min, and W. G. Read, Effects of 1997-1998 El Niño Southern Oscillation on tropospheric ozone and water vapor, *Geophys. Res. Lett.*, *25*, 3867–3870, 1998.

Chatfield, R. B., J. A. Vastano, H. B. Singh, and G. Sachse, A general model of how fire emissions and chemistry produce African/oceanic plumes (O_3, CO, PAN, smoke) in TRACE-A, *J. Geophys. Res.*, *101*, 24,279–24,306, 1996.

Chatfield, R. B., Z. Guo, G. W. Sachse, D. Blake, and N. Blake, The Subtropical Global Plume in PEM-T A, PEM-T B, and GASP: How Tropical Emissions Affect the Remote Pacific., *J. Geophys. Res.*, *manuscript in preparation*, 2002.

Cooke, W. F., B. Koffi, and J.-M. Gregoire, Seasonality of vegetation fires in Africa from remote sensing data and application to a global chemistry model, *J. Geophys. Res.*, *101*, 21,051–21,065, 1996.

Craig, R., *The Upper Atmosphere: Meteorology and Physics*, Academic, San Diego, Calif., 1965.

Cros, B., R. Delmas, D. Nganga, B. Clairac, and J. Fontan, Seasonal trends of ozone in equatorial Africa: Experimental evidence of photochemical formation, *J. Geophys. Res.*, *95*, 7521–7532, 1990.

Crutzen, P. J., The influence of nitrogen oxides on the atmospheric ozone content, *Q. J. R. Meteorol. Soc.*, *96*, 320–325, 1970.

Crutzen, P. J., A discussion of the chemistry of some minor constituents in the stratosphere and troposphere, *Pure Appl. Geophys.*, *106–108*, 1385–1399, 1973.

Crutzen, P. J., The role of NO and NO_2 in the chemistry of the stratosphere and troposphere, *Ann. Rev. Earth Plant Sci.*, *7*, 443–472, 1979.

Crutzen, P. J., Tropospheric ozone: A review, in *Tropospheric Ozone: Global and Regional Scale Interactions*, edited by I. Isaksen, pp. 3–32, D. Reidel., Norwell-Mass., 1988.

Crutzen, P. J., and M. O. Andreae, Biomass burning in the tropics: Impact on atmospheric chemistry and biogeochemical cycles, *Science*, *250*, 1669–1678, 1990.

Crutzen, P. J., and C. Brühl, A model study of atmospheric temperatures and the concentrations of ozone, hydroxyl, and some other photochemically active gases during the glacial, the preindustrial holocene, and the present, *Geophys. Res. Lett.*, *20*, 1047–1050, 1993.

Crutzen, P. J., and P. H. Zimmermann, The changing photochemistry of the troposphere, *Tellus A*, *43*, 136–151, 1991.

de Laat, A. T. J., and J. Lelieveld, Diurnal ozone cycle in the marine boundary layer, *J. Geophys. Res.*, *105*, 11,547–11,559, 2000.

de Laat, A. T. J., M. Zachariasse, G. J. Roelofs, P. F. J. van Velthoven, R. Dickerson, K. Rhoads, S. Oltmans, and J. Lelieveld, Tropospheric O_3 distribution over the Indian Ocean during spring 1995 evaluated with a chemistry-climate model, *J. Geophys. Res.*, *104*, 13,881–13,893, 1999.

Dentener, F. J., and P. J. Crutzen, Reaction of N_2O_5 on tropospheric aerosols: Impact on the global distributions of NO_x, O_3, and OH, *J. Geophys. Res.*, *98*, 7149–7163, 1993.

Dentener, F. J., J. Feichter, and A. B. M. Jeuken, Simulation of transport of ^{222}Rn using on-line and off-line global models at different horizontal resolutions: A detailed comparison with measurements, *Tellus*, *51B*, 573–602, 1999.

Dentener, F. J., W. Peters, M. C. Krol, M. van Weele, and J. Lelieveld, On the interannual variability and trend of OH and the lifetime of CH_4: 1979-1993 global CTM simulations, *J. Geophys. Res.*, *submitted manuscript*, 2002a.

Dentener, F. J., M. van Weele, M. C. Krol, S. Houweling, and P. F. J. van Velthoven, Trends and interannual variability of methane emissions derived from 1979-1993 global CTM simulations, *Atm. Chem. Phys. Disc.*, *2*, 249–278, 2002b.

Diab, R., et al., Vertical ozone distribution over southern Africa and adjacent oceans during SAFARI-92, *J. Geophys. Res.*, *101*, 23,823–23,833, 1996.

Disselkamp, R. S., M. A. Carpenter, J. P. Cowin, C. M. Berkowitz, E. G. Chapman, R. A. Zaveri, and N. S. Laulainen, Ozone loss on soot aerosols, *J. Geophys. Res.*, *105*, 9767–9771, 2000.

Dlugocencky, E. J., L. P. Steele, P. M. Lang, and K. A. Masarie, The growth rate and distribution of atmospheric methane, *J. Geophys. Res.*, *99*, 17,021–17,043, 1994.

Dockery, D. W., C. A. Pope, X. P. Xu, J. D. Spengler, J. H. Ware, M. E. Fay, B. G. Ferris, and F. E. Speizer, An association between air-pollution and mortality in 6 United States cities, *New England Journal of Medicine*, *329*, 1753–1759, 1993.

Duncan, B., R. Martin, A. Staudt, R. Yevich, and J. Logan, Seasonal and inter-annual variability of biomass burning emissions constrained by remote-sensed observations, *manuscript in preparation*, 2002.

Duncan, B. N., and W. L. Chameides, Effects of urban emission control strategies on the export of ozone and ozone precursors from the urban atmosphere to the troposphere, *J. Geophys. Res.*, *103*, 28,159–29,179, 1998.

Dwyer, E., M. C. Pereira, J.-M. Grégoire, and C. C. DaCamara, Characterization of the spatio-temporal patterns of global fire activity using satellite imagery for the period April 1992 to March 1993., *Journal of Biogeography*, *27*, 57–69, 1999.

Ehhalt, D. H., H.-P. Dorn, and D. Poppe, The chemistry of the hydroxyl radical in the troposphere, pp. 17–34, Proc Roy. Soc. Edinburgh, Ser. B., 97, 1991.

Eisinger, M., and J. P. Burrows, Tropospheric sulfur dioxide observed by the ERS-2 GOME instrument, *Geophys. Res. Lett.*, *25*, 4177–4180, 1998.

Elbern, H., J. Hendricks, and A. Ebel, A climatology of tropopause folds by global analysis, *Theor. and App. Climatol.*, *59*, 181–200, 1996.

Farman, J. C., B. G. Gardiner, and J. D. Shanklin, Large losses of total ozone in antarctica reveal seasonal ClO_x/NO_x interaction, *Nature*, *315*, 207–210, 1985.

Fenn, M. A., et al., Ozone and aerosol distributions and air mass characteristics over the South Pacific during the burning season, *J. Geophys. Res.*, *104*, 16,197–16,212, 1999.

Fishman, J., and J. C. Larsen, Distribution of total ozone and stratospheric ozone in the tropics: Implications for the distribution of tropospheric ozone, *J. Geophys. Res.*, *92*, 6627–6634, 1987.

Fishman, J., C. E. Watson, J. C. Larsen, and J. A. Logan, Distribution of tropospheric ozone determined from satellite data, *J. Geophys. Res.*, *95*, 3599–3617, 1990.

Fishman, J., V. G. Brackett, E. V. Browell, and W. B. Grant, Tropospheric ozone derived from TOMS/SBUV measurements during TRACE-A, *J. Geophys. Res.*, *101*, 24,069–24,082, 1996.

Fortuin, J. P. F., and H. Kelder, An ozone climatology based on ozonesonde and satellite measurements, *J. Geophys. Res.*, *103*, 31,709–31,734, 1998.

Fortuin, J. P. F., H. M. Kelder, and C. R. Becker, Evidence of inertial unstable flow over Suriname during the South American monsoon period, *manuscript in preparation*, 2002.

Frank, W. M., The Structure and Energetics of the East Atlantic Intertropical Convergence Zone, *J. Atmos. Sci.*, *40*, 1916–1929, 1983.

Fuelberg, H. E., R. O. Loring, M. V. Watson, M. C. Sinha, K. E. Pickering, A. M. T. G. W. Sachse, D. R. Blake, and M. R. Schoeberl, TRACE-A trajectory intercomparison 2. Isentropic and kinematic methods, *J. Geophys. Res.*, *101*, 23,927–23,939, 1996.

Fujiwara, M., K. Kita, T. Ogawa, S. Kawakami, T. Sano, N. Komala, S. Saraspriya, and A. Suripto, Seasonal variations of tropospheric ozone in Indonesia revealed by 5-year ground-based observations, *J. Geophys. Res.*, *105*, 1879–1888, 2000.

Galanter, M., H. Levy, and G. R. Carmichael, Impacts of biomass burning on tropospheric CO, NO_x and O_3, *J. Geophys. Res.*, *105*, 6633–6653, 2000.

Ganzeveld, L. N., J. Lelieveld, and G. J. Roelofs, A dry deposition parameterization for sulfur oxides in a chemistry-general circulation model, *J. Geophys. Res.*, *103*, 5679–5694, 1998.

Gery, M. W., G. Z. Whitten, J. P. Killus, and M. C. Dodge, A photochemical kinetics mechanism for urban and regional scale computer modeling, *J. Geophys. Res.*, *94*, 12,925–12,956, 1989.

Gibson, R., P. Kallberg, and S. Uppsala, The ECMWF re-analysis (ERA) project, *ECMWF Newslett.*, *73*, 7–11, 1997.

Guelle, W. Y., J. Balkanski, M. Schulz, F. Dulac, and P. Monfray, Wet deposition in a global size-dependent aerosol transport model, 1, Comparison of a 1 year ^{210}Pb simulation with ground measurements, *J. Geophys. Res.*, *103*, 11,429–11,445, 1998.

Guenther, A., et al., A global-model of natural volatile organic compound emissions, *J. Geophys. Res.*, *D5*, 8873–8892, 1995.

Guthrie, P. D., The CH_4-CO-OH conundrum: A simple analytical approach, *Global. Biogeochem. Cycles*, *3*, 287–298, 1989.

Haagen-Smit, A. J., and M. M. Fox, Ozone formation in photochemical oxidation of organical substances, *Ind. Eng. Chem. Res.*, *48*, 1484–1487, 1956.

Hao, W. M., and M.-H. Liu, Spatial and temporal distribution of tropical biomass burning, *Global Biogeochem. Cycles*, *8*, 495–504, 1994.

Hao, W. M., M. H. Liu, and P. J. Crutzen, Estimates of the annual and regional release of CO_2 and other trace gases to the atmosphere from fires in the tropics based on the FAO statistics for the period 1975-1980, in *Fire in the Tropical Biota, Ecol. Stud.*, edited by J. Goldman, pp. 440–462, Springer-Verlag, New York, 1990.

Hastenrath, S., On general circulation and energy budget in the area of the Central American seas, *J. Atmos. Sci.*, *23*, 604–711, 1966.

Hastenrath, S., On the upper-air circulation over the equatorial Americas, *Arch. Meteor. Geophys. Bioklimatol. Serie A.*, *25*, 309–321, 1977.

Hastenrath, S., Annual cycle of upper air circulation and convective activity over the tropical Americas, *J. Geophys. Res.*, *102*, 4267–4274, 1997.

Hastenrath, S., Interannual and longer-term variability of upper air circulation in the Northeast Brazil-tropical Atlantic sector, *J. Geophys. Res.*, *105*, 7327–7335, 2000.

Hastenrath, S., and P. Lamb, *Climatic Atlas of the Tropical Atlantic and Eastern Pacific Oceans*, Univ. of Wisconsin Press, Madison, 1977.

Hauglustaine, D. A., G. P. Brasseur, S. Walters, P. J. Rasch, J. F. Müller, L. K. Emmons, and M. A. Carroll, MOZART, a global chemical transport model for ozone and related chemical tracers, 2. Model results and evaluation, *J. Geophys. Res.*, *103*, 28,291–28,335, 1998.

Heimann, M., P. Monfray, and G. Polian, Long-range transport of ^{222}Rn – A test for 3D tracer models, *Chem. Geology*, *70*, 98–98, 1988.

Hess, P., and S. Madronich, On tropospheric chemical oscillations, *J. Geophys. Res.*, *102*, 15,949–15,965, 1997.

Holton, J. R., P. H. Haynes, M. E. McIntyre, A. R. Douglass, R. B. Rood, and L. Pfister, Stratosphere-Troposphere exchange, *Reviews of Geophysics*, *33*, 403–439, 1995.

Houweling, S., Global modeling of atmospheric methane sources and sinks, Ph.D. thesis, Utrecht University, 2000.

Houweling, S., F. J. Dentener, and J. Lelieveld, The impact of nonmethane hydrocarbon compounds on tropospheric photochemistry, *J. Geophys. Res.*, *103*, 10,673–10,696, 1998.

Houweling, S., T. Kaminski, F. J. Dentener, J. Lelieveld, and M. Heimann, Inverse modeling of methane sources and sinks using the adjoint of a global transport model, *J. Geophys. Res.*, *104*, 26,137–26,160, 1999.

Houweling, S., F. J. Dentener, and J. Lelieveld, Simulation of preindustrial atmospheric methane to constrain the global source strength of natural wetlands, *J. Geophys. Res.*, *105*, 17,243–17,255, 2000.

Hudson, R. D., and A. M. Thompson, Tropical Tropospheric Ozone from Total Ozone Mapping Spectrometer by a modified residual method, *J. Geophys. Res.*, *103*, 22,129–22,145, 1998.

Hudson, R. D., J. Kim, and A. M. Thompson, On the derivation of tropospheric column ozone from radiances measured by the Total Ozone Mapping Spectrometer, *J. Geophys. Res.*, *100*, 11,138–11,145, 1995.

IPCC-TAR, Atmospheric Chemistry and Greenhouse gases, in *Climate Change 2001: Contribution of Working group I to the Third assessment report of the Intergovernmental Panel on Climate Change.*, edited by J. Houghton et al., p. 881, Cambridge University press,Cambridge and New York, NY, USA, 2001.

Isaksen, I. S. A., and O. Hov, Calculation of trends in the tropospheric concentration of O_3, OH, CO, CH_4 and NO_x, *Tellus B*, *39*, 271–285, 1987.

Jacob, D. J., Origin of ozone and NO_x in the tropical troposphere: A photochemical analysis of aircraft observations over the south Atlantic basin, *J. Geophys. Res.*, *101*, 24,235–24,250, 1996.

Jaeglé, L., et al., Ozone production in the upper troposphere and the influence of aircraft during SONEX: Approach of NO_x-saturated conditions, *Geophys. Res. Lett.*, *26*, 3081–3084, 1999.

Jeuken, A. B. M., Evaluation of chemistry and climate models using measurements and data assimilation, Ph.D. thesis, R. Dutch Meteorol. Inst. (KMNI), Utrecht, 2000.

Jeuken, A. B. M., H. J. Eskes, P. F. J. van Velthoven, H. M. Kelder, and E. V. Hölm, Assimilation of total ozone satellite measurements in a three-dimensional tracer transport model, *J. Geophys. Res.*, *104*, 5551–5564, 1999.

Johnson, B. J., S. J. Oltmans, H. Vömel, T. Deshler, C. Kroger, and H. G. J. Smit, ECC ozonesonde pump efficiency measurements and sensitivity tests of buffered and unbuffered sensor solutions, *J. Geophys. Res.*, *in press*, 2002.

Johnston, H., and D. Kinnison, Methane photooxidation in the atmosphere: Contrast between two methods of analysis, *J. Geophys. Res.*, *103*, 21,967–21,984, 1998.

Kanakidou, M., F. J. Dentener, and P. J. Crutzen, A global three-dimensional study of the fate of HCFCs and HFC-134a in the troposphere, *J. Geophys. Res.*, *100*, 18,781–18,801, 1995.

Kentarchos, A. S., G. J. Roelofs, and J. Lelieveld, Altitude distribution of tropospheric ozone over the northern hemisphere during 1996, simulated with a chemistry-general circulation model at two different horizontal resolutions, *J. Geophys. Res.*, *106*, 17,453–17,469, 2000.

Kim, J.-H., R. D. Hudson, and A. M. Thompson, A new method of deriving time-averaged tropospheric column ozone over the tropics using Total Ozone Mapping Spectrometer (TOMS) radiances: Intercomparison and analysis using TRACE-A data, *J. Geophys. Res.*, *101*, 24,317–24,330, 1996.

Kim, K.-Y., and Q. Wu, A comparison study of EOF techniques: Analysis of nonstationary data with periodic statistics, *J. Clim.*, *12*, 185–199, 1999.

Kirchhoff, V. W. J. H., and R. A. Rasmussen, Time variations of CO and ozone concentrations in a region subject to biomass burning, *J. Geophys. Res.*, *95*, 7521–7532, 1990.

Kleinman, L. I., Low and high NO_x tropospheric photochemistry, *J. Geophys. Res.*, *99*, 16,831–16,838, 1994.

Kley, D., P. J. Crutzen, H. G. J. Smit, H. Vomel, S. J. Oltmans, H. Grassl, and V. Ramanathan, Observations of near-zero ozone concentrations over the convective Pacific: Effects on air chemistry, *Science*, *274*, 230–233, 1996.

Klonecki, A., and H. Levy, Tropospheric chemical ozone tendencies in a CO-CH_4-NO_y-H_2O system: Their sensitivity to variations in environmental parameters and their application to a global chemistry transport model study, *J. Geophys. Res.*, *102*, 21,221–21,238, 1997.

Komhyr, W. D., *Handbook- Ozone measurements to 40 km altitude with model 4A-ECC-ozone sondes*, NOAA Techn. Memorandum ERL ARL-149, 1986.

Komhyr, W. D., S. J. Oltmans, P. R. Franchois, F. J. Evans, and W. A. Matthews, The latitudinal distribution of ozone to 35 km altitude from ECC ozonesonde observations, Ozone in the Atmosphere, in *Proceedings of Quadrennial Ozone Symposium 1988 and Tropospheric Ozone Workshop*, edited by R. D. Bojkov and P. Fabian, pp. 147–150, Deepak, Hampton, VA, 1989.

Krishnamurti, T. N., H. E. Fuelberg, M. C. Sinha, D. Oosterhoff, E. L. Bensman, and V. B. Kumar, The meteorological environment of the tropospheric ozone maximum over the tropical South Atlantic, *J. Geophys. Res.*, *98*, 10,621–10,641, 1993.

Krishnamurti, T. N., M. Sinha, M. Kanamitsu, D. Oosterhof, H. Fuelberg, R. Chatfield, D. J. Jacob, and J. A. Logan, Passive tracer transport relevant to the TRACE-A experiment, *J. Geophys. Res.*, *101*, 23,889–23,908, 1996.

Krol, M. C., and J. Lelieveld, Can the variability in tropospheric OH be deduced from measurements of 1,1,1-trichlorethane (methyl chloroform)?, *J. Geophys. Res.*, *in press*, 2002.

Krol, M. C., and D. Poppe, Nonlinear dynamics in atmospheric chemistry rate equations, *J. Atmos. Sci.*, *29*, 1–16, 1998.

Krol, M. C., and M. van Weele, Implications of variations in photodissociation rates for global tropospheric chemistry, *Atmos. Environ.*, *31*, 1257–1273, 1997.

Krol, M. C., P. J. van Leeuwen, and J. Lelieveld, Global OH trend inferred from methylchloroform measurement, *J. Geophys. Res.*, *103*, 10,697–10,711, 1998.

Krol, M. C., W. Peters, P. J. F. Berkvens, and M. A. Botchev, A new algorithm for two-way nesting in global models: Principles and Applications, in *Proceedings of the 2nd international conference on air pollution modeling and simulation*, edited by B. Sportisse, Springer Geosciences, 2001.

Krol, M. C., J. Lelieveld, D. E. Oram, S. A. Penkett, and G. A. Sturrock, Evidence for substantial 1,1,1-trichloroethane emissions from europe, *Nature, submitted manuscript*, 2002.

Lamarque, J.-F., G. Brasseur, P. Hess, and J.-F. Müller, Three-dimensional study of the relative contributions of the different nitrogen sources in the troposphere, *J. Geophys. Res.*, *101*, 22,955–22,968, 1996.

Landgraf, J., and P. J. Crutzen, An efficient method for online calculation of photolysis and heating rates, *J. Atmos. Sci.*, *55*, 863–878, 1998.

Langner, J., and E. Rodhe, A global 3-dimensional model of the tropospheric sulfur cycle, *J. Atmos. Chem.*, *13*, 225–263, 1991.

Lawrence, M. G., P. J. Crutzen, P. J. Rasch, B. E. Eaton, and N. M. Mahowald, A model for studies of tropospheric photochemistry: Description, global distributions, and evaluation, *J. Geophys. Res.*, *104*, 26,245–26,277, 1999.

Lawrence, M. G., P. Jöckel, and R. von Kuhlmann, What does the global mean OH concentration tell us?, *Atmos. Chem. Phys.*, pp. 37–49, 2001.

Lelieveld, J., and P. J. Crutzen, Role of deep cloud convection in the ozone budget of the troposphere, *Science*, *264*, 1759–1761, 1994.

Lelieveld, J., and F. J. Dentener, What controls tropospheric ozone?, *J. Geophys. Res.*, *105*, 3531–3551, 2000.

Lelieveld, J., and R. van Dorland, Model simulations of ozone chemistry changes in the troposphere and consequent radiative forcings of climate during industrialization, in *Atmospheric ozone as a climate gas*, edited by W. C. Wang and I. S. A. Isaksen, pp. 227–258, NATO ASI Series, Springer-Verlag, Berlin, 1995.

Lelieveld, J., W. Peters, F. J. Dentener, and M. C. Krol, Stability of tropospheric hydroxyl chemistry, *J. Geophys. Res.*, *in press*, 2002.

Levy, H., W. J. Moxim, and P. S. Kasibhatla, A global three-dimensional time-dependent lightning source of tropospheric NO_x, *J. Geophys. Res.*, *101*, 22,911–22,922, 1996.

Levy II, H., Normal atmosphere: large radical and formaldehyde concentrations predicted, *Science*, *173*, 141–143, 1971.

Logan, J. A., Tropospheric Ozone: Seasonal behavior, trends and anthropogenic influence, *J. Geophys. Res.*, *90*, 10,463–10,482, 1985.

Logan, J. A., Trends in the vertical distribution of ozone: An analysis of ozonesonde data, *J. Geophys. Res.*, *99*, 25,553–25,585, 1994.

Logan, J. A., An analysis of ozonesonde data for the troposphere: Recommendations for testing 3-D models and development of a gridded climatology for tropospheric ozone, *J. Geophys. Res.*, *104*, 16,115–16,149, 1999.

Logan, J. A., and V. W. J. H. Kirchhoff, Seasonal variations of tropospheric ozone at Natal, Brazil, *J. Geophys. Res.*, *91*, 7875–7882, 1986.

Logan, J. A., M. J. Prather, S. C. Wofsy, and M. B. McElroy, Tropospheric chemistry: A global perspective, *J. Geophys. Res.*, *86*, 7210–7354, 1981.

Louis, J. F., A parametric model of vertical eddy fluxes in the atmosphere, *Boundary Layer Meteorol.*, *17*, 178–202, 1979.

Lu, R., C. Lin, R. Turco, and A. Arakawa, Cumulus transport of chemical tracers 1: Cloud-resolving model simulations, *J. Geophys. Res.*, *105*, 10,001–10,021, 2000.

Mackerras, D., and M. Darveniza, Latitudinal variation of lightning occurrence characteristics, *J. Geophys. Res.*, *99*, 10,813–10,822, 1994.

Martin, R. V., D. J. Jacob, J. A. Logan, J. R. Ziemke, and R. Washington, Detection of a lightning influence on tropical tropospheric ozone, *Geophys. Res. Lett.*, *27*, 1639–1642, 2000.

Martinerie, P., G. P. Brasseur, and C. Granier, The chemical composition of ancient atmospheres: A model study constrained by ice core data, *J. Geophys. Res.*, *100*, 14,291–14,304, 1995.

Marufu, L., F. J. Dentener, J. Lelieveld, M. O. Andreae, and G. Helas, Photochemistry of the African troposphere: The influence of biomass burning emissions, *J. Geophys. Res.*, *105*, 14,513–14,540, 2000.

Mauzerall, D. L., et al., Photochemistry in biomass burning plumes and implications for tropospheric ozone over the tropical South Atlantic, *J. Geophys. Res.*, *103*, 8401–8423, 1998.

McConnell, J. C., M. B. McElroy, and S. C. Wofsy, Natural sources of atmospheric CO, *Nature*, *233*, 187–188, 1971.

McPeters, R. D., and G. J. Labow, An assessment of the accuracy of 14.5 years of Nimbus TOMS Version 7 ozone data by comparison with the Dobson network, *Geophys. Res. Lett.*, *23*, 3695–3698, 1996.

Meijer, E. W., P. F. J. van Velthoven, D. W. Brunner, H. Huntrieser, and H. M. Kelder., Improvement and evaluation for the parameterisation of nitrogen oxide production by lightning, *Phys. Chem. of the Earth*, *26*, 557–583, 2001.

Molina, M. J., and F. S. Rowland, Stratospheric sink for chlorofluoromethanes: chlorine atom catalyzed destruction of ozone, *Nature*, *249*, 810–812, 1974.

Moxim, W. J., and H. Levy, A model analysis of the tropical South Atlantic Ocean tropospheric ozone maximum; The interaction of transport and chemistry, *J. Geophys. Res.*, *105*, 17,393–17,415, 2000.

Olivier, J. G. J., A. F. Bouwman, J. J. M. Berdowski, C. Veldt, J. P. J. Bloos, A. J. H. Visschedijk, C. W. M. van der Maas, and P. Y. J. Zandveld, Sectoral emission inventories of greenhouse gases for 1990 on a per country basis as well as on $1^\circ \times 1^\circ$, *Environ. Sci. Policy*, *2*, 241–264, 1999.

Olivier et al., J., Description of EDGAR version 2.0, Rijks-inst. voor Volksgezondheid en Milieu, Bilthoven, Rep. 771060002, 1996.

Oltmans, S. J., and H. Levy, Surface ozone measurements from a global network, *Atmos. Environ.*, *28*, 9–24, 1994.

Pacheco, P., *Parallel Programming with MPI*, Morgan Kauffman Publishers, 1996.

Pan, L., J. C. Gille, D. P. Edwards, P. L. Bailey, and C. D. Rodgers, Retrieval of tropospheric carbon monoxide for the MOPITT experiment, *J. Geophys. Res.*, *103*, 32,277–32,290, 1998.

Perner, D., et al., Measurements of tropospheric OH concentrations: A comparison of field data with model predictions, *J. Atmos. Chem.*, *5*, 185–216, 1987.

Peters, W., M. C. Krol, F. J. Dentener, and J. Lelieveld, Identification of an El Niño-Southern Oscillation signal in a multiyear global simulation of tropospheric ozone, *J. Geophys. Res.*, *106*, 10,389–10,402, 2001.

Peters, W., M. C. Krol, F. J. Dentener, A. M. Thompson, and J. Lelieveld, Chemistry-transport modeling of the satellite observed distribution of tropical tropospheric ozone, *Atmos. Chem. Phys.*, *2*, 103–120, 2002.

Petit, J. R., J. Jouzel, and D. Raynaud, Climate and atmospheric history of the past 420,000 years from the Vostok ice core, Antarctica, *Nature*, *399*, 429–436, 1999.

Pickering, K. E., A. M. Thompson, W. K. Tao, and T. L. Kucsera, Upper tropospheric ozone production following mesoscale convection during STEP/EMEX, *J. Geophys. Res.*, *98*, 8737–8749, 1993.

Pickering, K. E., A. M. Thompson, D. P. McNamara, M. R. Schoeberl, H. E. Fuelberg, R. O. Loring, M. V. Watson, K. Fakhruzzaman, and A. S. Bachmeier, TRACE-A trajectory intercomparison 1. Effects of different input analyses, *J. Geophys. Res.*, *101*, 23,909–23,925, 1996.

Pickering, K. E., Y. Wang, W. K. Tao, C. Price, and J. F. Müller, Vertical distributions of lightning NO_x for use in regional and global chemical transport models, *J. Geophys. Res.*, *103*, 31,203–31,216, 1998.

Pinto, J. P., and M. A. K. Khalil, The stability of tropospheric OH during ice ages, interglacial epochs and modern times, *Tellus B*, *43*, 347–352, 1991.

Pinty, B., F. Roveda, M. M. Verstraete, N. Gobron, Y. Govaerts, J. V. Martonchik, D. J. Diner, and R. A. Kahn, Surface albedo retrieval from Meteosat, 2. Applications, *J. Geophys. Res.*, *105*, 18,114–18,134, 2000.

Poppe, D., and H. Lustfeld, Nonlinearities in the gas phase chemistry of the troposphere: Oscillating concentrations in a simplified mechanism, *J. Geophys. Res.*, *101*, 14,373–14,380, 1996.

Pöschl, U., M. G. Lawrence, R. von Kuhlmann, and P. J. Crutzen, Comment on: 'Methane photooxidation in the atmosphere: Contrast between two methods of analysis' by Harold Johnston and Douglas Kinnison., *J. Geophys. Res.*, *105*, 1431–1432, 2000.

Pöschl, U., R. von Kuhlmann, N. Poisson, and P. J. Crutzen, Development and Intercomparison of Condensed Isoprene Oxidation Mechanisms for Global Modeling, *J. Atm. Chem.*, *37*, 29–52, 2000.

Prather, M., Lifetimes and eigenstates in atmospheric chemistry, *Geoph. Res. Let.*, *21*, 801–804, 1994.

Price, C., and D. Rind, A simple lightning parameterization for calculating lightning distributions, *J. Geophys. Res.*, *97*, 9919–9933, 1992.

Price, C., J. Penner, and M. Prather, NO_x from lightning, 1, Global distribution based on lightning physics, *J. Geophys. Res.*, *102*, 5929–5941, 1997.

Prinn, R. G., et al., Global average concentration and trend for hydroxyl radicals deduced from ALE/GAGE trichloroethane (methyl chloroform) data for 1978-1990, *J. Geophys. Res.*, *97*, 2445–2461, 1992.

Prinn, R. G., et al., Evidence for substantial variations of atmospheric hydroxyl radicals in the past two decades, *Science*, *292*, 1882–1888, 2001.

Randel, W. J., and J. B. Cobb, Coherent variations of monthly mean total ozone and lower stratospheric temperature, *J. Geophys. Res.*, *99*, 5433–5447, 1994.

Richter, A., F. Wittrock, M. Eisinger, and J. P. Burrows, GOME observations of tropospheric BrO in Northern Hemispheric spring and summer 1997, *Geophys. Res. Lett.*, *25*, 2683–2686, 1998.

Roelofs, G. J., J. Lelieveld, H. G. J. Smit, and D. Kley, Ozone production and transports in the tropical Atlantic region during the biomass burning season, *J. Geophys. Res.*, *102*, 10,637–10,651, 1997.

Russel, G., and J. Lerner, A new finite-differencing scheme for the tracer transport equation, *J. Appl. Meteorol.*, *20*, 1483–1498, 1981.

Shiotani, M., Annual, quasi-biennial and El Niño Southern Oscillation time-scale variations in Equatorial total ozone, *J. Geophys. Res.*, *97*, 7625–7634, 1992.

Singh, H. B., and L. J. Salas, Peroxyacetylnitrate in the free troposphere, *Nature*, *302*, 326–328, 1983.

Singh, H. B., M. Kanakidou, P. J. Crutzen, and D. J. Jacob, High concentrations and photochemical fate of oxygenated hydrocarbons in the global atmosphere, *Nature*, *378*, 50–54, 1995.

Snow, J. W., The Climate of Northern South America, in *World Survey of Climatology, Vol 12*, edited by H. E. Landsberg, chap. 6, pp. 305–321, Elsevier Scientific Publ. Amsterdam, 1976.

Spivakovsky, C. M., R. Yevich, J. A. Logan, S. C. Wofsy, M. B. McElroy, and M. J. Prather, Tropospheric OH in a three-dimensional chemical tracer model: An assessment based on observations of CH_3CCl_3, *J. Geophys. Res.*, *95*, 18,441–18,471, 1990.

Spivakovsky, C. M., et al., Three-dimendional climatological distribution of tropospheric OH: Update and evaluation, *J. Geophys. Res.*, *105*, 8931–8980, 2000.

Stewart, R. W., Dynamics of the low to high NO_x transition in a simplified tropospheric photochemical model, *J. Geophys. Res.*, *100*, 8929–8943, 1995.

Stohl, A., and N. E. Koffi, Evaluation of trajectories calculated from ECMWF data against constant volume balloon flights during ETEX, *Atmos. Environ.*, *32*, 4151–4156, 1998.

Stolarski, R. S., P. Bloomfield, R. D. McPeters, and J. R. Herman, Total ozone trends deduced from Nimbus 7 TOMS data, *Geophys. Res. Lett.*, *18*, 1015–1018, 1991.

Thompson, A. M., The oxidizing capacity of the Earths atmosphere: Probable past and future changes, *Science*, *256*, 1157–1165, 1992.

Thompson, A. M., and R. D. Hudson, Tropical tropospheric ozone (TTO) maps from Nimbus 7 and Earth Probe TOMS by the modified-residual method: Evaluation with sondes, ENSO signals, and trends from Atlantic regional time series, *J. Geophys. Res.*, *104*, 26,961–26,975, 1999.

Thompson, A. M., K. E. Pickering, D. P. McNamara, M. R. Schoeberl, R. D. Hudson, J. H. Kim, E. V. Browell, V. W. J. H. Kirchhoff, and D. Nganga, Where did tropospheric ozone over Southern Africa and the tropical Atlantic come from in October 1992? Insights from TOMS, GTE/TRACE-A, and SAFARI-92, *J. Geophys. Res.*, *101*, 24,251–24,278, 1996.

Thompson, A. M., B. G. Doddridge, J. C. Witte, R. D. Hudson, W. T. Luke, J. E. Johnson, B. J. Johnson, S. J. Oltmans, and R. Weller, A tropical Atlantic ozone paradox: Shipboard and satellite views of a tropospheric ozone maximum and wave-one in January-February 1999, *Geophys. Res. Lett.*, *27*, 3317–3320, 2000.

Thompson, A. M., J. C. Witte, R. D. Hudson, H. Guo, J. R. Herman, and M. Fujiwara, Tropical Tropospheric Ozone and Biomass Burning, *Science*, *291*, 2128–2132, 2001.

Thompson, A. M., et al., The 1998-2000 SHADOZ (Southern Hemisphere ADditional OZonesondes) Tropical Ozone Climatology. 1. Comparisons with TOMS and Ground-based Measurements, *J. Geophys. Res.*, *in press*, 2002a.

Thompson, A. M., et al., The 1998–2000 SHADOZ (Southern Hemisphere ADditional OZonesondes) tropical ozone Climatology. 2. Stratospheric and Tropospheric Ozone Variability and the Zonal Wave-One, *J. Geophys. Res.*, *in press*, 2002b.

Tiedtke, M. A., A comprehensive mass flux scheme for cumulus parameterization in large-scale models, *Mon. Weather Rev.*, *117*, 1779–1800, 1989.

Tuck, A. F., et al., The Brewer-Dobson circulation in the light of high-altitude in situ aircraft observations, *Q. J. R. Meteorol. Soc.*, *123*, 1–69, 1997.

US–EPA, National Air Quality and Emission Trends Report, *Tech. Rep. EPA 454/R-97-013*, US Environmental Protection Agency, Research Triangle Park, NC, 1998.

van Aardenne, J. A., F. J. Dentener, and J. G. J. Olivier, A 1 degrees x 1 degrees resolution data set of historical anthropogenic trace gas emissions for the period 1890-1990, *Global Biogeochem. Cycles*, *4*, 909–928, 2001.

Wang, Y., D. J. Jacob, and J. A. Logan, Global simulation of tropospheric O_3-NO_x-hydrocarbon chemistry, 3, Origin of tropospheric ozone and effects of nonmethane hydrocarbons, *J. Geophys. Res.*, *103*, 10,757–10,768, 1998.

Wang, Y., S. C. Liu, H. Yu, S. T. Sandholm, T.-Y. Chen, and D. R. Blake, Influence of convection and biomass burning outflow on tropospheric chemistry over the tropical Pacific, *J. Geophys. Res.*, *105*, 9321–9333, 2000.

Weller, J. W., R. Lilischkis, O. Schrems, R. Neuber, and S. Wessel, Vertical ozone distribution in the marine atmosphere over the central Atlantic Ocean (56°S–50°N), *J. Geophys. Res.*, *101*, 1387–1399, 1996.

Wesely, M. L., Parameterization of surface resistance to gaseous dry deposition in regional-scale numerical models, *Atmos. Environ.*, *23*, 1293–1304, 1989.

WMO, *Scientific assessment of ozone depletion: 1994*, World Meteorological Organization, 37 ed., 1995, Geneva.

Yienger, J. J., and H. Levy, Global inventory of soil-biogenic NO_x emissions, *J. Geophys. Res.*, *100*, 11,447–11,464, 1995.

Yonemura, S., H. Tsuruta, S. Kawashima, S. Sudo, L. C. Peng, L. Fook, , Z. Johar, and M. Hayashi, Tropospheric ozone climatology over peninsular Malaysia from 1992 to 1999, *J. Geophys. Res.*, *107*, DOI 10.1029/2001JD000,993, 2002a.

Yonemura, S., H. Tsuruta, T. Maeda, S. Kawashima, S. Sudo, and M. Hayashi, Tropospheric ozone variability over Singapore from August 1996 to December 1999, *Atmos. Env.*, *36*, 2061–2070, 2002b.

Yonemura, S., H. Tsuruta, S. Sudo, L. C. Peng, L. Fook, , and Z. Johar, Annual and El Niño/Southern Oscillation variations in observations of in-situ stratospheric ozone over peninsular Malaysia, *J. Geophys. Res.*, *107*, DOI 10.1029/2001JD000,742, 2002c.

Zachariasse, M., P. F. J. van Velthoven, H. G. J. Smit, J. Lelieveld, T. K. Mandal, and H. Kelder, Influence of stratosphere-troposphere exchange on tropospheric ozone over the tropical Indian Ocean, *J. Geophys. Res.*, *105*, 15,403–15,416, 2000.

Ziemke, J. R., S. Chandra, R. D. McPeters, and P. A. Newman, Dynamical proxies of column ozone with applications to global trend models, *J. Geophys. Res.*, *102*, 6117–6129, 1997.

Ziemke, J. R., S. Chandra, and P.-K. Bhartia, Two new methods for deriving tropospheric column ozone from TOMS measurements: The assimilated UARS MLS/HALOE and convective-cloud differential techniques, *J. Geophys. Res.*, *103*, 22,115–22,128, 1998.

Ziemke, J. R., S. Chandra, and P.-K. Bhartia, Seasonal and interannual variabilities in tropical tropospheric ozone, *J. Geophys. Res.*, *104*, 21,245–21,442, 1999.

Summary

This thesis discusses transport and photochemistry of trace gases in the tropical troposphere. The Inter Governmental Panel on Climate Change (IPCC) expects the composition of the troposphere to change in the future due to global population growth, industrialization, deforestation, desertification, and agricultural development. Momentarily, we cannot reliably predict what changes will occur, and what the consequences for global climate will be. Firstly because the links between the expected changes and the atmospheric response are not understood well enough, and secondly because natural variability of the climate system (for instance due to El Niño) might alter this response. These two aspects also complicate attempts to understand measurements made in the (recent) past.

The aim of the research presented here is to acquire knowledge of the (past, present, and future) composition, stability, sensitivity, and variability of the troposphere. We focus mostly on the tropical regions because it has received little attention so far, measurements here are scarce, and large changes are expected to occur in the future. Special attention is given to ozone as it plays a key role in tropospheric photochemistry. Not only is it a greenhouse gas, it is also the most important precursor of the hydroxyl radical (OH) which is responsible for the removal of many trace gases from the troposphere. Furthermore, ozone is an important indicator for atmospheric transport and photochemistry. The involvement of ozone in many different processes also renders it an excellent compound to test our knowledge of coupled transport-chemistry systems.

The research questions that we set out to answer in this work can be summarized as follows:

1. Do we understand the horizontal and vertical distribution of ozone in the tropical troposphere, and specifically over the equatorial Atlantic Ocean?

2. Do we understand the variability of ozone in the tropical troposphere?

3. What is the nature of photochemical feedbacks involving ozone, and how do they contribute to the apparent constancy of oxidant levels?

4. Does the human induced changing atmospheric composition destabilize tropospheric hydroxyl photo-chemistry?

The first research question is topic of Chapter 2, where we present the measurements of ozone performed since the inauguration (1999) of a new ozone monitoring

station in Paramaribo, Suriname. This station was started under the Research on Atmospheric Dynamics and Chemistry in Suriname (RADCHiS) project. The choice for this location was partly due to the historical ties with Suriname, but also because of the unique location of Paramaribo with respect to the Atlantic Ocean, the equator (northern hemisphere), and the Inter Tropical Convergence Zone (ITCZ). Because the ITCZ passes Suriname twice per year the station samples both the meteorological northern and southern hemispheres. This leads to strong contrast with nearby southern hemisphere stations (Ascension and Natal) during February and March.

Using simple model simulations we describe two meteorological situations that can cause photochemical ozone production following biomass burning to enhance ozone at Paramaribo. Also, the measurements at Paramaribo are used to show that satellite observations of ozone, that are also used in this thesis, show a systematic bias in the northern hemisphere due to an unconfirmed assumption in the algorithm used to create the dataset. The most important conclusion from Chapter 2 is that although the station resembles nearby stations in August through November, samples taken during February and March bring new information and insights on ozone in the equatorial Atlantic, and can be used to improve existing satellite observations.

Chapter 3 describes the variability of ozone in the tropics, and our ability to reproduce this variability (on time scales of months to years). For that purpose we use a model simulation that spans the period 1979-1993, and that includes trends of anthropogenic emissions, and day-to-day variability of meteorology. The model calculated seasonal cycle of ozone in the tropics shows that we are able to reproduce observations for stations in the remote Pacific Ocean quite well, but that the more polluted Atlantic Ocean is more problematic. At times, the model underestimates ozone by more than 30%.

Furthermore, our results show that the model realistically reproduces the changing convection patterns in the Walker circulation during the positive phase of the El Niño-Southern Oscillation (ENSO). This causes an increase of ozone due to downward transport over Indonesia, and a decrease of ozone over the Pacific region close to South America. These results are in good agreement with satellite observations, even though other influences on ozone that change during ENSO (e.g. biomass burning in dry areas) were not included in our model simulation. This work presents the first ENSO signal in a multi-year model simulation of ozone.

To better understand, and possibly solve, the large underestimate of ozone over the Atlantic Ocean we have investigated the zonal distribution of ozone in more detail in Chapter 4. Since ozone monitoring stations in the tropics are not abundant, and usually only span a few years, we have used satellite observations of ozone (1979-1992) to compare our model to. First, we introduce a method to compare model and measurements quantitatively and systematically, and then use this method to identify times and regions where model underestimates are largest.

Largest underestimates occur in the months from August through November, over the Atlantic Ocean, adjacent continents, and even part of the Indian Ocean. Analysis of the sources and sinks of ozone shows that the local ozone concentrations are determined almost equally by all relevant processes in the model, e.g. biomass burning, soil NO_x emissions, industrial emissions, lightning, and stratosphere-troposphere exchange. The influence of biomass burning emissions and soil NO_x emissions on ozone

display the largest asymmetry between Atlantic and Pacific though, because these sources are close to the surface and are transported through the troposphere more slowly. A large number of sensitivity simulations, in which specific model parameters were altered to study their influence on ozone, indicate that ozone is very insensitive to changes in model description because efficient feedbacks in the budget of ozone tend to stabilize its concentration.

This means that with the current knowledge of the system, and the calculated sensitivities, we cannot find systematic improvements to bring models and satellite observations within one standard deviation. Our recommendations based on this chapter are to focus future research on transport of ozone and precursors from the planetary boundary layer, and on the treatment of biomass burning in the tropics. Also, a reduction of the uncertainties in the satellite observations would help studies such as this.

Chapter 5 treats the stability of photochemistry in the tropics, and the largely unchanged levels of OH since industrialization. We focus specifically on OH levels, which are strongly coupled to ozone levels because together with water vapor and sunlight, they determine OH production rates.

We introduce a new concept called 'recycling efficiency' which describes to what extent OH production depends on ozone photolysis (primary production) relative to other processes (secondary production). We find that the role of primary ozone production is less important in industrialized areas, but of major importance to remote regions where advection of ozone has prevented strong decreases of OH levels. The regions that depend strongly on primary production are also most sensitive to disturbances in photochemistry such as through increases of methane or nitrogen oxide levels. This has important consequences, since these remote regions are mostly in the tropics where economical development is expected to introduce large changes in the (near) future.

It seems a paradox that global OH has remained nearly constant since industrialization despite large increases in levels of carbonmonoxide and methane. Our calculations show that global OH has remained constant through a 50% increase in primary OH production, and a 75% increase in secondary production. Locally, the OH distribution has changed substantially since industrialization with increases of more than 200% in urban areas, and decreases of more than 30% in remote marine areas.

Samenvatting

Het onderzoek in dit proefschrift richt zich op het transport en de fotochemische omzetting van sporegassen in de tropische troposfeer. Het Inter Governmental Panel on Climate Change (IPCC) verwacht dat de samenstelling van de troposfeer in de toekomst zal veranderen tengevolge van de toename van de wereldbevolking, voortschrijdende industrialisatie, grootschalige ontbossing, verwoestijning en verandering in agrarische methoden. Op dit moment kunnen wij nog niet betrouwbaar voorspellen hoe de samenstelling van de atmosfeer zal veranderen en wat de gevolgen zijn voor het wereldklimaat. Dit komt ten eerste doordat de verbanden tussen de genoemde veranderingen en de atmosferische respons niet goed begrepen zijn en ten tweede doordat natuurlijke variabiliteit (denk bijvoorbeeld aan El Niño) de respons kan veranderen, of zelfs teniet kan doen. Deze twee aspecten bemoeilijken ook pogingen om reeds waargenomen veranderingen in het recente verleden te verklaren.

Het doel van het hier gepresenteerde onderzoek is om meer inzicht te krijgen in de samenstelling, stabiliteit, gevoeligheid en variabiliteit van de troposfeer. Deze aspecten beschouwen we zowel in de huidige als in de vroegere en de toekomstige troposfeer. We richten ons voornamelijk op de tropen omdat deze regio erg groot is, van oudsher weinig aandacht heeft gekregen, weinig bemonsterd is door metingen en er de grootste veranderingen in de nabije toekomst te verwachten zijn. In het bijzonder gaat de aandacht uit naar ozon, dat een sleutelrol vervuld in de fotochemie van de troposfeer. Ozon is niet alleen een broeikasgas in de troposfeer, het is ook de belangrijkste voorloper van het hydroxyl-radicaal (OH) dat verantwoordelijk is voor de verwijdering van vele schadelijke stoffen uit onze atmosfeer. Bovendien is het ozon molecuul een goede indicator voor het atmosferisch transport en de fotochemische omzettingen die een luchtmassa heeft ondergaan. Vanwege zijn betrokkenheid bij zeer veel processen in de atmosfeer is ozon ook een uitstekende stof om onze kennis van gekoppelde systemen te testen.

De onderzoeksvragen die aan bod komen in dit proefschrift luiden als volgt:

1. Begrijpen we de horizontale en verticale verdeling van ozon in de tropische troposfeer en specifiek in het gebied rond de evenaar boven de Atlantische Oceaan?

2. Begrijpen we de interjaarlijkse variabiliteit van ozon in de tropen?

3. Wat is de aard van fotochemische terugkoppelingen waar ozon bij betrokken is en hoe dragen deze terugkoppelingen bij aan de stabiliteit van ozon en OH

concentraties?

4. Leidt menselijk handelen tot een destabilisatie van de fotochemie van het OH-radicaal?

De eerste onderzoeksvraag wordt behandeld in Hoofdstuk 2, waar we de metingen van ozon presenteren die gedaan zijn sinds de oprichting in 1999 van een nieuw meetstation in Paramaribo, Suriname. Dit station is opgebouwd onder het project RADCHiS, waar ook dit proefschrift onder valt. De keuze voor een meetstation in Paramaribo werd ingegeven door de historische banden met Suriname, en door de unieke ligging van Paramaribo ten opzichte van de Atlantische Oceaan, de evenaar (noordelijk halfrond) en de inter-tropische convergentiezone (ITCZ). Omdat de ITCZ twee maal per jaar het station passeert, kan zowel het meteorologische noordelijke als zuiderlijke halfrond bemonsterd worden. Dit leidt tot sterke contrasten met nabij gelegen stations op het zuidelijk halfrond (Ascension en Natal) tijdens de maanden februari en maart.

Met behulp van simpele modelsimulaties worden twee meteorologische situaties geschetst die kunnen zorgen voor foto-chemische verhoging van de ozon concentraties in Paramaribo tengevolge van de verbranding van biomassa in de tropen. Ook wordt met behulp van de meetgegevens aangetoond dat satellietwaarnemingen van ozon, die ook in dit proefschrift gebruikt zijn, een afwijking vertonen op het gehele noordelijk halfrond tengevolge van een onjuiste aanname in het gebruikte algoritme.

De belangrijkste conclusie uit Hoofdstuk 2 luidt dat dit station weliswaar sterk lijkt op nabij gelegen stations tijdens de maanden juni-november, maar dat het bemonsteren van het noordelijk halfrond in februari-maart nieuwe informatie oplevert die onze kennis over de equatoriale Atlantische regio vergroot en kan helpen om bestaande satelliet waarnemingen te verbeteren.

Hoofdstuk 3 gaat in op de variabiliteit van ozon in de tropen en ons vermogen om deze variabiliteit (op tijdschalen van maanden tot jaren) te reproduceren. Hiervoor is een model simulatie uitgevoerd die de periode 1979-1993 bestrijkt en waarin zowel de ontwikkeling van industriële emissies als de dag-tot-dag variabiliteit van meteorologie wordt meegenomen.

Uit de door het model berekende seizoensgang van ozon op een viertal lokaties in de tropen blijkt dat we goed in staat zijn om de concentraties boven stations in de afgelegen Grote Oceaan te reproduceren. Echter, de sterker vervuilde troposfeer boven de stations in de Atlantische Oceaan is problematisch. Het model onderschat ozon daar soms met meer dan 30%.

Daarnaast blijkt dat het model, door het gebruik van de juiste meteorologie, in staat is om de invloed van de El-Niño Southern Oscillation (ENSO) op de ozon concentraties te reproduceren. Het verschuiven van sterke convectiecentra in de Walker circulatie richting de kust van Zuid-Amerika zorgt daar voor een lokaal minimum van ozon, terwijl boven Indonesië een maximum van ozon ontstaat door neerwaarts ozontransport. Deze bevindingen komen goed overeen met satellietwaarnemingen, ondanks het feit dat andere aspecten die ozon beïnvloeden tijdens ENSO (denk bijvoorbeeld aan extra biomassa verbranding in droge tijden) niet in het model gestopt zijn. Dit werk is het eerste ooit dat de invloed van ENSO op ozonconcentraties beschrijft middels een simulatie van meerdere jaren.

Om de onderschatting van ozonconcentraties boven de Atlantische Oceaan beter te begrijpen, en mogelijk te verhelpen, zijn we in Hoofdstuk 4 gedetailleerder gaan kijken naar de longitudinale verdeling van ozon in ons model. Omdat ozonmeetstations in de tropen dun gezaaid zijn en vaak pas over slechts enkele jaren aan observaties beschikken, hebben we nu gekozen om satellietwaarnemingen (1979-1992) van ozon te gebruiken. In dit hoofdstuk introduceren we eerst een methode om model en waarnemingen op een kwantitatieve, systematische manier met elkaar te vergelijken. Deze methode wordt vervolgens gebruikt om in kaart te brengen waar en wanneer de onderschatting van ozon door het model het sterkst is.

De grootste onderschattingen komen voor tijdens de maanden augustus tot en met november, en over de gehele Atlantische Oceaan, aangelegen continenten en zelfs een deel van de Indische Oceaan. Een analyse van de bronnen van ozon in de tropen leert ons dat de ozonconcentratie bijna evenredig bepaald wordt door alle processen die we beschouwen: stratosfeer-troposfeer uitwisseling, biomassa verbranding, industriële emissies, bliksem, en bodememissies van NO_x. Desalniettemin lijken biomassa verbranding en bodememissies de sterkste asymmetrie te vertonen tussen de Grote Oceaan en de Atlantische Oceaan omdat deze emissies laag aan de grond plaatsvinden en zich minder snel verspreiden door de troposfeer. Een groot aantal gevoeligheidssimulaties, waarin we specifieke parameters veranderen om hun effect op berekend ozon te bestuderen, leert ons dat ozon nauwelijks gevoelig is voor veranderingen in de randvoorwaarden van het model, doordat terugkoppelingen in de productie en verwijdering van ozon en zijn voorlopers een stabiliserende werking hebben op de concentraties.

Dit betekent dat we met de huidige kennis van het systeem en de berekende gevoeligheden geen systematische verbetering kunnen vinden die de modelberekeningen en satellietwaarnemingen binnen één standaard deviatie brengen. Onze aanbevelingen in dit hoofdstuk zijn om toekomstig onderzoek vooral te richten op transport van ozon en op de beschrijving van biomassa verbranding in de tropen. Daarnaast is een reductie van de onzekerheid in de satellietmetingen gewenst.

Hoofdstuk 5 beschouwt de stabiliteit van fotochemie in de tropen en het vrijwel onveranderde niveau van OH sinds de het begin van de industrialisatie. We richten ons in dit hoofdstuk vooral op OH niveaus, die sterk gekoppeld zijn aan die van ozon omdat ozon samen met waterdamp en zonlicht mede de productie van OH bepaalt.

We introduceren een nieuw concept dat we 'recycling efficiency' hebben genoemd. Dit concept beschrijft hoe sterk de productie van OH afhangt van ozon (primair), ten opzichte van OH productie via andere kanalen (secundair).

Het blijkt dat vlakbij geïndustrialiseerde gebieden de rol van primaire ozonproductie minder belangrijk is geworden, maar dat juist op verafgelegen gebieden de aanvoer van ozon voorkomen heeft dat OH niveaus ingestort zijn. De plekken die sterk afhankelijk zijn van ozon om de OH productie in stand te houden zijn ook het meest gevoelig voor verstoringen van de chemie door bijvoorbeeld toenames van methaan of stikstofoxiden. Dit heeft belangrijke implicaties omdat deze gebieden voornamelijk in de tropen liggen waar door snelle economische groei grote veranderingen kunnen gaan plaatsvinden.

Het lijkt paradoxaal dat OH niveaus zo constant zijn sinds het begin van de industrialisatie, ondanks het feit dat de emissies van koolstofmonoxide en methaan, die met OH reageren, zo sterk gegroeid zijn. Onze berekeningen laten zien dat globaal

gemiddelde OH niveaus constant zijn gebleven door een 50% toename van primaire OH productie uit ozon en een 75% toename van secundaire OH productie. Bovendien is de verdeling van OH sinds de industrialisatie sterk veranderd met toenames met meer dan 200% in verstedelijkte gebieden, en afnames met meer dan 30% in afgelegen marine gebieden.

Nawoord

Honderd-vier-en-veertig pagina's heeft U doorgeworsteld om hier uiteindelijk het antwoord te vinden op de vraag: "Sta ik er in, sta ik er niet in?". Tegen degenen die er in staan zou ik zeggen: "Uiteraard...", tegen degenen die buiten de boot vallen door ruimtegebrek: "Ik maak het nog wel eens goed...", en tegen diegenen die ik (expres?) vergeten ben: "Sorry...". Een fijne dooddoener is misschien dat de dank die ik verschuldigd ben aan iedereen die mij de afgelopen jaren geholpen, gesteund en geïnspireerd heeft toch vele malen groter is dan ik op deze pagina's kwijt kan.

Ik wil Jos Lelieveld graag bedanken voor de uitstekende begeleiding. Als geen ander weet je de balans tussen vrijheid en sturing op de juiste manier in te vullen. Dit heeft mij altijd het gevoel gegeven heeft dat ik al mijn eigen ideeën kon uitproberen, maar dat het nooit tot een mislukking van mijn promotie kon leiden. Jouw enthousiasme voor, maar ook relativerende benadering van de wetenschap is een voorbeeld voor me. Ik waardeerde vooral sterk de mogelijkheid om je op te kunnen bellen over niet 'wetenschappelijk inhoudelijke' zaken, maar gewoon met de vraag: "Jos, hoe pak ik dit aan?". Naast af en toe een bezoekje aan Mainz hoop ik ook dat in de toekomst te kunnen blijven doen.

Maarten Krol is de grote motor achter mijn (en vele andere!) promotie, zonder hem waren deze vier jaar nooit zo soepel verlopen. Ons dagelijks overleg, je vele adviezen, de technische hulp, de nauwe samenwerking, de aanmoedigingen, en ook de nodige bijsturingen hebben me enorm veel geleerd en sterk bijgedragen aan mijn wetenschappelijke vorming tot nu toe. Ik heb vooral genoten van de projecten waar we samen aan gewerkt hebben, en die enorm inspirerend en leerzaam zijn geweest. In dit opzicht wil ook Frank Dentener bedanken die van grotere afstand altijd interesse in mijn werk en voortgang heeft getoond. Ik hoop nog lange tijd met jullie te kunnen blijven werken.

I would like to thank Anne Thompson for her hospitality, enthusiasm, and constant interest in my work. I have greatly enjoyed our collaboration on the two chapters in this thesis, and the three months spent in your group in Maryland have enriched my scientific career. The way you welcomed me in the States, took close interest in my work, always answered all my questions quickly, and was never too busy to go through my manuscripts has amazed me, and inspired me. I'm very happy that you are present at my thesis defense, and I will certainly look for opportunities to keep working together.

While abroad, many people have contributed to my scientific, and especially social, well-being. These people make science such a fine business to be in. First of all Karen and Dave Thornton, for adopting me into their family and making my stay

in the US so much nicer. Also Yukako, for our great discussions, wonderful dinners, and pleasant (quiet!) evenings. Jacquie and Christian for showing me around, and Maryland's own 'Space Bastards' for memorable weekend trips and loads of fun.

Mijn verblijf in Suriname zou niet zo'n succes geweest zijn zonder het aangename gezelschap en vele meteorologische lessen van Truus Warsodikromo, en de zeer hartelijke ontvangst en goede zorgen van de heer Cor Becker en zijn familie.

Natuurlijk koester ik fijne herinneringen aan (al) mijn jaren bij het IMAU, waar staf, secretaresses, ondersteunend personeel, en mijn (ex-) collega's bijdragen aan de fantastische sfeer die ik tot nu toe nog nergens anders heb meegemaakt.

Sandra, veel van de energie en het enthousiasme waarmee ik aan mijn promotie gewerkt heb putte ik uit jouw aanwezigheid. Ik hoop dat we onze perfecte balans volhouden in de spannende tijden die gaan volgen. Tot slot wil ik degenen bedanken die de meest fundamentele rol gespeeld hebben in alle jaren leidend tot mijn promotie, en zonder wie ik niet gekomen was tot waar ik nu ben: André, Rita, Susan, en Jenny.

Curriculum Vitae

Wouter Peters is geboren op 15 mei 1975 in Hoorn. Hij behaalde in 1993 zijn VWO diploma aan de Regionale Scholen Gemeenschap in Enkhuizen, waarna hij een jaar Natuurkunde studeerde aan de Vrije Universiteit te Amsterdam. In 1994 vervolgde hij zijn opleiding aan de Universiteit Utrecht waar de bovenbouw studie 'Meteorologie en Fysische Oceanografie' gevolgd werd. Dankzij een zeer interessant afstudeeronderzoek dat hem naar het tropische Suriname leidde, werd zijn interesse voor de wetenschap gewekt. En tijdens een enerverende autorit van Zanderij naar Paramaribo besloot hij op de aanbieding van zijn passagiers Jos Lelieveld en Paul Crutzen in te gaan en per september 1998 zijn promotie onderzoek te beginnen.

Het promotie onderzoek bracht hem in de gelegenheid veel te reizen, onder andere nog twee keer terug naar Suriname. In de laatste fase van het onderzoek verbleef hij nog enkele maanden in Washington DC, onder de plezierige begeleiding van Dr Anne Thompson.